AERODYNAMIC BEHAVIOUR OF BRIDGES.

by

William Iain Linn, B.Sc.

Thesis presented for the degree of M.Sc.

to the Faculty of Engineering,

The University of Glasgow.

Department of Aeronautics
and Fluid Mechanics.

October, 1974.

ProQuest Number: 10647008

ProQuest 10647008

AERODYNAMIC BEHAVIOUR OF BRIDGES

SUMMARY

For a number of years, under various contracts, the Department
of Aeronautics and Fluid Mechanics has been wind-tunnel testing bridge
models for static loads.   A recent development has been to include
dynamic testing of models to determine the stability of the bridge
in winds.   The interest of the writer was in applying aeroelstic
techniques to the prediction of the stability of the bridge models.

Tests on section models of a proposed road bridge were carried
out in the low speed wind-tunnel of the Aeronautics Department.   The
unusual feature of the bridge under consideration was its composite
nature, the road deck being suspended between a pair of parabolic
arch ribs.   In the classic suspension bridges, or cable-stayed bridges,
the deck is suspended from cables and the stability resolved using the
deck alone in the tests.   In the case of the proposed bridge, the deck
and the supporting arch rib would interact, and each would contribute
to the dynamic behaviour of the bridge as a whole.   However, because
of the differing modes of motion of the parts it was thought that the
aerodynamic stability of the complete structure could be determined
from tests of section models of each part.   Interaction between the
parts would tend to reduce motion and increase stability.   The size
of the wind-tunnel working section usually prohibits testing of
complete models at an acceptable scale.   The radius of curvature of
the arch rib was such that straight sections could be used for the
model with very small errors.

The separate section models were tested on the three-component
balance to determine the steady wind forces on the bridge, which were
also compared with predictions using British Standards data, and then
on a dynamic mounting to examine their aerodynamic stability.

Both the arch rib and the deck had a low speed resonant vibration caused by the natural frequency of the structure matching that of the shedding of vortex pairs from the top and bottom surfaces. The amplitudes of vibration of both were greatly reduced by cutting holes in the webs of the spanwise girders of the deck, and in the side plates of the arch ribs. These holes bled air from the leading edges, and reduced the strength of the vortices.

The deck had a divergent pitch oscillation at high speeds, induced by a vortex phenomenon. The speed at which this occurred was increased by about 30% by adding a trapezoidal fairing to the edge of the roadway parapet. This reduced the strength of the upper surface vortex by smoothing the airflow.

The low speed instability can be predicted using the Strouhal number for the structure, and amplitudes of vibration can be estimated for a number of damping levels. The pitch instability could only be determined experimentally, and as it will lead to catestrophic failure of the structure, it is essential that the critical speed is well above that likely to be experienced by the prototype. Detail changes have a very important effect on this motion and extrapolation to the full-size prototype must be done with great care.

Much more dynamic experimental data are needed from full-size prototypes to allow more confident predictions to be made from model testing.

CONTENTS.

FIGURES.

ACKNOWLEDGEMENTS.

AERODYNAMIC BEHAVIOUR OF BRIDGES.

INTRODUCTION.

For a number of years, under various contracts, the Department of Aeronautics and Fluid Mechanics has been wind-tunnel testing bridge models for static loads. A recent development has been to include dynamic testing of section models to determine the stability of the bridge in winds. The interest of the writer was in applying aeroelastic techniques to the prediction of the stability of the bridge models.

At the request of Messrs. W. A. Fairhurst and Partners, consultants to the Scottish Development Department, tests on section models of a proposed road bridge were carried out in the 1.14m x 0.8m low speed wind tunnel of the Aeronautics Department. The unusual feature of the bridge under consideration was its composite nature, the road deck being suspended between a pair of parabolic arch ribs.

The proposed bridge consisted of a light steel and reinforced concrete deck forming a two-lane carriageway, with side footpaths, supported by the steel arch ribs at 13 metre intervals. The ribs were of hollow rectangular cross-section, and presented a frontal area approximately one and a half times that of the deck.

The deck and arch ribs would each contribute to the dynamic behaviour of the bridge as a whole, but it was thought that the aerodynamic stability of the complete structure could be determined from section model tests of each part. Also, the size of the wind-tunnel working section prohibited testing of a combined deck-arch model at an acceptable scale. A scale of $\frac{1}{32}$ full-size was used for both models, representing a full scale span of 36.2 metres for the sections.

The separate models were tested on the three component balance to determine the steady wind forces on the bridge, and then on a dynamic mounting to examine their aerodynamic stability.

Following tests on the original models, a series of modifications to the basic design were investigated. The final configuration showed improved dynamic characteristics at both the lower and upper critical wind speeds.

NOTATION.

a	Acceleration.
A	Area.
A_i	Unsteady aerodynamic derivative
b	Width
C_D	Drag force coefficient.
C_H	Horizontal force coefficient.
C_L	Lift force coefficient.
C_M	Moment coefficient.
C_N	Normal force coefficient.
d	Displacement.
D	Drag force.
E	Youngs Modulus.
f	Damping constant.
f_{CR}	Critical damping.
F	Force
g	Acceleration due to gravity.
G	Shear modulus
h	Vertical degree of freedom, and projected section height.
H_i	Unsteady aerodynamic derivative.
I	Inertia in bending.
I_p	Inertia in pitch.
J	Inertia in torsion.
k	spring stiffness.
l	Length.
L	Lift.
m	Mass.
n	Number of cycles.
N	Amplitude ratio.

s	Scale factor.
S	Strouhal number.
t	Time.
v,V	Velocity.
V	Volume.
w	Angular velocity, frequency.
w_o	Natural frequency.
w_{TOR}	Torsional frequency.
y	Vertical degree of freedom.
y_R	Amplitude.
α	Incidence.
γ	Damping ratio.
δ	Logarithmic decrement.
λ	$1/w^2$.
μ	Viscosity of air.
ρ	Mass density of air.
Ω_d	Frequency of cosine wave of diminishing amplitude.

HISTORICAL REVIEW.

The collapse of the Tacoma Narrows suspension bridge in November 1940, only five months after it was opened to traffic, came as a very great shock to the engineering profession, and started the investigations into the aerodynamic stability of suspension bridges (Reference 1). Although it was the most spectacular and best documented collapse of a suspension bridge, it was certainly not the first such event. Throughout the 19th century, suspension bridges had been damaged or destroyed by wind in Europe and the United States. In Great Britain alone, five bridges failed in a period of 21 years, and others experienced trouble many times before the final collapse. The following British bridges destroyed by wind induced oscillations had the effect of dissuading British engineers for many years from constructing major suspension bridges. The recent Forth Road Bridge was the first new major bridge in over 120 years.

Near Dryburgh Abbey, in 1818, a footbridge 80 metres long and 1.2 metres wide was destroyed six months after it was built (Reference 1). The walkway was stiffened in the vertical direction by the side parapets, and the inference that can be made is that it caused Karman vortices to be formed, leading to a destructive torsional oscillation.

Across the river Tweed, at Berwick, the Union Bridge was the first vehicular suspension bridge, and the first large eyebar chain bridge in Britain. It was destroyed in high winds six months after it was completed (Reference 1).

The Brighton Chain Pier, of four spans of 68 metres, was partially destroyed in 1833 and 1836. An officer in the Royal Engineers, Lieutenant-Colonel Reid, was an eye witness to the 1836 occurrence, and wrote a very full account of the event, with graphic sketches (Reference 2), Fig. 1. He concluded that a torsional oscillation in the third span
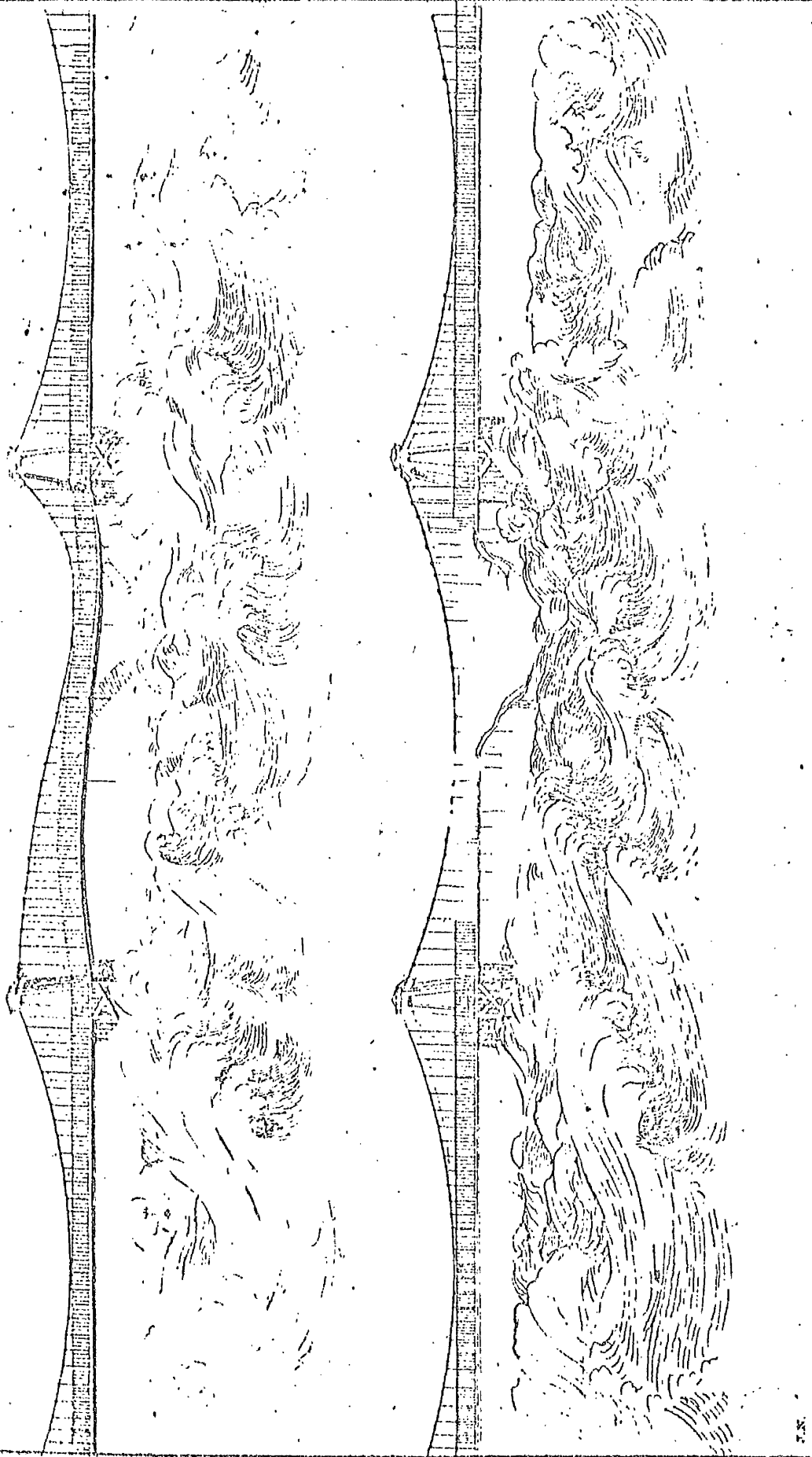
BRIGHTON CHAIN PIER

FIGURE I

overloaded the roadway until it broke.   This relieved the load enough
on the other spans to save them.

The suspension bridge across the Esk at Montrose collapsed once due
to an overload of people watching a boat race, and again in a storm.
The roadway was carried away by the storm, but the rest of the structure
was sound.   The bridge was rebuilt with the roadway made very stiff in
bending and torsion, and no further trouble was experienced (References
3, 4), Fig. 2.

The Menai Straits Bridge was damaged in 1826 and 1836, and serious-
ly damaged in 1839. Fig. 3.   It was considerably altered when rebuilt,
and remained in use until 1939, when the suspended structure was com-
pletely replaced.   An excellent report on this bridge is presented by
W. A. Provis in the Transactions of the Institute of Civil Engineers
(Reference 5).

- The reports on the Brighton Chain Pier, the Montrose Suspension
Bridge, and the Menai Straits Bridge by qualified engineers indicate
that the failures of the structures were due to wind induced oscillations.
Various theories were put forward as to the causes of the oscillations.
The principle ones were that the wind rebounded off the water, or came
down on the bridge at an angle of incidence, forcing vertical displace-
ments.

With the present knowledge of the atmosphere, and hindsight, an
indication of the requirements for instability can come from comparing
two similarly constructed bridges, the Menai Straits and the Conway.
The Menai bridge was high over the water, and violently affected by the
wind.   The Conway bridge was 5 metres above the sea, and wind effects
were slight.   (Reference 5).   Now it would be said that the Conway
bridge was in the turbulent boundary layer of the atmosphere, very close
to the ground, where the mean wind speed in any one direction is low.
The turbulence prevents any steady-state flow patterns developing.

SKETCH OF THE SUSPENSION BRIDGE OF MONTROSE IN ELEVATION.

AS IT APPEARED AFTER THE STORM OF THE 11TH OCTOBER 1833.

C.W. PASLEY, C.B. COLONEL, R.E.

THE ORIGINAL LENGTH OF ROADWAY BETWEEN THE PIERS 412 FEET

FIG. 1.

HIGH WATER
LOW WATER
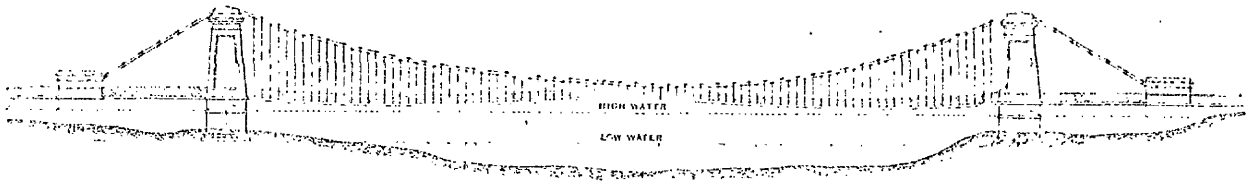
FIG 2.
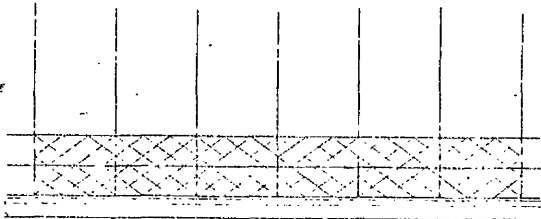
SKETCH OF THE SIDE RAILING OF THE BRIDGE AT MONTROSE

FIG. 5.
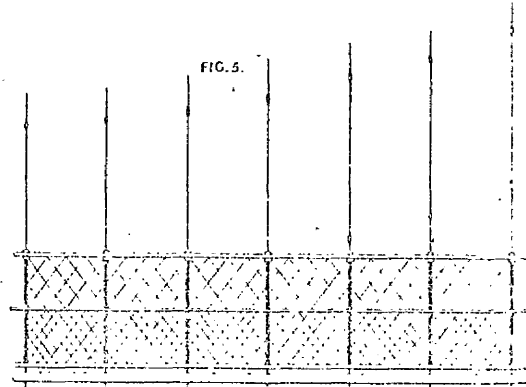
SIDE RAILING OF THE MENAI BRIDGE

FIG. 4.
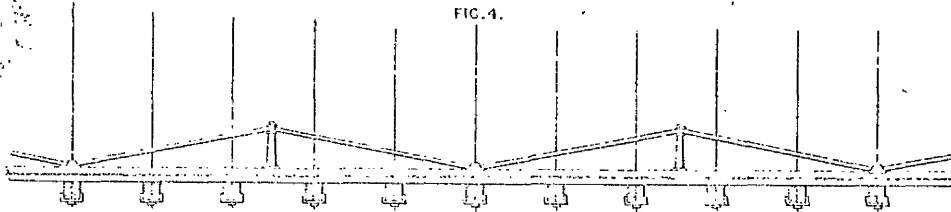
CENTRAL TRUSSING OF THE BRIDGE AT HAMMERSMITH

FIG. 6.

FIG. 3.
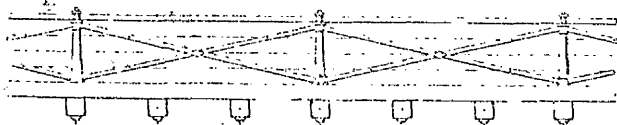
SIDE RAILING OF THE BRIDGE AT HAMMERSMITH
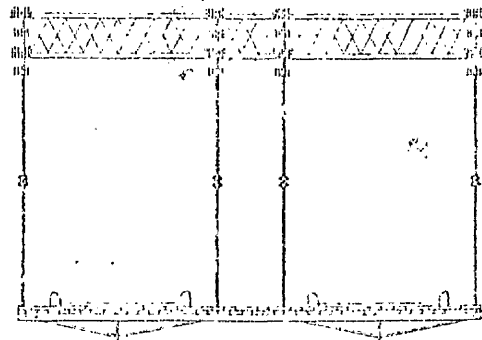
TRANSVERSE SECTION OF THE MENAI BRIDGE

SCALE FOR FIGS 2 3 4 5 AND 6.
10   5   0   10   20 FEET

FIGURE 2

THE MENAI BRIDGE.

AS IT APPEARED AFTER THE STORM OF JANUARY 6.7.1839.

HIGH WATER

LOW WATER

ANGLESEY

CAERNARVONSHIRE

PLAN.

NORTH EAST CARRIAGE WAY

FOOTWAY

SOUTH WEST CARRIAGE WAY

SCALE OF

FEET
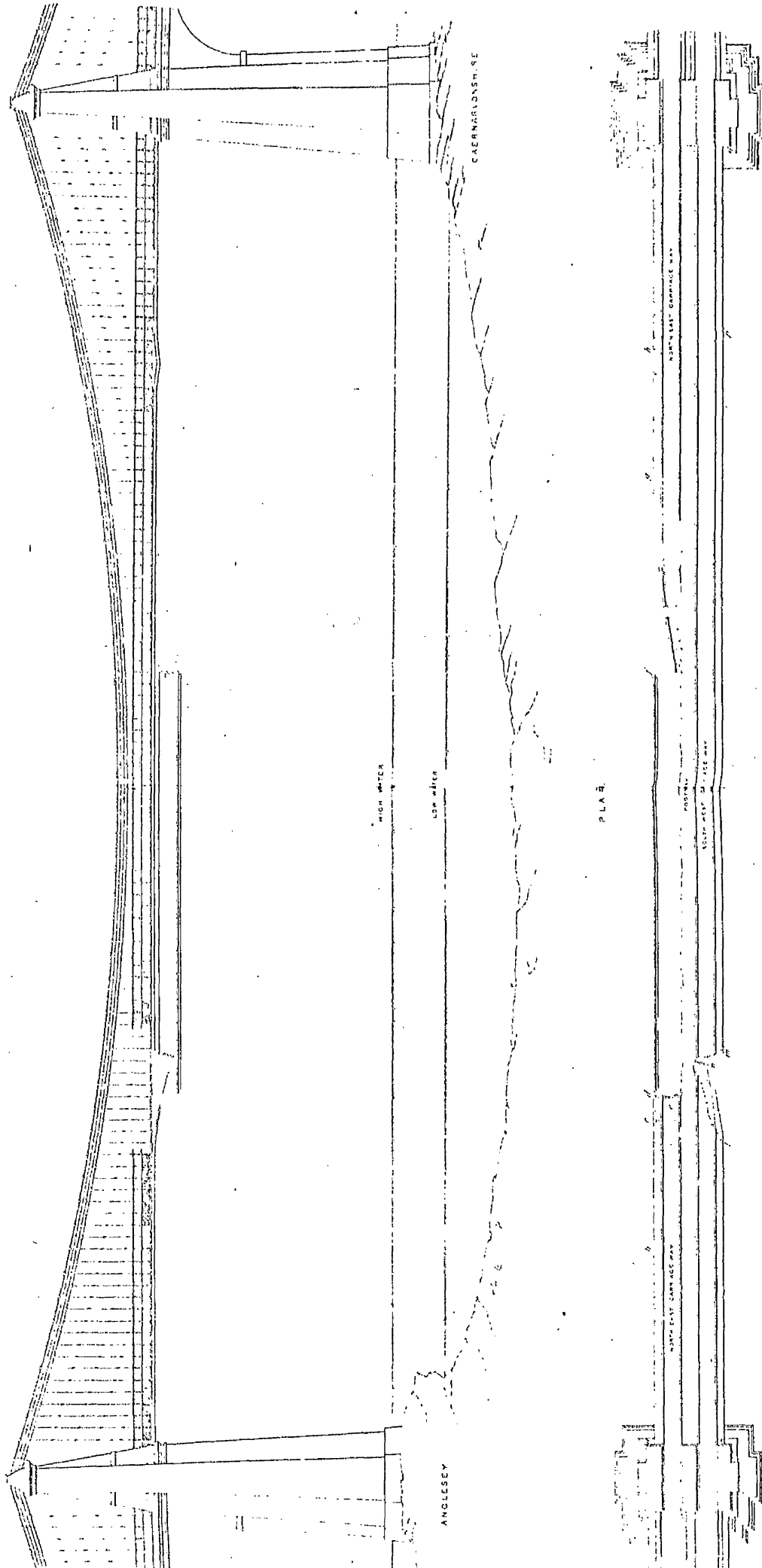
FIGURE 3

On the other hand, the Menai bridge was high enough in the shear layer

of the atmosphere for the mean velocity to be high, with low turbulence

levels allowing steady-state flow patterns to develop.

It was also recognised that the stiffness of the roadway was very

important.   The Hammersmith Bridge in London (Reference 5) had deep

trussed frames longitudinally, Fig. 2, but was close to the river surface

so the two effects on stability could not be separated.   An inland site

meant that the average wind velocity was lower than on an exposed coast.

No high bridge had been built with deep trusses, but when all the damaged

bridges had been substantially stiffened, they experienced no more

unstable oscillations.

J. S. Russell, in his paper "On the Vibration of Suspension Bridges

and other Structures" (Reference 2), compared the vibration of structures

to the vibration of a musical string.   He came by the comparison when

watching a tower of wooden scaffolding 25 metres high in strong winds.

The tower was braced in the middle, and guyed from the top   The upper

half of the beams vibrated in the wind, causing an opposite motion in

the sheltered lower half, with no movement at the bracing.   With the

bracing moved to the $\frac{1}{3}$ point, three waves developed, and four waves when

at the $\frac{1}{4}$ point.   The waveforms were identical to those on a vibrating

string with 1, 2 and 3 nodes.   If the position of the bracing was such

that the ratios were not integral, no oscillation occurred.   Russell

carried the analogy over to suspension bridges, resulting in a simple

method of guying to prevent induced oscillation.   His method for finding

the distance of the stay from one end was to square the length (1) of the

bridge, half the result, $1^2/2$, and extract the square root of this.   The

result $1/\sqrt{2}$ is a non-integral portion of the length (1) of the bridge.

Although the paper demonstrated the forms taken by the oscillating

structures, and their analogy with vibrating strings, the basic exciting

mechanism was not understood (and is still not fully understood).

The legacy of these disasters was that British engineers became very cautious about building big suspension bridges, and it was left to the Americans to develop this form of construction.

In 1855, a railway bridge was built at Niagara by George Roebling using his wire cable spinning machine (References 6, 7). This eliminated the unwieldy chains previously used, and made the erection of the suspension cables very much easier, since the cable could be built up strand by strand as the machine went to and fro across the river. Chains had to be raised into position en masse. Cables had the added advantage of being failsafe, where chains were not. The Niagara bridge had a span of 250 metres, and was guyed from the centre to the foot of the abutments. Wind caused some damage, and as a result, subsequent United States bridges were made very robust and ungainly to give high stiffnesses.

The first bridge to use steel wire cables instead of wrought iron was the Brooklyn Bridge, built in 1883 (References 7, 8).

With the advent of the motor car, and the relaxing of roadway gradient requirements, the trend changed towards lighter structures, culminating in the Bronx-Whitstone and Tacoma Narrows bridges. Both were very light, slender structures stiffened by plate-girders. The Tacoma bridge was at least half the weight per foot span of any other bridge, and generally closer to one-quarter, the extreme in ribbon-like bridges. This design was adequate for static wind loads, but not enough aerodynamic information was available to avoid the dynamic effects of wind induced oscillation. These effects were captured on cine film during the destruction of the Tacoma Narrows bridge by a torsional oscillation in a wind of 18 m/sec. (Reference 1). Bridges had suffered from vibrations before even the truss-stiffened Golden Gate bridge (Reference 9), but nothing had attracted such worldwide attention as this.

The collapse led to extensive research into suspension bridge
stability in the United States of America, especially at the University
of Washington, where a wind tunnel 30 metres wide was specially built for
testing model bridges.   Using the cine film, vibration modes of the
original bridge were duplicated in the models, and with confidence from
this correlation, a safe design for the new bridge was determined. Fig.4.
From the investigation, the technique developed of using section models
of the bridge deck to determine the behaviour of the complete bridge.
Testing could then be carried out more easily and cheaply in the normal
wind-tunnel, and the models were much more amenable to changes in design.
The researches also led to substantial increases in the torsional and
bending stiffnesses of existing bridges, to prevent a similar occurrence,
and to reduce any slight oscillation.

At this time, Britain also began intensive research into suspension
bridge aerodynamic stability for a proposed crossing of the River Severn.
The main span of the bridge was to be 900 metres, and the side spans 330
metres, and the investigations were prompted by the troubles in the United
States of America.   The tests were carried out by Frazer and Scruton of
the National Physical Laboratory, using a specially built 13 metre wide
wind tunnel. (References 10, 11).. A stable design with a truss stiff-
ened suspended structure was developed, and then used for a crossing of
the River Forth instead of the Severn.   Fig. 5 (Reference 12).

Further research for the Severn crossing produced a significant new
design (Reference 13).   The suspended structure was a box-section of
approximately aerofoil shape, which was aerodynamically stable at all
possible wind speeds.   This was a major advance in bridge design, giving
a very elegant structure, which was easy to fabricate and erect.
Another advantage is that the basic shape can be used for other bridges,
such as the Erskine Bridge across the River Clyde, Fig. 6, or the bridge
across the Bosphorus at Istanbul (Reference 14).
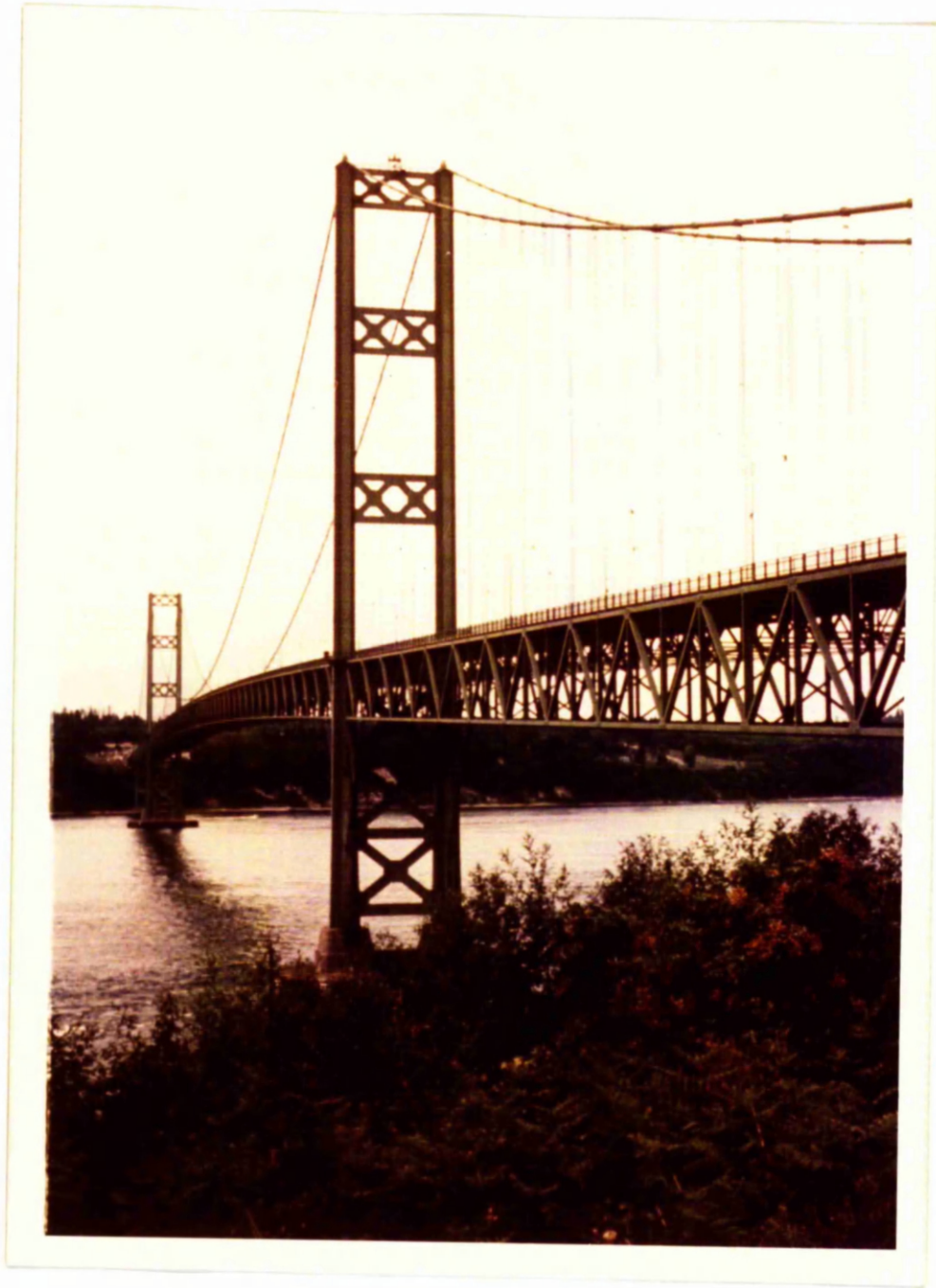
TACOMA NARROWS BRIDGE

FIGURE 4
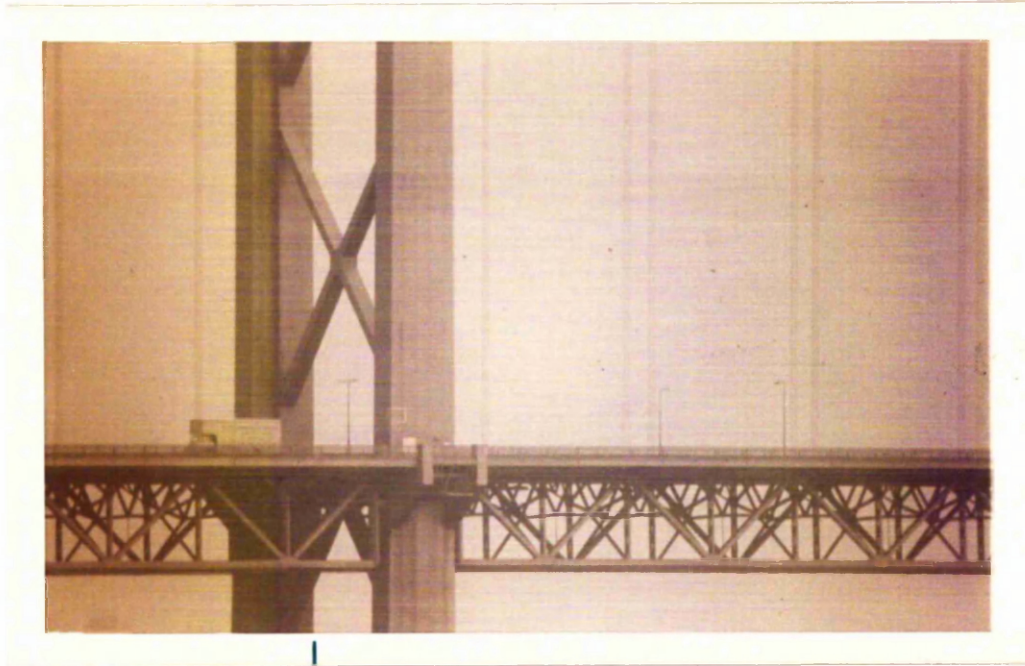
FORTH ROAD BRIDGE
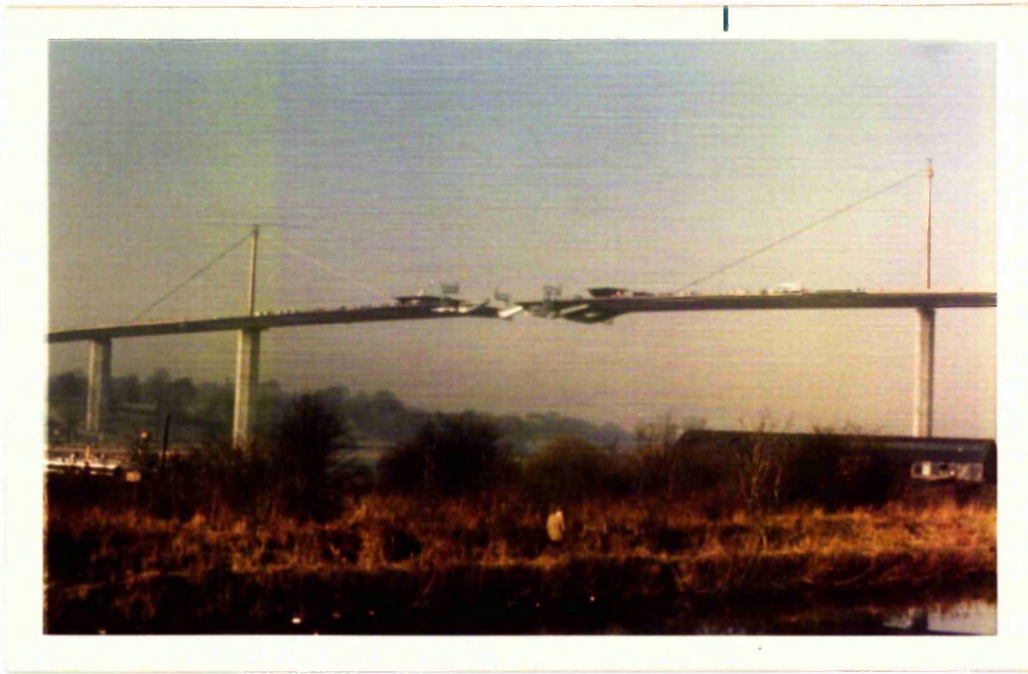
FIGURE 5

ERSKINE BRIDGE

FIGURE 6

Contemporary American designs such as the Verrazano Narrows Bridge (Reference 15) in New York, the Tagus Bridge (Reference 16) in Portugal and the Orinoco Bridge (Reference 17) in Venezuela still used truss-stiffened structures. One advantage is that two or more levels of roadway can be incorporated for large volumes of traffic. Nevertheless, it seems that Britain has made up for the century in the doldrums.

THE PROBLEM OF SCALE OF A MODEL.

The laws of similarity and dimensional analysis governing the scaling of the various properties and functions of any model are determined by the laws of mechanics. Two bridge systems are dynamically similar when the relationship between them is such that the forces on one system are multiples of the forces on the other at the corresponding time. The displacements of both systems will then be similar, and so one system will copy the movements of the other. This is the whole reason for making dynamic scale models of bridges, as the model will show the behaviour of the prototype under all conditions represented by the tests.

The movement of a suspension bridge in the wind depends on its size, shape, density, elastic module, the damping of the materials used, the friction properties inherent in the mode of construction, and the wind forces.

The relation between the motion of a model and that of the prototype is dependent on the linear and time scales of the model. Denoting the linear scale, model to prototype, as 's' and the time scale as 't', velocities will be to the scale s/t, and accelerations to s/t^2. With the same gravitational constants for both systems, and air densities normally the same, gravitational forces will be to the scale s^3, and inertial forces s^4/t^2, and for equality of these scales $t = \sqrt{s}$. Model wind speeds are thus to the scale $\sqrt{s}$, and frequencies to the scale $1/t$ or $1/\sqrt{s}$.

The wind forces acting on a body are partly viscous, from the friction between the wind stream and the body, and partly inertial, from the pressure of the wind against the body. If exact similarity of behaviour is required between the model and prototype, wind and gravitational forces must be reduced by the same scale, which must also match the scales of the other functions. The ratio of inertial to viscous

wind force is as follows:-

$$\frac{\text{Inertial Force}}{\text{Viscous Force}} = \frac{\rho l^3 a}{\mu l^2 (\frac{v}{l})}$$

v - velocity

l - representative length

ρ - mass density of air

μ - viscosity of air

a - acceleration

$$= \frac{\rho l^3 (v^2/l)}{\mu l^2 (v/l)}$$

$$= \frac{\rho v l}{\mu} \quad \text{(the Reynolds Number)}$$

One of the uncertainties of model testing is the effect of viscosity and Reynolds Number when comparing model and prototype, as the linear scale factor is usually large. Air flow patterns may not be the same as a result of this. Fortunately, most bridges are bluff bodies with sharp edges, giving the same flow pattern for the model and prototype, and no Reynolds number corrections are necessary. This was shown in correlating the model tests of the first Tacoma Narrows Bridge with the prototype, and in later tests of the Golden Gate and new Tacoma Narrows bridges (Reference 1). Where gaps and slots are present on the prototype, care must be taken when modelling them, as their small sizes make the effects of Reynolds number very important. In some cases, it is necessary to have a slightly incorrect geometric shape in order to make the model flow pattern the same as that of the prototype.

The ratio of inertial force to gravitational force is expressed as

$$\frac{\text{Inertial Force}}{\text{Gravitational Force}} = \frac{ma}{mg}$$

$$= \frac{v^2/l}{g}$$

$$= \frac{v^2}{lg}$$

$$= \text{constant (the Froude number)}$$

Since the acceleration due to gravity, g, is constant, the relationship between model and prototype is

$$\frac{v^2_m}{l_m} = \frac{v^2_p}{l_p}$$

$$\text{so } \frac{v_m^2}{v_p^2} = \frac{l_m}{l_p} = s, \text{ where } s \text{ is scale factor}$$

Thus, the model wind velocity is to the scale of $\sqrt{s}$ of the prototype.

In bridge model testing, the Froude number is used for scaling wind speeds, as the Reynolds number correlation is generally ignored for bluff bodies.

Elastic forces must be accounted for in the construction of the model, the members of which have areas to the scale s^2. As it is difficult to find materials with elastic moduli scaled by s to give correct elastic forces, material with the same moduli as the prototype is used. Fairings and mass are then added to give the correct shape and density to compensate for the wrong moduli. This procedure is used when testing a complete model of a bridge. Sectional models are rigidly constructed from suitable materials, and the required stiffnesses, mass distributions, and inertias achieved using external springs and weights.

The importance of damping cannot be overestimated. The damping, or decay, of any oscillations is usually specified by the logarithmic decrement, δ, of the oscillations, where

$$\delta = \frac{1}{n} \log_e N \qquad \text{for } \delta \ll 1$$

where N is the ratio of the amplitude at the first cycle to that at the nth cycle of the damped oscillation. This is a non-dimensional number, and so the model and prototype should have the same value. Structural damping is caused by the internal damping of the material, the fretting action of joints, sliding friction, or any artificial damping provided. There is a lack of information about the damping of full scale structures, which leads to uncertainty of the aerodynamic stability predicted from models. A compromise is to test the model with as low a damping as can be achieved realistically, bearing in mind that welded structures

tend to have a lower structural damping than bolted structures.   Using
the experience of the aircraft industry, with its experimental data on
the structural damping of aircraft, a reasonable damping level can be
assumed, in order that the model tests do not appear too pessimistic.

A short table of scale factors for various functions follows:-

Function.		Dimension.		Scale.	
Length	l	L	l_m/l_p	$= s$	
Area	A	L^2	A_m/A_p	$= s^2$	
Volume	V	L^3	V_m/V_p	$= s^3$	
Moment of Inertia	I, J	L^4	I_m/I_p	$\doteq s^4$	
Time	T	T	T_m/T_p	$= \sqrt{s}$	
Frequency	w	$1/T$	w_m/w_p	$= 1/\sqrt{s}$	
Velocity	v	L/T	v_m/v_p	$= \sqrt{s}$	
Acceleration	a	L/T^2	A_m/A_p	$= 1$	
Mass	m	M	M_m/M_p	$= s^3$	
Elastic Modulus	E, G	M/LT^2	E_m/E_p	$= s$	
Stiffness	EI, GJ	ML^3/T^2	$(EI)_m/(EI)_p$	$= s^5$	

CONSTRUCTION OF MODELS.

The working section dimensions of the University's low speed wind tunnel are such that testing a model of the complete bridge would be impracticable, and would not give meaningful results.   Sectional models of the arch rib and road deck were constructed from drawings provided by the consultants to a scale of $\frac{1}{32}$ full size.

A strip-laminated plank of white pine was used to model the reinforced concrete deck.   This would avoid any warping of the finished model, and provide a very solid basic structure for the attachment of the other components.   The main spanwise deck girders were made to the correct scale geometry using 24 S.W.G. and 22 S.W.G. aluminium alloy sheet.   Channel sections were formed from the 24 S.W.G. material, to which were bonded flange strips using 22 S.W.G. material.   The transverse deck girders were of the correct overall scale dimensions, but the web and flange thicknesses were 26 S.W.G. and 2 x 26 S.W.G.   Fig. 7. This small departure from the true dimensions because of construction problems was considered acceptable since the airflow would be parallel to the axes of these members.   Correctly scaled safety railings were made from brass strip, and the wire mesh infill was initially represented by a woven nylon net.   This was subsequently replaced by a rectangular mesh of tinned copper wire, Fig. 8 (Reference 18) fitted to the inboard face of the railings.

For the static load tests, mounting brackets were attached to the underside of the deck and the rear central hanger support pad for connecting the model to the three-component balance Fig. 7.   For the dynamic tests, special end-plate fittings were machined from aluminium alloy, and were an integral part of the model.   To them were attached the stub axles, Figs. 7 and 9, which could be fixed in a number of positions, so altering the axis of rotation.   The stub axles were removed for the static tests, and the mounting brackets removed for the

UNDERSIDE OF DECK

FIGURE 7
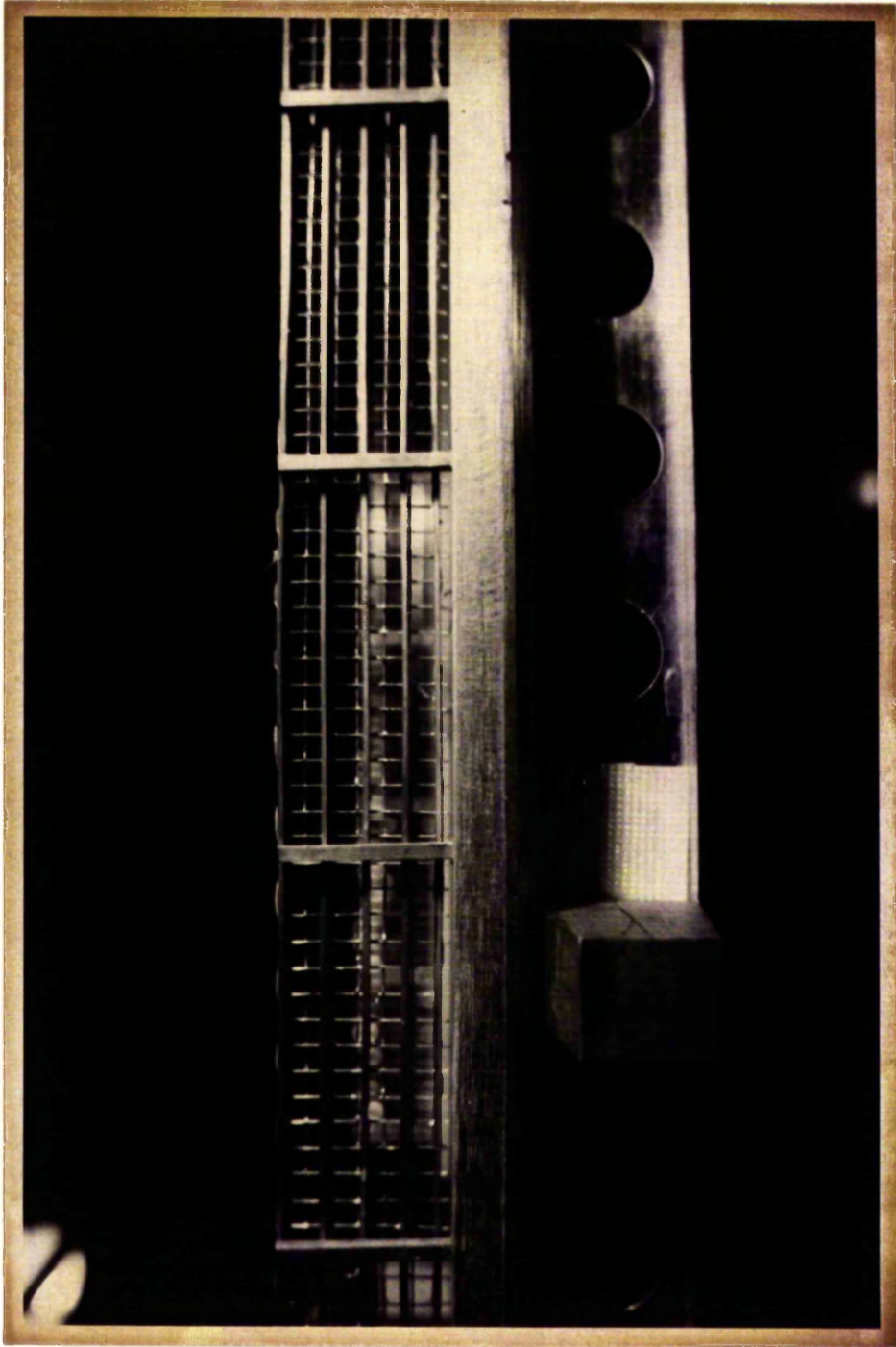
RAILINGS AND WIRE MESH
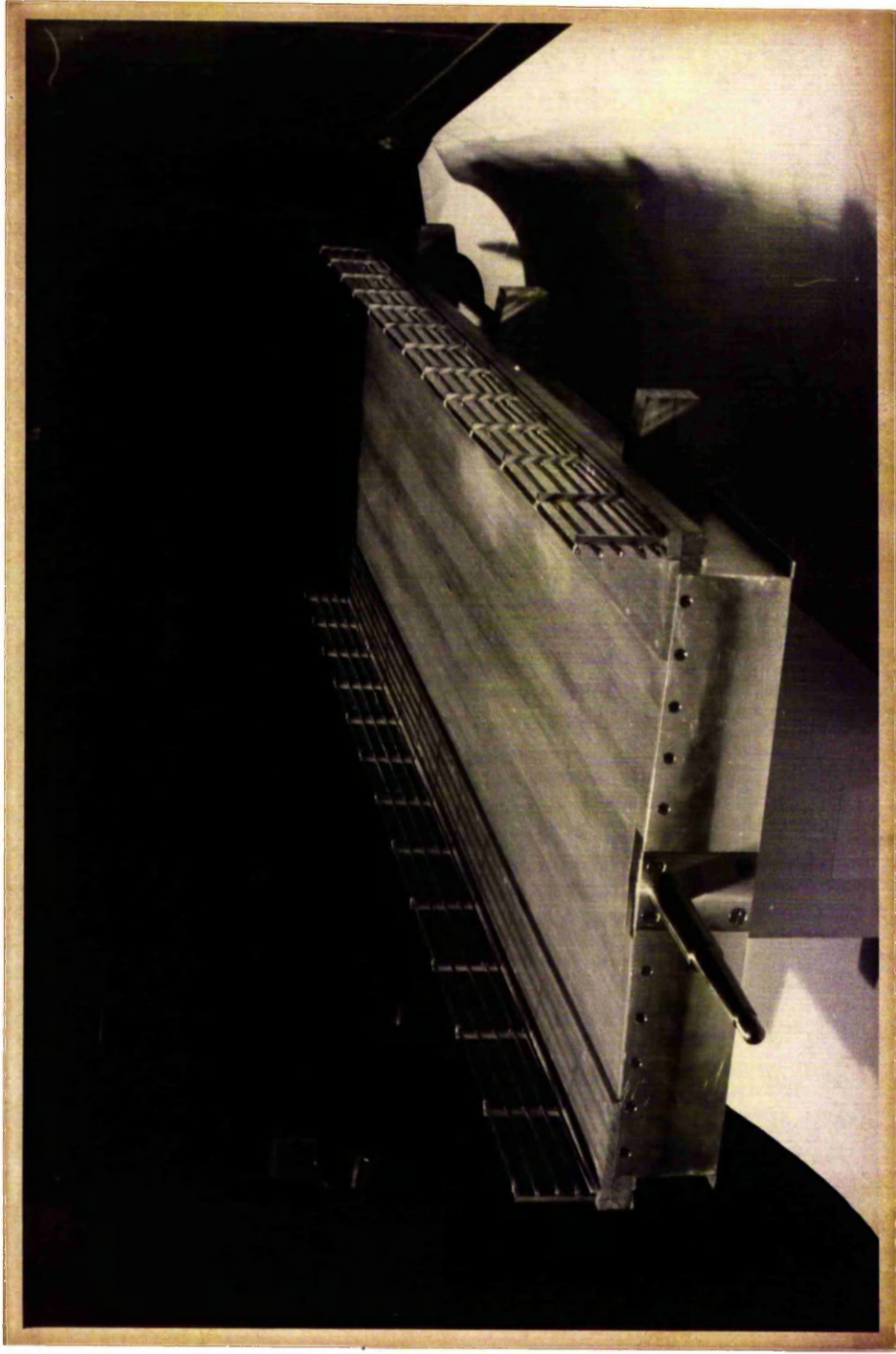
FIGURE 8

DECK AND STUB AXLES

FIGURE 9

dynamic tests, Fig. 10.

The mass of the deck model, less the stub axles, was 4.5 kg. This is approximately one third of the correct scale mass, since the effective mass for the dynamic tests must include all the parts of the dynamic mounting which move with the model. With the model in its original configuration, the effective mass was 13.3 kg., compared with the correct value of 12.8 kg. After the first series of tests, involving vertical translation only, the effective mass was increased by external balance weights to 14.9 kg. This combined the mass of the deck with 50% of the estimable scale mass of the arch rib and hangers. For all the stability tests of the deck model involving rotational movement, the effective mass moment of inertia was 0.210 kg.m^2, compared with the correct mass moment of the deck alone of 0.174 kg.m^2.

The sectional model of the arch rib was in the form of two straight parallel box beams rigidly connected together by plywood end-plates. The end plates fulfilled the same purpose as the alloy ones on the deck model, providing the attachment for the stub axles for the dynamic tests. Neither the curve, nor the angle of inclination of the arch rib was represented, and no provision was made to permit displacement of one rib relative to the other. Fig.11. The model was constructed from balsa wood sheet, with the correct scale geometry for the cross-sections and spacings of the ribs and bracing members. The effective mass was 12.9 kg. in the dynamic mountings, representing the estimated scale mass of the arch rib and hangers, plus 66% of the scale mass of the deck alone. In the tests involving rotation, or pitch, the axis of rotation coincided with the axis of symmetry of the model. The mass moment of inertia about this axis was 0.210 kg.m^2, equal to the correct scale moment of inertia of the arch rib, plus 20% of the scale moment of inertia of the deck.
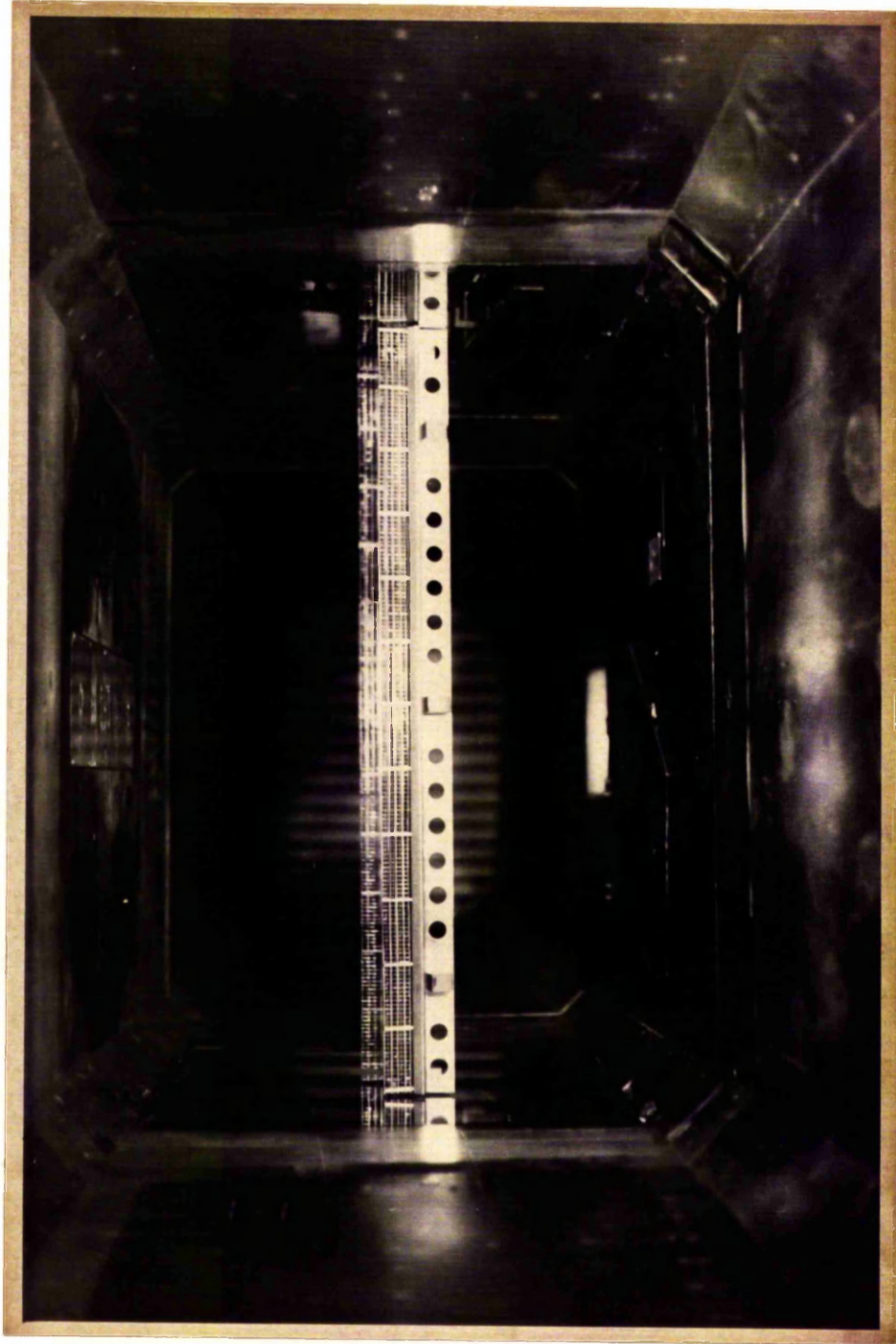
DYNAMIC TEST OF DECK

FIGURE 10

ARCH RIB

FIGURE 11
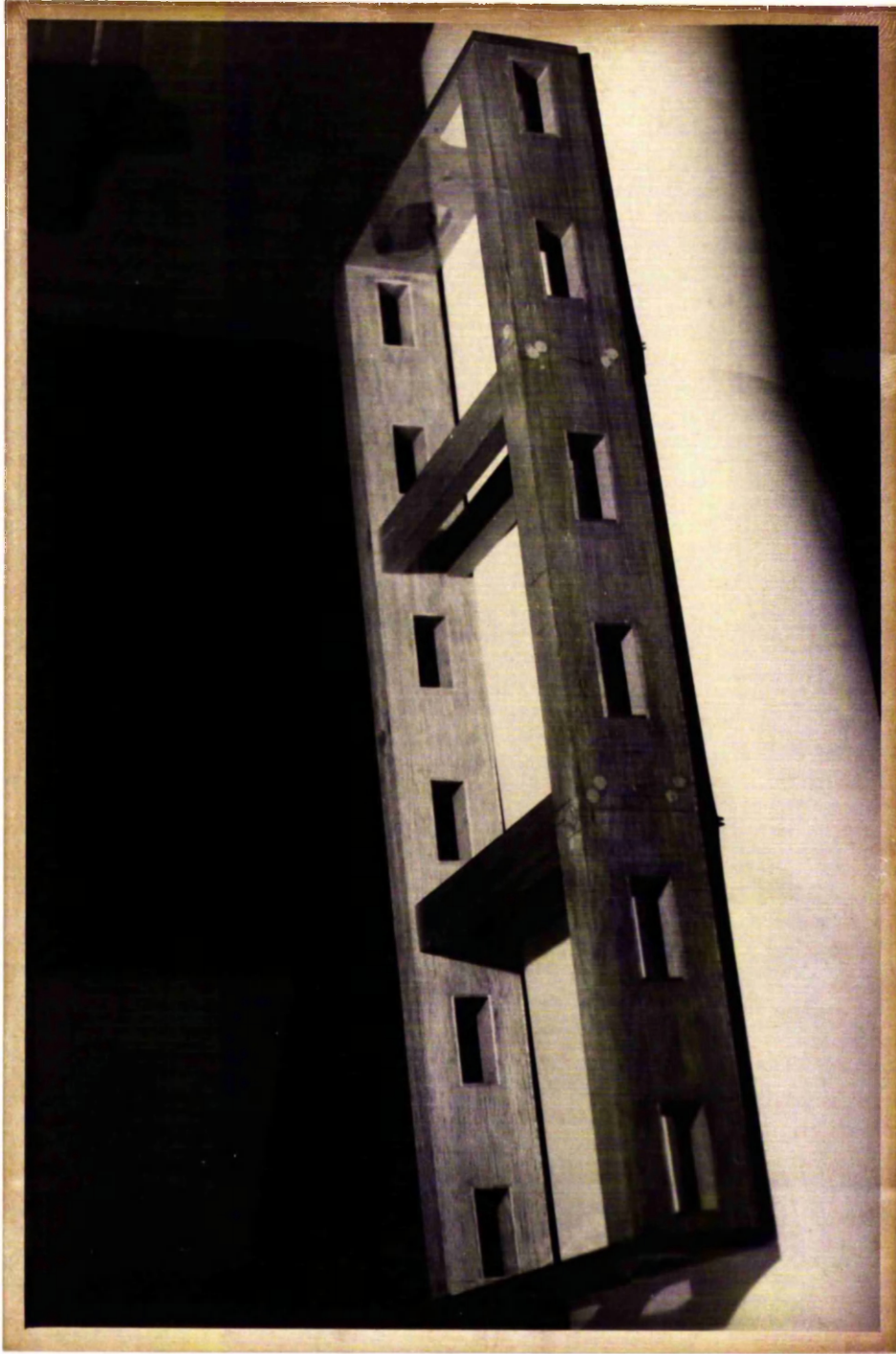
Dynamic Mountings.

The investigation into the dynamic behaviour of the section models was carried out using special mountings designed for the tests. The two mountings were bolted to the outside of the tunnel working section, and the model connected via the stub axles through holes in the windows, Fig. 12. The model could oscillate in two degrees of freedom, vertical translation, and pitch, and viscous damping could be applied if required. The stub axles run in self-aligning ball-races carried in the vertical main links. Horizontal radius arms constrain the main links, to allow vertical translation only, and are connected to the side plates through flat spring flexures to allow relative movement of the parts. Sideways restraint is provided by the double lower radius arm, the upper one being single.

A coil spring between the vertical link and the side plate gives the necessary vertical stiffness. Quick release fittings allow the spring to be easily changed to vary the stiffness. The spring can be tensioned to take out any backlash if the amplitude of oscillation becomes large.

The outer end of the stub axle is tapered, on which the torsion link is keyed and securely held. The horizontal arms from the hub of the link carry the fittings for the two coil springs which provide the torsional sitffness. Similar arms from the top of the vertical link carry the fittings for the other ends of the springs. The torsion link is thus elastically constrained to the vertical link, and the stiffness altered by varying the radius of the spring fittings from the hub. A small screw through the hub to the vertical link locks the torsion link in place to isolate the vertical translation mode of the system. A small plate locks the top of the vertical link to the side plate if only the torsion mode is required. The lower end of the torsion link has two horizontal rods to which balance weights are attached. The mass

ELECTRO-MAGNETS
ALLOY PLATE
SIDE PLATE
VERTICAL COIL SPRING
MAIN LINK
RADIUS ARMS
FLAT SPRING
CAPACITANCE TRANSDUCER
TORSION LINK
TORSION SPRINGS
HORIZONTAL ARMS
BALANCE WEIGHTS

DYNAMIC MOUNTINGS

FIGURE 12
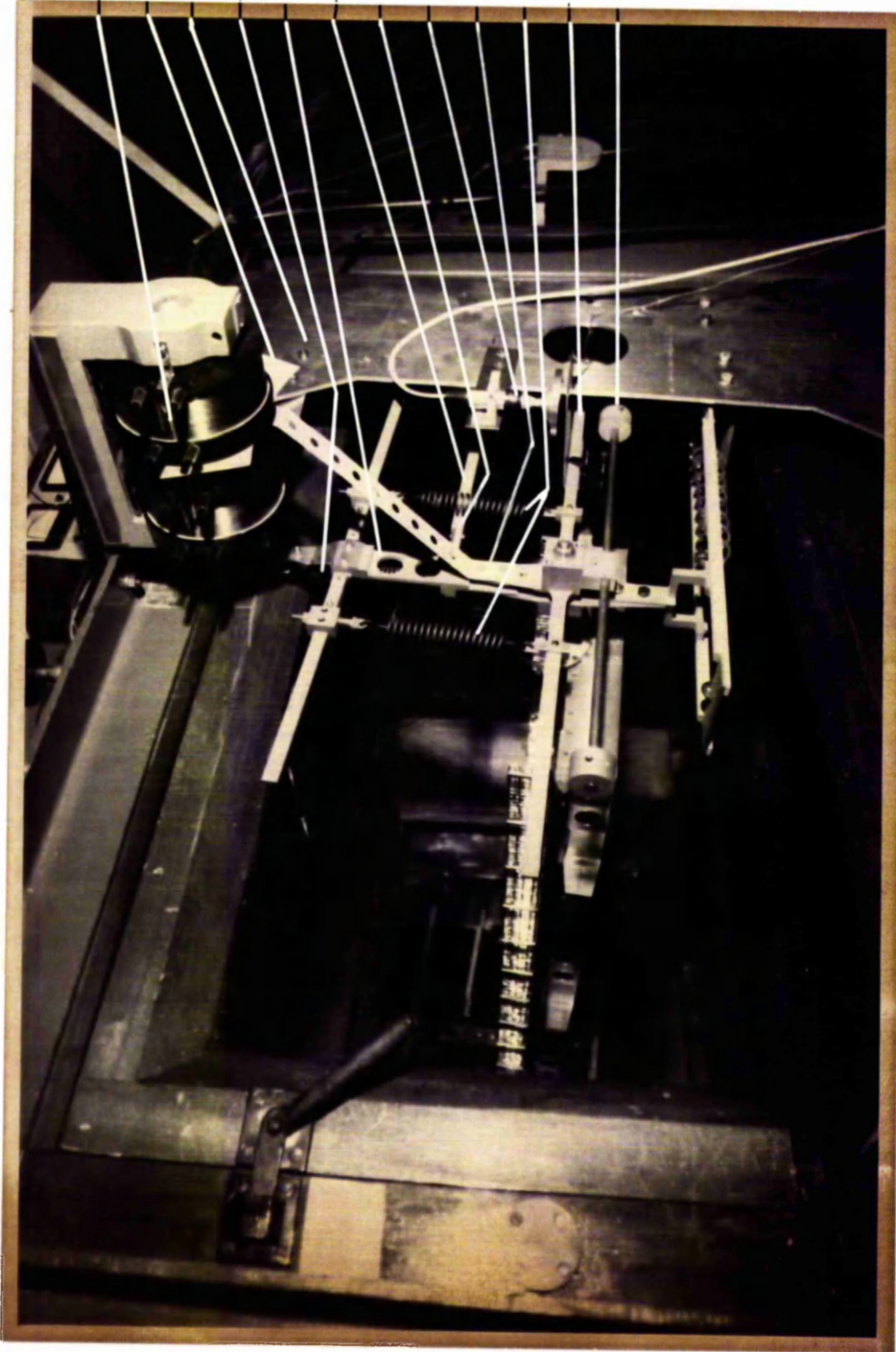
can be varied to give the required effective mass, and the radius arm varied to give the required mass moment of inertia.

Viscous damping is provided by eddy currents induced in thin aluminium alloy plates passing between the poles of powerful electromagnets. The magnets are bolted to the wind-tunnel structure, and the alloy plates are attached to the hub of the torsion link by a cantilever arrangement. The required level of damping is obtained by varying the current supplied to the coils of the electromagnet.

The spring and link arrangement allows translation in the direction normal to the model, i.e. vertical translation with respect to the model, and rotation about the axis of twist of the model. The position of the axis of twist can be altered on the deck model by changing the stub axle. The complete dynamic mounting can be moved to give an incidence range of -15° to $+15^\circ$ referred to the tunnel centre-line.

VIBRATION CALCULATIONS.

The calculations to determine the structural vibration modes and frequencies were carried out by the Civil Engineering Department. The structural stiffness matrix was calculated for the bridge as made up of plane frames, resulting in the only degree of freedom being vertical translation.

By using the "Second Law of Motion" and the stiffness and mass matrices, the equation to be solved, using matrix notation is

$$\left[\lambda I - k^{-1}m\right]\left[d\right] = 0$$

where I = unit matrix

λ = $1/w^2$ where w is angular velocity in radians/sec.

k = structural stiffness

m = mass matrix

d = displacement of node points, i.e. mode shape.

Solving the matrix equation for the latent roots and vectors gives the frequencies and mode shapes for each of the vibration modes.

The mass of the deck was 6,600 kg/m. and that of the arch was 2,815 kg/m up to 0.29 of half span, 3,325 kg./m from 0.29 to 0.72 of half span, and 2,635 kg./m, from 0.72 to mid span.

The bridge is symmetrical about the centre-line, (Fig. 13) so the calculation can be reduced in size by using half the mass and stiffness matrices.

The stiffnesses of the structural elements were defined in kN.m units.

If the weight is measured in Newtons, then

$$1N = 1kg \times 1m/sec.^2$$
$$\simeq \frac{1}{10} kg \times g \quad \text{where } g = 9.81 \text{ m/sec}^2$$
$$1kN \simeq 100 kg \times g.$$
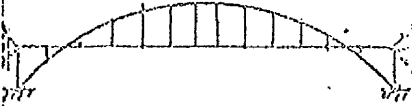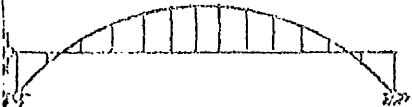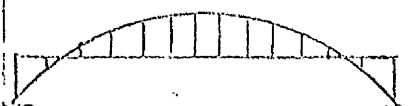
Using kN as the force unit makes the equivalent mass unit 10^3 kg, so the latent roots have to be scaled by 10^{-3}.

In Fig. 13, the Case 2 weights were the final ones, and the first mode frequency used was 0.444 Hz.

Since the arch rib is built in a parabolic arc the first vertical bending mode must be asymmetric about the centre-line, as is demonstrated by the mode shapes in Fig. 14 for the arch rib. The first bending mode of the deck is symmetrical about the centre-line, so the influence of the arch would be to reduce any forced vibration giving symmetrical bending in the deck.

The bridge arch diagram with node numbering (2–28), panel dimensions, height 22.2 and 15.1, total span 183.
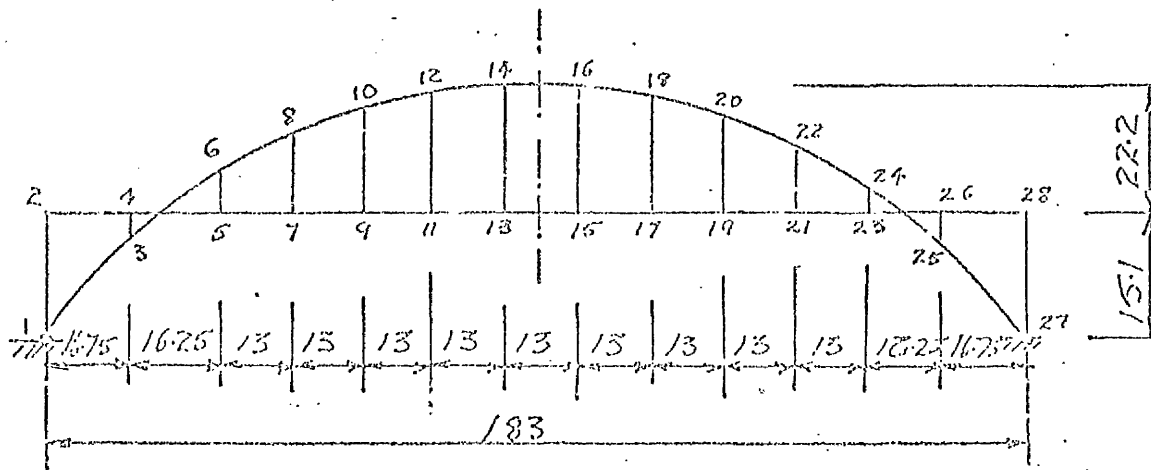
SUPPORT CONDITION	WEIGHTS : CASE 1.			WEIGHTS : CASE 2.		
	ω (rad/sec)	f (Hertz)	p (Secs)	ω (rad/sec)	f (Hertz)	p (Secs)
50 x 50 Matrix	6.279	0.999	1.000	2.791	0.444	2.252
	10.409	1.657	0.603	5.768	0.918	1.089
	15.625	2.487	0.402	10.286	1.637	0.6108
51 x 51 Matrix	5.62	0.89	1.12	2.78	0.44	2.26
	9.46	1.51	0.66	5.75	0.92	1.09
	13.62	2.17	0.46	10.24	1.63	0.61
52 x 52 Matrix	2.54	0.40	2.48	1.84	0.29	3.41
	9.17	1.46	0.69	3.31	0.53	1.90
	9.51	1.51	0.6	5.76	0.92	1.09

BRIDGE DATA

FIGURE 13

50 DEGREES OF FREEDOM
MODE 1. G.U. ○ ω = 2·791
MODE 1. B.A.C. × ω = 2·8

(G.U.)

(B.A.C.)
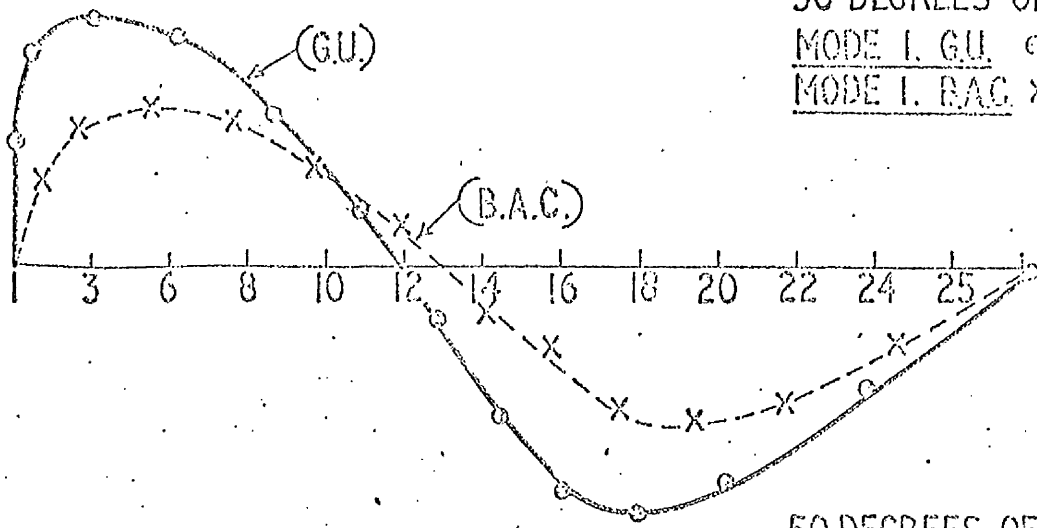
(a)

50 DEGREES OF FREEDOM
MODE 2. G.U. ○ ω = 5·768
MODE 2. B.A.C. × ω = 5·8

(G.U.)

(B.A.C.)
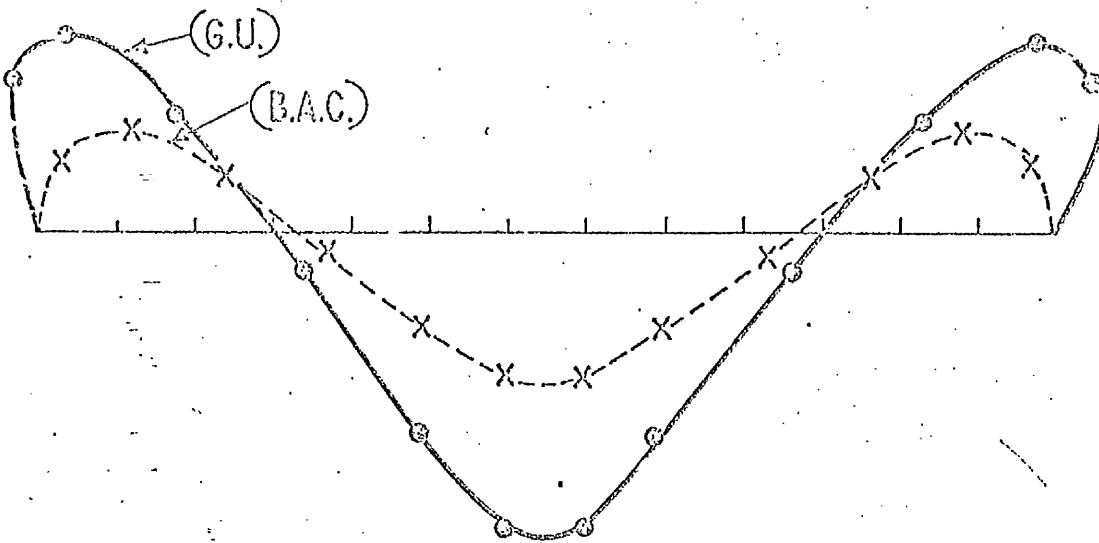
(b)

50 DEGREES OF FREEDOM
MODE 3. G.U. ω = 10·286
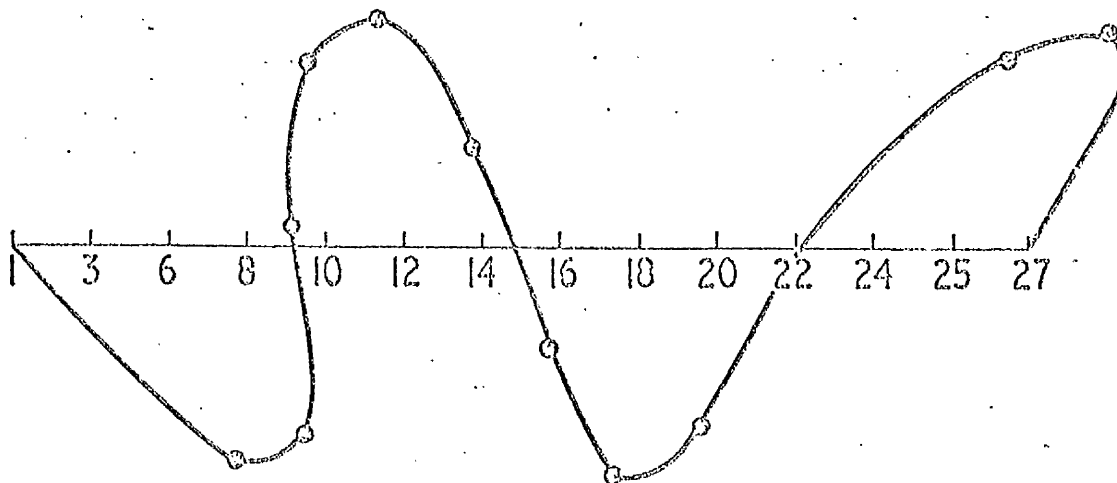
(c)

VIBRATION MODES FOR ARCH RIB

FIGURE 14

TESTING PROCEDURE.

Models of sections of the deck and arch rib, were used to predict
the static aerodynamic loads and the dynamic characteristics of the full
size structure.   This procedure of using section models accords with
standard practice, based on results from wind tunnel tests of both
complete and section models of the Tacoma Narrows Bridge (Reference 1)
the Severn Road Bridge (Reference 10) and others.   The deck and arch
rib models were tested separately.   It was considered that the results
obtained from the tests of the individual units would give a reasonable
indication of the structure as a whole.   In the vibration analysis,
the first bending mode of the deck was symmetrical bending, whereas
the first arch rib mode was asymmetrical bending.   Thus, the influence
of one on the other was deemed to be beneficial in reducing amplitudes.

On the full size structure, the aerodynamic interference effects
between the arch rib and the deck would help to reduce any displacements.
Where the elements are closest, the arch rib is at a steep angle to the
deck, and so any relative motions will be out of phase with one another.
This region will also give rise to very turbulent air flow, reducing
the possibility of regular airforces developing.

The conclusions reached were that the majority of the aerodynamic
forcing in the dynamic cases would come from the central $\frac{2}{3}$ of the bridge,
away from the arch rib-deck cross-over.   Also, since the dynamic
effects were more important, any small errors in the static aerodynamic
coefficients as a result of ignoring the aerodynamic interference
effects between the arch rib and the deck were allowable.   The tests
would also be much simpler, and their number greatly reduced.

Static Tests.

Each model was mounted in turn on the wind tunnel three component
balance for the measurement of the static forces components, and the
pitching moment.   The test data obtained were reduced and then

processed using a simple computer programme (Table 1) to obtain the horizontal and normal force coefficients (C_H, C_N) and the moment coefficients (C_M) for various wind speeds and inclinations to the horizontal. These tests were done in smooth airflow, with the turbulence levels less than 0.1%.

The procedure was repeated for the variety of deck and arch rib configurations as follows:-

Static Test Configurations.

Deck Model.

Test 1: Deck alone.

Test 2: Deck with railings.

Test 3: Deck with railings with a nylon mesh fitted to the inboard face of each set of railings.

Test 4: Deck and railings. The model was modified by cutting 6 holes, 25.4 mm diameter at 50.8 mm pitch in the webs of the two span-wise girders, between adjacent support pads. (Figs. 8, 10). The ratio of cutaway area to the frontal area of the deck (less railings and mesh) between adjacent support pads was 0.125.

Test 5: As for Test 4, with nylon net replaced by a rectangular mesh of soldered tinned copper wire (0.56 mm diameter, 1.58 per cm) fitted to the inboard face of each set of railings.

Test 6: As for Test 4, with trapezoidal section fairings added to the outboard vertical faces at the parapets.

Test 7: As for Test 5, with the addition of the parapet fairings (Fig. 8). This represented the final deck configuration with all the accepted modifications incorporated.

Two other tests were carried out with the following modifications to the final configuration.

```
EGTRAN COMPILER         MARK NO. 302        DATE    16/11/71        TIME    15.21.15
C     TO FIND THE HORZ. FORCE COEFF,NORMAL FORCE COEFF.,AND
C     MOMENT COEFF. OF BALLACHULISH BRIDGE
      REAL L,MC,MO
      DIMENSION H(20),RN(20),CH(20),CN(20),CMO(20),R(20),LALPHA(20)
      I=0
      PI=.3141593E1
      READ 1,M
6     READ 1,N
      DO 2 K=1,N
      READ 1,LALPHA(K),L,D,MC,DELTAP                                    MA101700
1     FORMAT(80Z)
100   ALPHA=LALPHA(K)*(PI/180.0)
      QH=5.20*1.208*DELTAP                                              MA101500
      DELTAO=0.0962*D                                                   MA101600
      QC=QH*DELTAO                                                      MA101700
      H(K)=D*COS(ALPHA)+L*SIN(ALPHA)                                    MA101800
      RN(K)=L*COS(ALPHA)-D*SIN(ALPHA)                                   MA101900
      MO=MC+3.125*RN(K)-2.250*H(K)                                      MA102000
      V=0.305*0.00119*SQRT(QC)                                          MA102100
      R(K)=((0.06*V)/1.48)*10.0E4                                       MA102200
      CH(K)=H(K)/(0.733*QC)                                            MA102300
      CN(K)=RN(K)/(4.6*QC)
      CMO(K)=MO/(4.6*14.8*QC)
2     CONTINUE
      PRINT 4                                                           MA102600
4     FORMAT(23H1   IAIN LINN   AERO ENG//6H ALPHA,10X,13H REYNOLDS NO,,MA102800
     C10X,19H HORZ. FORCE COEFF.,10X,20H NORMAL FORCE COEFF.,10X,       MA102801
     C14H MOMENT COEFF.,//)                                             MA102802
      DO 7 K=1,N                                                        MA102900
7     PRINT 5,LALPHA(K),R(K),CH(K),CN(K),CMO(K)                         MA102801
5     FORMAT(I3,3X,F10.6,3(10X,F8.4))                                   MA103000
      PRINT 8                                                           MA103001
8     FORMAT(80X,18H VALUE OF H AND RN//)                               MA103002
      DO 9 K=1,N                                                        MA103003
9     PRINT 10,H(K),RN(K)                                               MA103004
10    FORMAT(82X,2(F8.4,4X))                                            MA103005
      I=I+1                                                             MA102501
      IF(I.NE.M)GO TO 6                                                 MA103100
      CALL EXIT                                                         MA103100
      END                                                               MA103200
```

REFERENCE TABLES

| 0 | 00000/0 | 6 | 00005/5 | 1 | 00024/0 | 2 | 00073/3 | 4 | 00077/4 |
| 3 | 00100/4 | 5 | 00122/1 | 8 | 00123/4 | 9 | 00124/4 | 10 | 00136/1 |

```
      ROUTINE COMPILED
      TIME  LESS THAN 5 SECS
      NUMBER OF INSTRUCTION WORDS 99
      * * * * * * * * * * * * * * * *


NUMBER OF INSTRUCTION WORDS 0099


EXTERNAL ROUTINES REQU.
         WONT30   WONT31   WONT32   DONT83   COS   SIN   SQRT   WONT40   WONT42
   WONT41   DONT05   EXIT
*DATA
JOB ORGANISED  15.21.21        16/11/71
```

PROGRAMME TO DETERMINE FORCE AND MOMENT COEFFICIENTS

TABLE 1

Firstly, instead of the tinned copper mesh, a woven brass mesh (0.51 mm. diameter, 3.94 per cm) was used.

Secondly, a test was run with the configuration as for Test 7, except that the holes in the girder webs were blanked off.

The first was to check the effect of a mesh giving increased blockage, such as may occur with the standard mesh blocked by ice or snow.

The effect of the parapet fairings and tinned copper mesh alone had not been investigated; thus the need for the second test.

Arch Rib.

Only two static tests were required in this case, the first with the model in the basic shape. After the initial dynamic tests, the model was modified by cutting transverse rectangular holes through both the beams. (Fig. 11). Two holes were cut through each beam between each pair of transverse members, giving a ratio of cutaway area to frontal area per "bay" of 0.132.

The final arrangement decided by the consultants was of four elliptical cut-outs at the quarter, and three-quarter points. This was to make the stress analysis easier, and was more pleasing visually, but this arrangement was never tested.

Dynamic Tests.

Each model was mounted in turn on the dynamic test rig, on which three modes of motion were possible. These were as follows:-

1. The model could be allowed to translate vertically.

2. The model could be allowed to rotate in pitch about its mounting spindles, which were located in the plane of symmetry of each model section.

3. It could be made free to translate vertically, and rotate in pitch simultaneously.

The facility for independent testing of each mode of vibration is essential for model testing, as some of the dynamic effects are due to coupling between translation and pitch. Isolating each mode, and determining its effect on the two degree of freedom motion is necessary in order to understand the aerodynamic mechanism causing the excitation, and effect a cure. Two degrees of freedom are sufficient for suspension bridges, as their length makes a small section approximate an idealized body with infinite aspect ratio, and any disturbing force will cause motion either vertically or in pitch. Horizontal motion is ignored in the case of dynamic stability, although it is essential for the lateral buckling stability of the structure (Reference 19).

The other variable parameters used in the tests were as follows:-

1. Wind Speed, from 0 to 30 m/sec.

2. Wind Inclination, up to $\pm 10^{\circ}$ to the horizontal.

3. Viscous Damping. This was produced by applying currents in the range 0-0.5 amperes to the coils of the two electromagnets, inducing eddy currents in the damping plates (Fig. 12). The measure of the damping applied was assessed by ascertaining the logarithmic decrement of the appropriate damped oscillation at zero wind speed, and comparing it with the value obtained when no eddy current was applied. The logarithmic decrement, δ , is a measure of the amplitude decay rate of an oscillating system after an initial displacement, and is the logarithm of the amplitude ratio of two successive cycles. When the damping factor is small, less than 0.1, the amplitude ratio can be measured over non-successive cycles, and the result divided by the number of cycles, as was the case with these tests.

4. Spring Stiffness. Different springs could be substituted to investigate the effect of different values of stiffness. The torsion arm for the torsion springs could also be altered (Fig. 12).

5. Mass and Inertia.   This could be varied by means of balance weights on the horizontal rods at the lower end of the torsion link. (Fig.12).

6. The Axis of Rotation.   On the deck model this could be changed by altering the vertical position of the mounting spindles.   Most of the tests were done with the spindles coincident with the underside of the road slab (Fig. 15).   Check tests were run with the spindles in two other locations, nominally 25 mm above and below the original setting.   This was to cover the effect of the hangers on the centre of rotation of the prototype.   For the deck alone, this was in the basic location, but it was thought that the hanger stiffness would alter this to some extent.

7. Degree of turbulence.   This could be varied by placing a grid of steel rods upstream of the model.   The spacing of the rods was constant, and no attempt was made to simulate the velocity profile of the atmosphere.

Instrumentation.

An ultraviolet paper trace recording galvanometer was used throughout the tests to record the oscillatory motion of the model. An inductance type displacement transducer and an accelerometer, used initially, were replaced by a Wayne Kerr capacitance probe.   This was mounted on the frame of the rig, and measured the capacitance between the probe and the adjacent face of an aluminium plate located at a convenient point on the spring-mounted part of the rig.   (Fig. 12). This was on the torsion link, at a radius of 193 mm from the axis of rotation of the model.   The signal from the probe was amplified to give about 10x gain to the trace on the recorder chart.   Only one probe was used, as the basic requirements were frequency and amplitude measurements.   Phase differences between vertical and pitch motions in the coupled mode were not investigated at the beginning of the tests, and as the tests proceeded, it was found that the basic high speed
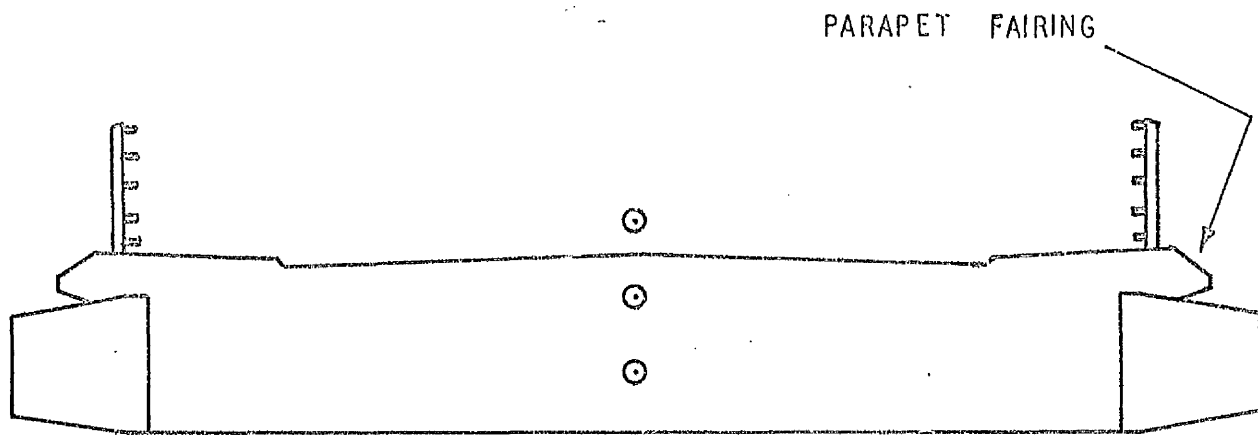
PARAPET FAIRING

⊙ PIVOT CENTRES

SECTION ACROSS DECK SHOWING PIVOT POSITIONS

FIGURE 15

instability was one of pitch, with very little translation. No asymmetric motion, such as roll, was encountered, and thus the simple installation of one capacitance probe was sufficient for all tests.

Only the deck exhibited the pitch instability, but both the deck and the arch rib had the vertical oscillation caused by the shedding of Karman vortices.

Test Method.

The appropriate model with its particular configuration was mounted in the tunnel working section on the test rig. (Fig. 10). Eleven deck and three arch rib configurations were tested. A "wind-off" amplitude calibration was carried out, using a dial test gauge to determine the relationship between model displacement and recorder paper trace displacement. The model position was varied manually by known increments, and the corresponding chart recordings taken. The linearity of the capacitance probe and recorder system was proved, and a scale factor obtained for the working range of the tests. The maximum model deflection used was about 5 mm, and the scale factor was about 11:1.

Chart recordings were made of the damped oscillation occurring when the model was released after manual displacement, for "wind-off" and for "wind-on" conditions. Using mechanical stops, this initial displacement was kept constant at 5 mm. The chart recordings were done for various steady wind speeds, eddy current damping values and model incidences, and the final steady state oscillation was also recorded. (Fig. 16).

Particular attention was given to model behaviour in the region of a critical wind speed where the logarithmic decrement showed a marked decrease, and the steady state amplitude a marked increase. (Fig. 17). For the low-speed "bounce", a forced vibration caused by Karman vortex shedding, very fine speed increments were necessary to determine the

$$\delta = \left[\frac{1}{30} \ln \frac{6 \cdot 60}{1 \cdot 19} \right]$$

$$= \frac{1}{30} \left[\frac{1 \cdot 887}{-474} \right] = \frac{1 \cdot 887 - 474}{1 \cdot 713} = \cdot 0571$$

0.83 c/s

PAUSE IN RECORD

TIME
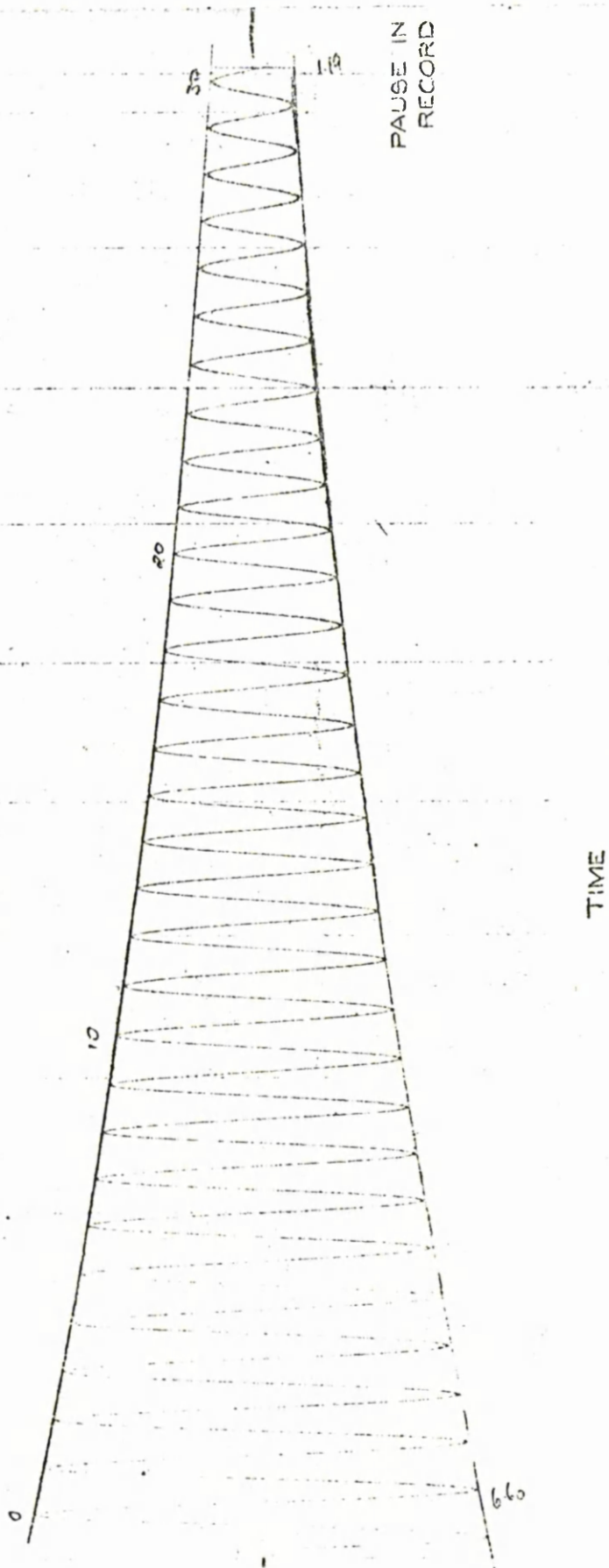
Facsimile of oscillograph record of test on deck model with holes in webs of main beams but otherwise in original configuration.

Vertical translation and rotation. $\alpha = 0$. $\quad \varepsilon_{z\theta_o} = 0.044$.

Tunnel speed   1.0m/sec.   Equivalent wind speed 5.0 m/sec.

FIGURE 16

DAMPED OSCILLATION
$\delta = .009$

SUSTAINED OSCILLATION.

$\beta = 2.86 \text{ Hz}$

PAUSE IN RECORD.

TIME
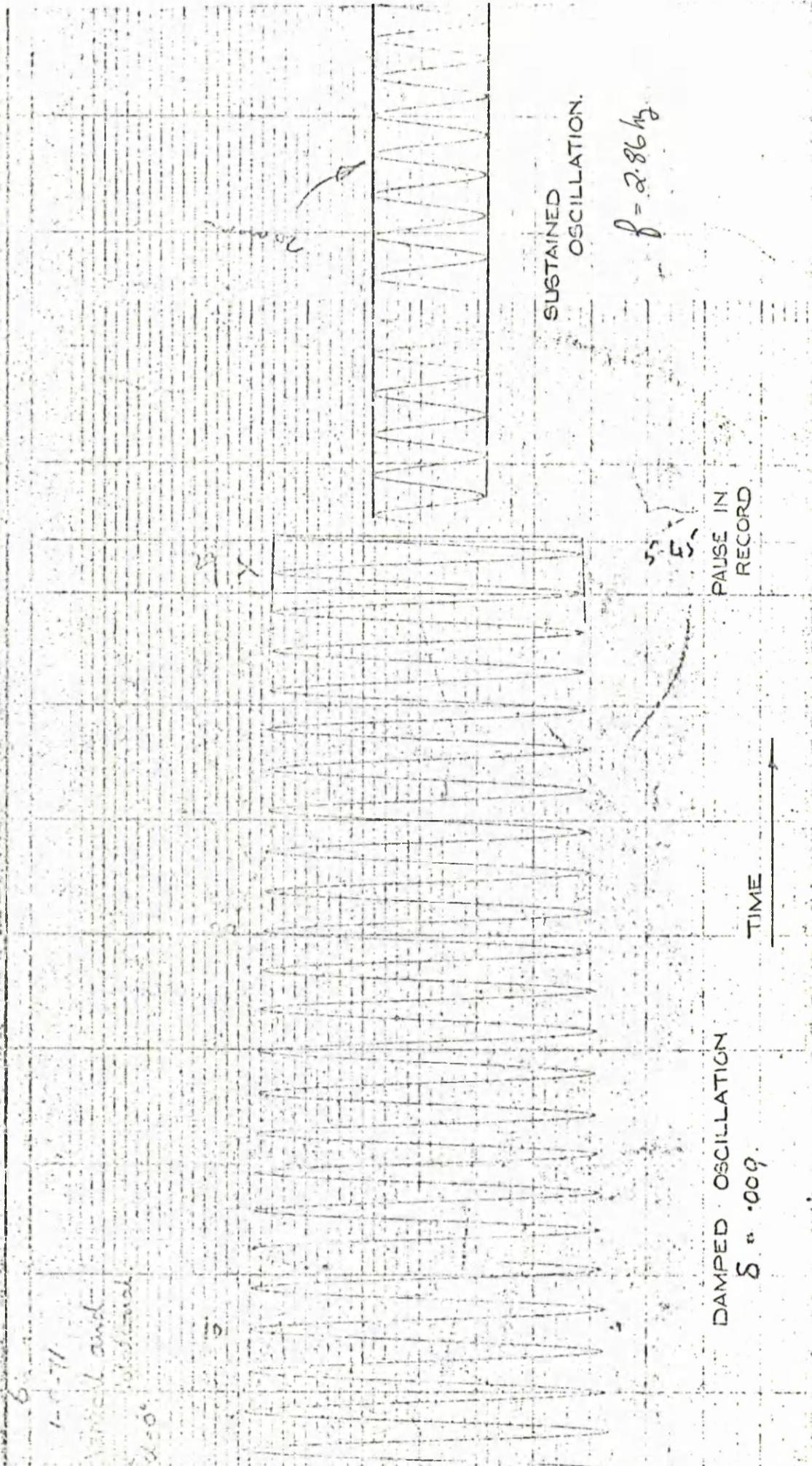
Facsimile of oscillograph record of test on deck model in original configuration with nylon gauze.

Vertical translation and rotation. $\alpha = 0.$ $S_{z\theta_0} = 0.033$

Tunnel speed   1.7m/sec.   Equivalent wind speed 8.4 m/sec.

FIGURE 17

resonance peak.   As this was a non-catastrophic oscillation, no damage
was done to the model.   The high speed instability was a divergent
oscillation, and catastrophic, starting over a very small velocity
increment, and care was needed to safeguard the model.   A position of
neutral stability could be achieved by very fine adjustment of the
speed, and this point was used as the factor defining the critical
speed.

Each chart recording then yielded the steady state amplitude, the
frequency of oscillation, and the logarithmic decrement associated with
that particular wind speed.

AERODYNAMIC THEORIES.

Until the investigation into the collapse of the Tacoma Narrows
Bridge, only two theories were in use to explain the instability of
suspension bridges. The first assumed that the nature of the surround-
ing terrain caused turbulence in the wind which excited the motion. The
second was inspired by the similarity between bridge motion and that of
long transmission wires under the action of the wind.

Buffet.

It was thought that a turbulent wind might act on the structure
in such a way as to give rise to a period variation in lift force.
This periodic force would be nearly coincident with the natural frequency
of the structure, and would result in the building up of a mode of motion
corresponding to that frequency. It is possible that a gusty wind
would have the required characteristics, but it is highly unlikely.
The only record of wind turbulence affecting a bridge was at the Golden
Gate Bridge in 1951 (Reference 9) where a hill to the north-west caused
the wind from there to blow down on the bridge and reduce the amplitude
of motion. During this storm, the bridge had an edge amplitude of ± 2
metres in the torsion mode, but the greater amplitude in symmetrical
bending which was later predicted, was absent due to the deflected wind.
A suspension bridge will probably never be so close to catastrophic
failure due to flutter and survive. Later, the bridge was stiffened
across the bottom of the trusses, and no further vibration problems
have occurred.

The failures of the Menai Straits Bridge and the Brighton Chain
Pier were thought to be caused by the wind being deflected to strike
the underside of the roadway, thus lifting the structure and destroying
it. A study of the accounts now reveals that the wind caused a tor-
sional oscillation, due either to vortex shedding, or flutter, which led

to failure in the structures.   (References 2, 5).

A case in which turbulence from other objects can cause problems
is where one bridge is in the wake of another.   At certain wind speeds
and directions, the upwind bridge will shed regular vortices, i.e.
Karman vortex streets, which will cause forced vibrations of the down-
wind bridge.   Once the vortex shedding frequency of one bridge is
known, the other, if it is a new structure, can have its frequency
response altered, or situated where its influence is least.

Two cases where this could have occurred, if not for wind tunnel
tests, were the proposed Runcorn-Widnes suspension bridge, and the
Tamar suspension bridge.

The Runcorn-Widnes bridge was to be built very close to an existing
railway bridge.   Section model wind tunnel tests showed that the pro-
jected bridge oscillated severely in the vortex field of the bluff
railway bridge, which was level with the suspension bridge deck.   The
problem would have been solved by stiffening the suspended structure,
and siting it very close to the original bridge, but by this time an
arched design had been adopted.   (Reference 20).

The Tamar bridge at Plymouth was in a similar situation, forced
by circumstances to be close to an existing bridge.   The design was
basically a $\frac{1}{2}$ scale model of the Forth Road bridge, and so was aero-
dynamically stable.   Model tests showed that vertical oscillations were
produced by the proximity of the other bridge, and the presence of a
train on the other bridge increased them.   The critical wind speed
was over a very limited range at 22 m/sec., and was not thought to be
a problem, and the deck was 5.4 m above the existing bridge.   No
problems have been reported in use.   (Reference 21).

Autorotation.

The second theory was commonly known as "autorotation", and was proposed by Den Hartog as an explanation for galloping transmission lines (Reference 22). When coated with ice, the lines had been observed to oscillate with large amplitudes in the wind. In Picture 18 of Reference 22, the section motion is assumed positive downwards, and the angle, α, of the resultant wind is $\tan^{-1} v/V$.

The total vertical force developed by the wind is

$$F = L \cos \alpha + D \sin \alpha .$$

As the bridge moves vertical with variable velocity v, the resultant force, F, varies with angle α, so

$$\frac{dF}{d\alpha} = \frac{d}{d\alpha} (L \cos \alpha + D \sin \alpha)$$

$$= \frac{dL}{d\alpha} \cos \alpha - L \sin \alpha + \frac{dD}{d\alpha} \sin \alpha + D \cos \alpha$$

$$= \sin \alpha \left[\frac{dD}{d\alpha} - L \right] + \cos \alpha \left[\frac{dL}{d\alpha} + D \right]$$

Since v is small with respect to V, $\tan^{-1} v/V$ is very small

$$\frac{dF}{d\alpha} = \frac{dL}{d\alpha} + D$$

If $dF/d\alpha$ is negative, the increasing force for decreasing α produces a divergent oscillation by putting energy into the system. When $dF/d\alpha$ is positive, the resulting force opposes motion, and energy is absorbed. Thus the bridge is unstable when

$$\frac{dL}{d\alpha} + D < 0$$

The static aerodynamic forces are usually plotted as non-dimensional coefficients, so

$$\frac{dC_L}{d\alpha} + C_D < 0$$

Thus the bridge will be aerodynamically unstable if the negative slope of the lift curve is greater than the accompanying drag coefficient.

Similarly for the pitching moment curve, where $dC_m/d\alpha$ is negative, it will give rise to a moment which increases v, and the input of energy to the system; on the other hand, positive $dC_m/d\alpha$ will give a stabilising moment. (Fig. 18).

Iced up transmission wires have an irregular shape, and once a small gust causes motion to start, it can build up an oscillation under the above conditions. In "galloping", the wires can move up to 50-60 diameters at a steady speed across the direction of the wind, and so it is possible to explain the motion using static coefficients. For a bridge, the amplitude of the movement is small compared to its size, and unsteady aerodynamic derivatives are needed to explain the motion.

It can be seen from the graphs of the static coefficients (Figs. 21-29) that the slope of the lift and moment coefficients versus angle, α, are positive in nearly every case over the working range, and yet the bridge deck always oscillated in pitch at some speed. Other investigations have also shown this to be the case, notably the original Tacoma Narrows Bridge, with the H-section unstable in pitch, but which has positive slopes for the static force coefficients. (Reference 1).

Thus, it can be seen from the above that the "autorotation" theory cannot be used to explain bridge motion although it has relevance for iced up transmission lines.

Vortex Excitation.

Oscillations of bluff bodies in wind are commonly excited by vortices formed at the sides of the body, and shed alternately into the wake. This is the mechanism behind the Aeolian harp. If the frequency of vortex shedding coincides with a natural frequency of the body, oscillations transverse to the wind direction may occur. The frequency of vortex shedding depends on the wind speed, cross-section shape, and

L

D

V''

V

$\propto \quad \tan^{-1}\left(\dfrac{V''}{V}\right)$

RESULTANT
WIND, V_R

MOTION

V''

M

V

V_R
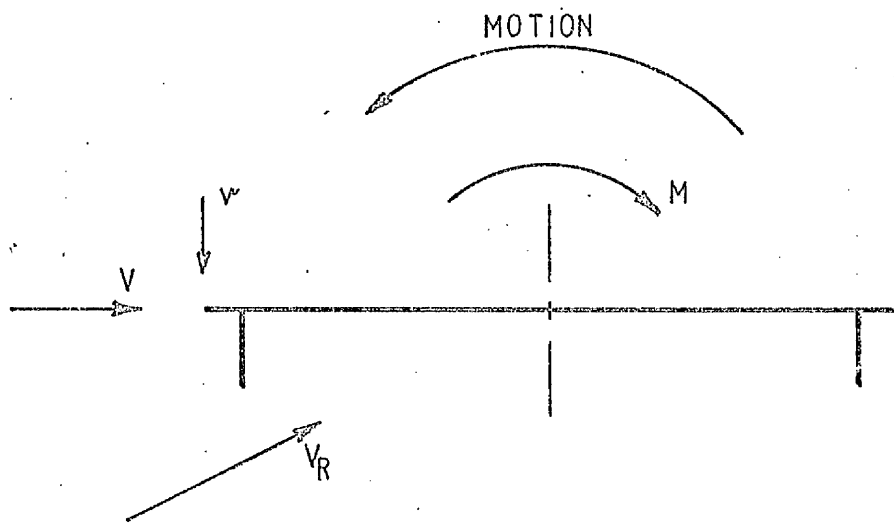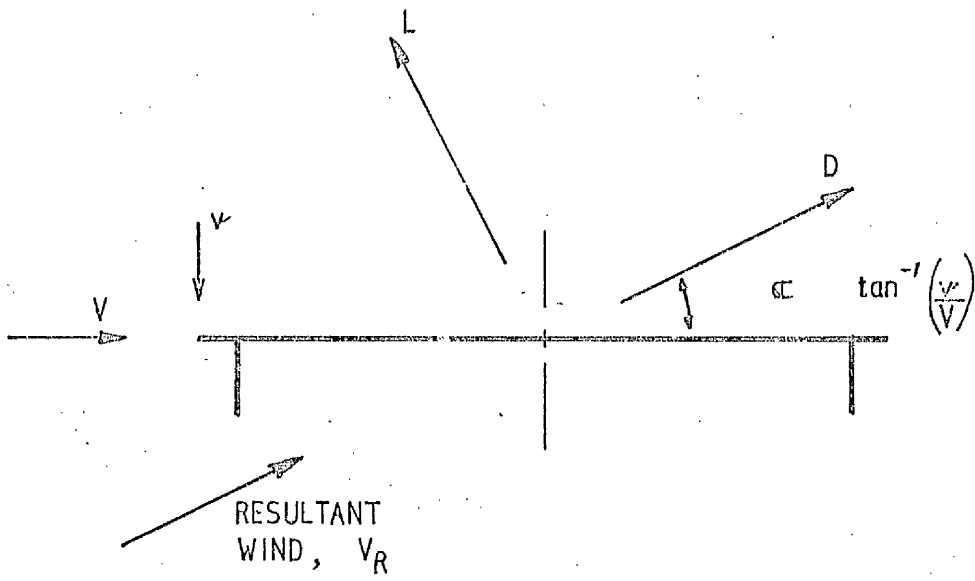
AUTOROTATION

FIGURE 18

Reynolds Number, and is defined by the non-dimensional Strouhal number

$$S = \frac{nl}{v}$$

where n is the frequency of shedding vortex pairs, l is a typical length, and v the wind speed.

For cross-sections with sharp edges, S is independent of Reynolds number, as the positions of flow separation are fixed at the corners. For cylinders and other rounded sections, the separation position, and so S, varies with Reynolds number. Bridges in general are sharp edged bodies, and so the Strouhal number is independent of Reynolds number, and model test results can be applied to the full-size prototype with a good degree of confidence. Girder type bridges exhibit this type of forced oscillation more than the truss type, as they tend to have a larger solidity factor. The air-flow through a truss structure is more turbulent, with consequently less chance of regular vortex shedding. A solution for girder bridges follows, so that by making holes in the webs of the girders, transverse oscillations can be greatly reduced. The vibration is restricted within a certain wind velocity range, and has a maximum amplitude. Although it is non-catastrophic, it could eventually cause fatigue failure in structural members, and is noticeable and unpleasant to the public.

Assuming that the forced vibration is caused by a Karman vortex street, it is possible to calculate the lift coefficient, C_L, at resonance. The equation of motion for a one degree of freedom system in the airflow is

$$my'' + fy' + ky = F = \tfrac{1}{2}\rho \, v^2 hl C_L e^{iwt}$$

Critical damping, $f_{CR} = 2mw_0 = 2\sqrt{km}$

$$\gamma = f/f_{CR}, \qquad w_0^2 = \frac{k}{m}$$

where

m = mass

f = damping constant

k = spring constant

w_o = natural frequency

w = frequency of forced vibration

ρ = density of air

v = wind velocity

h = projected section height

l = length

C_L = lift coefficient

From vibration theory, the amplitude, Y_R, of a forced vibration is

$$Y_R = \frac{F/k}{\sqrt{\left(1 - \frac{w}{w_o}\right)^2 + \left(2\frac{f}{f_{CR}} \cdot \frac{w}{w_o}\right)^2}}$$

At resonance, $w/w_o = 1$

$$Y_R = \frac{F/k}{2\ f/f_{CR}}$$

$$= \frac{F}{2k} \cdot \frac{2mw_o}{f}$$

$$= \frac{F}{fw_o}$$

$$= \frac{F}{mbw_o} \qquad \text{where } b = \frac{f}{m}$$

$$= \frac{F}{2m\gamma\, w_o{}^2}$$

$$= \frac{\tfrac{1}{2}\rho v^2 hl C_L}{2m\gamma\, w_o{}^2}$$

Taking Strouhal number, $S = \dfrac{w_o h}{2\pi v}$

$$w_o = \frac{2\pi S v}{h}$$

$$C_L = \frac{2m\gamma\, w_o{}^2 Y_R}{\tfrac{1}{2}\rho\, v^2 hl}$$

$$= \frac{2m\gamma \cdot 4\pi^2 S^2 v^2 Y_R}{\frac{1}{2}\rho v^2 hl \cdot h^2}$$

$$= \frac{16m\gamma \pi^2 S^2 Y_R}{\rho h^2 l \quad h}$$

$$= 16\pi^2 \mu \, S^2 \gamma \frac{Y_R}{h} \qquad \text{where } \mu = \text{mass ratio}$$

$$= \frac{m}{\rho h^2 l}$$

Damping Relationships (Reference 23)

$$\delta \cong 2\pi\gamma \qquad \text{where} \qquad \gamma \ll 1$$

$$\cong \pi g \qquad\qquad\qquad g \ll 1$$

$$\text{and } g = \frac{\delta}{\pi} \qquad \text{where } \delta \text{ is the logarithmic decrement}$$

Using data from Fig. 17, and the other deck model parameters, in the above equations

$$C_L = 16\pi^2 \mu \, S^2 \gamma \frac{Y_R}{h} \qquad\qquad m = 13.3 \text{ kg}$$

$$= 16\pi^2 \frac{m}{\rho h^2 l} \cdot \frac{w_0^2 h^2}{4\pi^2 v^2} \cdot \frac{\delta}{2\pi} \cdot \frac{Y_R}{h} \qquad w_0 = 18 \text{ r/s}$$

$$\qquad\qquad\qquad\qquad\qquad\qquad\qquad\qquad v = 1.7 \text{ m/s}$$

$$= \frac{2m w_0^2 \delta}{\rho l v^2 \pi} \frac{Y_R}{h} \qquad\qquad\qquad \delta = .009$$

$$\qquad\qquad\qquad\qquad\qquad\qquad\qquad Y_R = 1.45 \times 10^{-3} \text{ m}$$

$$= \frac{2 \times 13.3 \times 18^2 \times .009 \times 1.45 \times 10^{-3}}{1.293 \times 1.14 \times 1.71^2 \times \quad \times .06} \quad \begin{array}{l} = 1.293 \text{ kg/m}^3 \\ l = 1.14 \text{ m} \end{array}$$

$$= \underline{0.138} \qquad\qquad\qquad\qquad\qquad h = .06 \text{ m}$$

This value is in good agreement with the static values of the lift or normal force coefficients from Figs. 22 and 25.

Stall Flutter.

The final aerodynamic instability in a single degree of freedom system is stall flutter. This is caused by negative aerodynamic damping forces produced by negative phase lag of the aerodynamic forces.

(Reference 23). Torsional motion predominates, and the amplitude of the bending moment is negligible, whereas in classical flutter, bending and torsion are of the same order of magnitude. Stall flutter is best illustrated by the hysteresis effect on the pitching moment versus incidence curve (Fig. 19). A positive slope to the curve gives a pitching moment which acts in a direction to reduce incidence.

At small angles of incidence, a perturbation due to a gust causes the pitching moment to increase, which tends to reduce the incidence increased by the gust, so giving a positive stability. At the stall, the airflow remains attached to the surface under a small increase in incidence, when it would normally separate, and after separation, the flow reattachment is delayed until a much lower incidence is reached. The airforces at this point depend on the direction of motion, and cause a forced vibration (Reference 24).

It is unlikely that this instability would occur on a suspension bridge deck, as the angle of incidence on the deck is small, usually less than $\pm 5°$. It could occur with the cable support towers, but with an inherently high torsional stiffness, the wind speed would have to be very high. In Figs. 23 and 26, the shape of the moment coefficient versus incidence curves could indicate stall flutter, but the shape of the curves in Fig. 29 is completely different. The dynamic tests showed that the type of motion was the same for all the configurations and only at a higher speed for that of Fig. 29

Classical Flutter.

Classical flutter, an oscillatory motion involving coupling between the pitch and translation modes of vibration, is one of difficult theoretical problems in bridge aerodynamics. The problems arise in the calculation of the unsteady airforces needed to solve the equations of motion. After the collapse of the Tacoma Narrows Bridge, much work was done in the United States on the theoretical aspects of
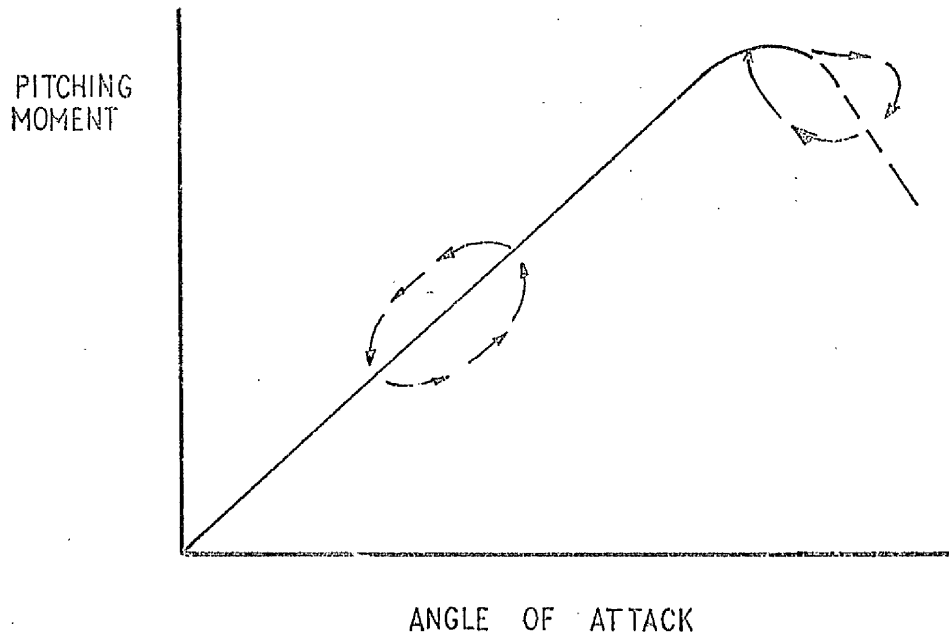
STALL FLUTTER

PITCHING
MOMENT

ANGLE OF ATTACK
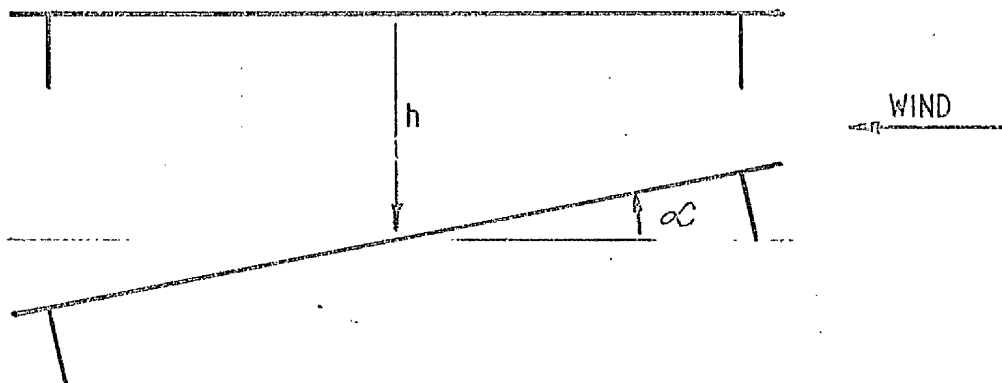
FIGURE 19

CLASSICAL FLUTTER

h

WIND

α

FIGURE 20

bridge vibration, the most important contribution coming from Bleich. He applied Theodorsen's classical flutter theory for flat plates directly to suspension bridge decks, and calculated the aerodynamic coefficients necessary for the equations of motion for the new Tacoma Narrows Bridge. Good agreement was obtained between theory and model tests for this bridge, but not when applied to the Golden Gate Bridge. (References 1, 25, 26). Flutter theory for thin aerofoils assumes that the airflow is attached at the trailing edge, which is generally not the case with a bluff body such as a bridge deck. The new bridge was a truss design, and the deck was very thin, approximating to a thin aerofoil. The Golden Gate Bridge was thicker, and agreement between model tests and theory was reached when a correction was applied using vortex forces on the leading edge, which were experimentally determined. The critical effects of bridge geometry was the shortcoming of Bleich's analyses. Later authors (Rocard, Selberg, Frandsen) developed the theme, and advocated applying it to new forms of bridge decks, but the problems of separated airflow still remained.

At the National Physical Laboratory, during the aerodynamic investigation into the River Severn suspension bridge, a new type of deck structure was proposed and developed. (Reference 13). This was a steel box section, which would cut construction costs and weight and also be very stiff in bending and torsion. A concurrent theoretical investigation into the aeroelastic stability of the final configuration was able to predict the critical speeds using Theodorsen flat plate airforces in a classical flutter analysis (Reference 27). The unusual shape of the cross-section, with thin walkways cantilevered on either side of the main box results in the flow remaining attached across the top and bottom surfaces, so simulating the required flat plate.

About the same time, in Norway and Denmark, an aerodynamic investigation into a box type bridge across the Lillebaelt was carried out under Professor Selberg, and similar conclusions reached (Reference 28). Thus, by careful choice of the box cross-section, thin aerofoil or flat plate aerodynamics can be used to predict critical speeds in a classical flutter analysis. To do this, the flow must remain attached across the box section, and for the Lillebaelt bridge small slats at the bottom of the guard rail were used to achieve this.

A recent development in the United States of America by Professor Scanlan (et al) is an analytical method in which the aerodynamic forces used are derived in real form from tests on bridge section models. (References 29, 30, 31, 32). This follows ideas set out by Duncan and Frazer in their initial work on flutter (References 33, 34). The equations of motion are set out for bending-torsional flutter, with the aerodynamic lift and moment force functions of the various displacements, velocities and accelerations. The aerodynamic force derivatives can then either be calculated using thin aerofoil theory, or measured, depending on the section under test. This approach, using simple equations of motion, and allowing for the complexities of the Theodorsen function to appear only in the calculation of the aeroderivatives is a better approach, as it leads to an easier understanding of the problem. This was emphasized by Pugsley in the discussion of Bleich's paper (Reference 25). Scanlan has simplified the equations of motion further, by separating structural and aerodynamic components, and ignoring aerodynamic inertia terms completely. Although theory depends on linear aerodynamic characteristics, and bridge decks have a tendency to non-linearity, at the exact critical speed, the amplitudes of the unstable motion are very small, and linearity can be assumed.

Considering a section of a symmetrical bridge deck, with the c.g. on the centre-line, and with vertical and torsional degrees of freedom,

h and α , (Fig. 20) the equations of motion can be written as:-

$$h'' + 2\gamma_h w_h h' + w_h^2 h = \frac{L_h}{m}$$

$$= H_1 h' + H_2 \alpha' + H_3 \alpha \qquad (1)$$

$$\alpha'' + 2 \gamma_\alpha w_\alpha \alpha' + w_\alpha^2 \alpha = \frac{L\alpha}{I_D}$$

$$= A_1 h' + A_2 \alpha' + A_3 \alpha \qquad (2)$$

The coefficients H_i and A_i are the unsteady aerodynamic derivatives which can be evaluated either theoretically for thin aerofoils or experimentally for bluff bodies. Scanlan's papers deal with the experimental evaluation for bluff bodies, and the verification of the technique using a thin aerofoil. The motion of the original Tacoma Narrows Bridge was also checked using this technique. Its usefulness is such that the method of deriving the coefficients will be dealt with in full.

The section model under investigation is placed in the wind tunnel. With the wind-off, equations (1) and (2) are satisfied with H_i and A_i equal to zero. The aerodynamic inertia terms in h'' and α'' are omitted, as being negligible. This is generally the case in aeroelastic problems, and the terms are easily incorporated if an unusual configuration is being tested.

With the wind on, equations (1) and (2) are satisfied at a steady state sinusoidal oscillation. With the α motion locked out, equation (1) is satisfied for $H_1 \neq 0$. A decaying oscillation gives a good approximation to a flutter motion if the damping is low enough. The amplitude record of h can then be used to calculate H_1.

Thus, $\qquad h'' + 2\gamma_h w_h h' + w_h^2 h = H_1 h' \qquad (3)$

$$h'' + 2\gamma_1 w_h h' + w_h^2 h = 0$$

Where $\gamma_1 = \gamma_h - \frac{H_1}{2w_h}$

From vibration theory

$$\delta_h = \frac{2\pi \, \gamma_1}{\sqrt{1 - \gamma^2}}$$

$$= \frac{1}{n} \ln \frac{h_0}{h_n} \qquad = \text{Logarithmic decrement}$$
$$\text{of vertical motion}$$

$$\gamma_1^2 = \frac{1}{1 + 4\left(\frac{\pi}{\delta_h}\right)^2} \qquad \cong \qquad \frac{1}{4}\left(\frac{\delta_h}{\pi}\right)^2$$

$$H_1 = 2w_h\left(\gamma_h - \gamma_1\right) \tag{4}$$

Similarly, with the vertical motion locked, equation (2) is satisfied with $A_1 = 0$, and excellent approximations for A_2 and A_3 are obtained in a similar manner.

Thus,

$$\alpha'' + 2\,\gamma_\alpha\,w_\alpha\,\alpha' + w_\alpha^2\,\alpha = A_2\,\alpha' + A_3\,\alpha$$

$$\alpha'' + 2\,\gamma_2 w_\alpha\,\alpha' + \Omega_\alpha^2\,\alpha = 0 \tag{5}$$

where $\quad 2\,\gamma_2 w_\alpha = 2\,\gamma_\alpha\,w_\alpha - A_2 \tag{6}$

and $\quad \Omega_\alpha^2 = w_\alpha^2 - A_3 \tag{7}$

Then $\quad \delta = \frac{1}{n}\ln\frac{\alpha_0}{\alpha_n} = \frac{2\,\gamma_2\pi}{\sqrt{1 - \gamma_2^2}}$

$$\gamma_2^2 = \frac{1}{1 + 4\left(\pi/\delta_\alpha\right)^2} \tag{8}$$

and $\Omega_d = \Omega_\alpha\sqrt{1 - \gamma_2^2} \tag{9}$

where Ω_d is the frequency of the cosine wave of diminishing amplitude.

Substituting into (6) and (7) yields A_2 and A_3.
At the onset of flutter, the solutions are sinusoidal. thus

$$h = h_0 \sin wt \qquad\qquad w = \text{flutter frequency.}$$

$$\alpha = \alpha_0 \sin (wt - \theta)$$

Using those for h and α in equations (1) and (2), the following expressions for A_1, H_2 and H_3 are derived

$$A_2 = \frac{1}{w} \cdot \frac{\alpha_0}{h_0}\left[(w^2 - w_\alpha^2 + A_3)\sin\theta + (2\gamma_\alpha w_\alpha - A_\alpha)w\cos\theta\right]$$

$$H_2 = \frac{1}{w} \cdot \frac{h_0}{\alpha_0}\left[(w_h^2 - w^2)\sin\theta + (2\gamma_h w_h - H_1)w\cos\theta\right]$$

$$H_3 = - \cdot \frac{h_0}{\alpha_0}\left[(w^2 - w_h^2)\cos\theta + (2\gamma_h w_h - H_1)w\sin\theta\right]$$

Although this method is general for sectional models, its use depends on the ease of separating bending from torsional motion in the wind tunnel. This is a factor in the design of the model support system. The method also depends on the nature of the flutter motion as it must be possible to keep the model in a small amplitude flutter motion for sufficient time to obtain good amplitude traces. On some models this is difficult to do as the motions may be very divergent. The calculations eliminate model structural damping, so an answer may be to increase this damping enough to allow a steady state, or slowly divergent oscillation to occur. The time span need only be enough to allow the operator to take the necessary readings, and then stop the flutter by hand. The viscous damping can be applied in the usual manner using oil filled dashpots, or electromagnetic means.

Another approach, proposed by Dicker, is based on quasi-steady aerodynamic coefficients, this assumption being made since the motions of the structures are slow. This allows him to base his coefficients on their static values. (References 35, 36). This approach is incorrect, as the time scale for suspension bridges is within the range where unsteady aerodynamic coefficients are required. Current aero-industry practice is to assume quasi-steady aerodynamics for modern jet transports at frequencies less than 0.1 hz. First vibration modes of suspension bridges occur at frequences greater than 0.1 hz as shown by the following examples. The original Tacoma Bridge was 0.13 hz, the Golden Gate was 0.12 hz, the Forth Road Bridge was 0.13 hz and the Severn 0.13 hz.

Static Tests.

The results of the static tests on the deck and arch rib models are given in coefficient form in Figures 21-31. Figures 21, 22, 23 give the horizontal force coefficient, C_H, the normal force coefficient, C_N, and the pitching moment coefficient, C_M, for the original deck model, without railings, for two tunnel speeds. The Reynolds numbers are 4.78×10^6, and 9.56×10^6. Figures 24, 25, 26 show C_H, C_N and C_M respectively for the original deck model with railings, and also the effect of holes in the webs of the main beams. The Reynolds numbers were the same. As expected, C_H is increased by the addition of the railings, and the holes do not influence the separated flow from the main beams very much, so C_H with the holes is not much different from that without the holes. The non-linearity of the C_N curve is probably caused by a change in the position of the centre of pressure. The flow is attached to the top surface at some small negative angle of incidence, but is always separated from the flanges of the main beams on the bottom surface. With holes in the webs, the flow on the underside between the main beams will be more regularly turbulent, and give less movement of the centre of pressure. In Figure 25, the gradient of C_N/α is more uniform with the holes than the other cases without them.

The shape of the C_M curve is such that the dynamic instability of the nature of stall flutter, or autorotation could occur. At incidences close to zero, the flow separates at the leading edge, but reattaches itself to the top surface, and at higher incidences is separated over all the deck surface. Thus the deck has no stall angle of incidence in the normal aerofoil sense. Movement of the line of action of the drag force can account for the change in C_M with incidence. A force equilibrium calculation gives the resultant force
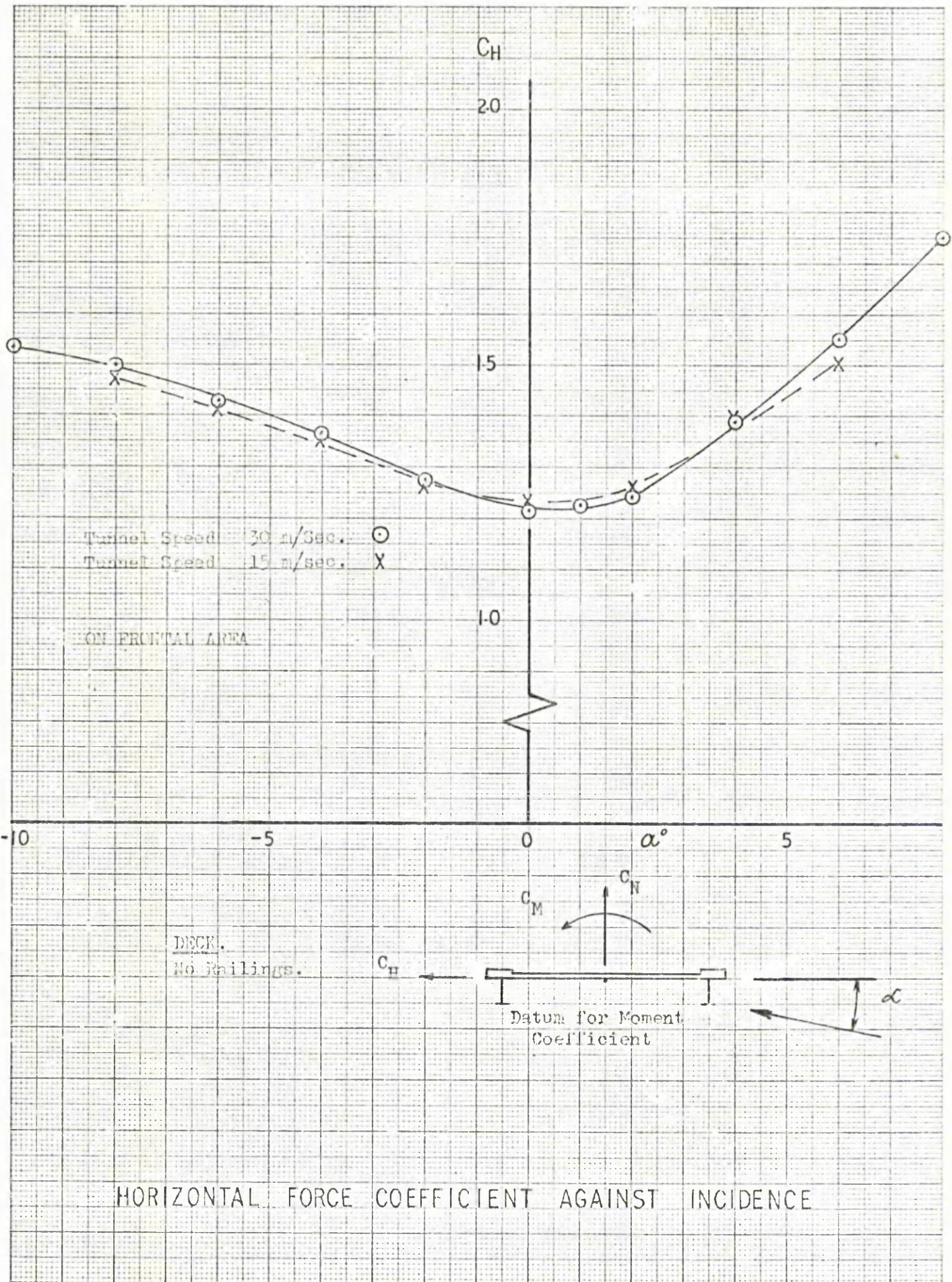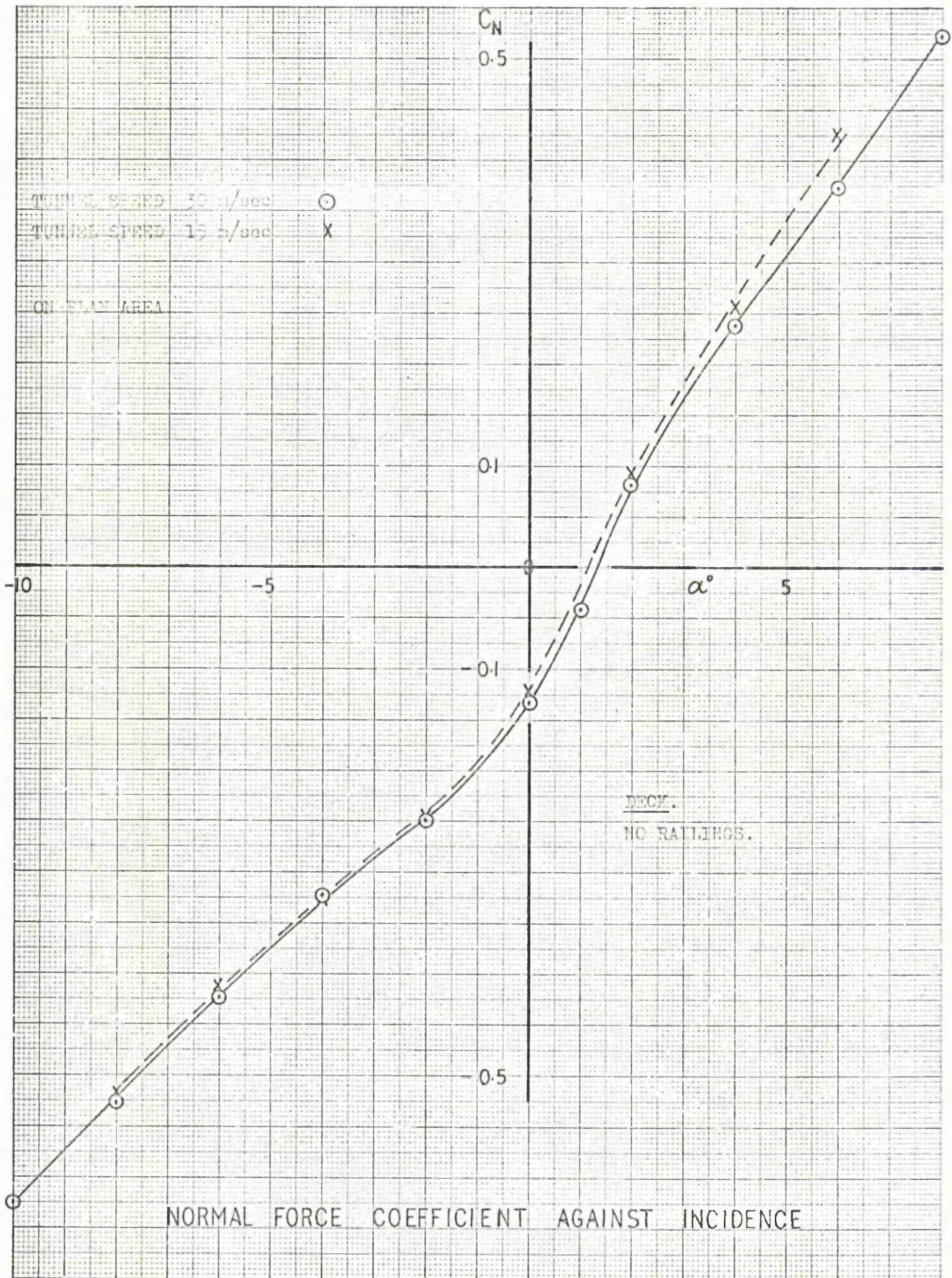
Tunnel Speed   30 m/Sec.   ⊙
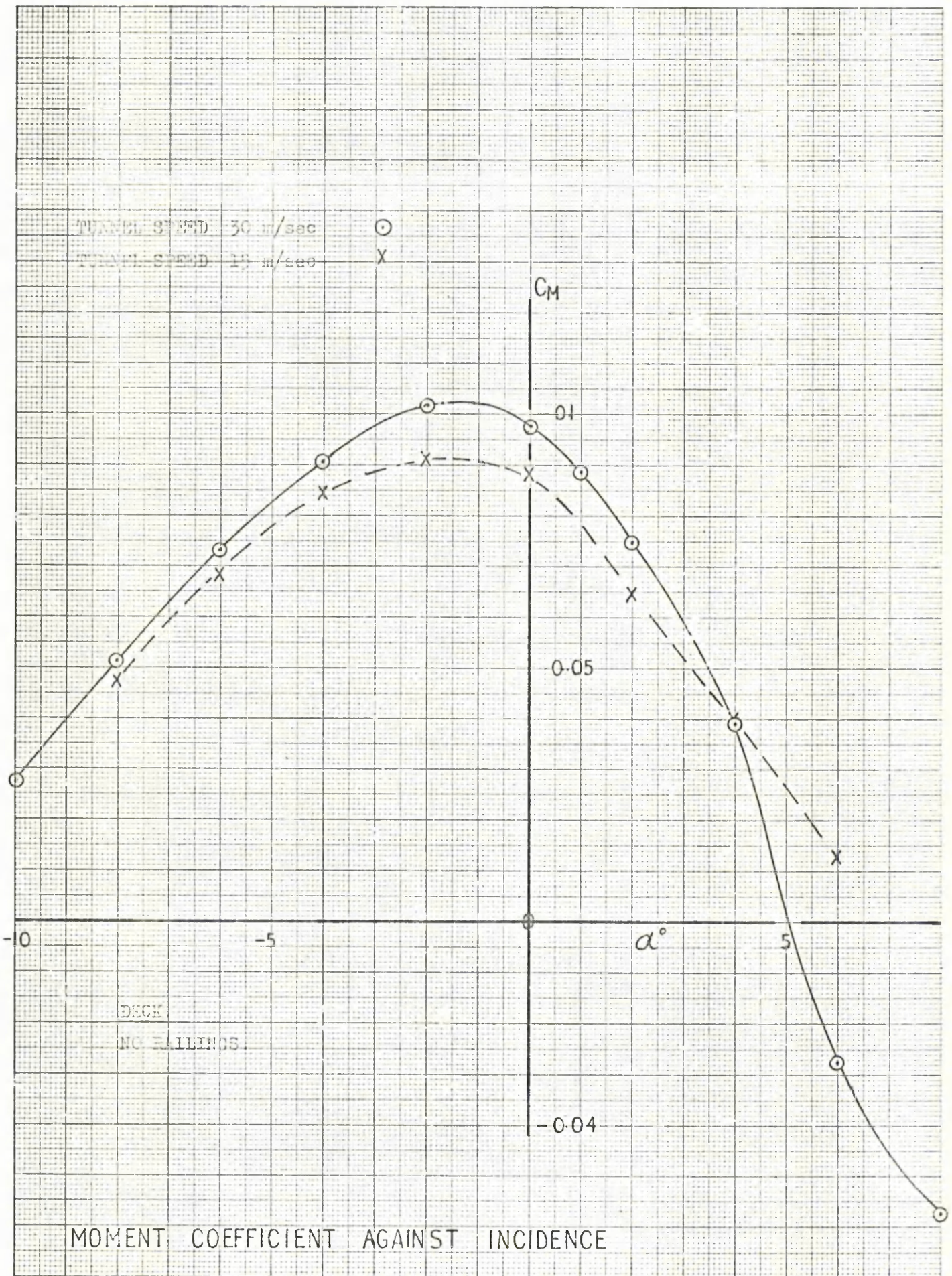Tunnel Speed   15 m/Sec.   X

ON FRONTAL AREA

DECK.
No Railings.

Datum for Moment Coefficient

HORIZONTAL FORCE COEFFICIENT AGAINST INCIDENCE

FIGURE 21

NORMAL FORCE COEFFICIENT AGAINST INCIDENCE

FIGURE 22

C_M

·01

0·05

-10   -5 $\alpha°$ 5

DECK
NO RAILINGS

-0·04

MOMENT COEFFICIENT AGAINST INCIDENCE

FIGURE 23

NO HOLES

HOLES

TUNNEL SPEED 30 m/sec   ⊙
    "   "   15 m/sec.   ×
    "   "   15 m/sec   +

DECK.
With Railings
Effect of holes in webs of Spanwise Girders.

HORIZONTAL FORCE COEFFICIENT AGAINST INCIDENCE

FIGURE 24

NORMAL FORCE COEFFICIENT AGAINST INCIDENCE

FIGURE 25

TUNNEL SPEED 30 m/sec. ⊙
"   "   15 m/sec. ✕
"   "   15 m/sec. +

NO HOLES

0·08

0·06

0·04

HOLES

0·02   DECK
        With Railings

        Effect of holes in webs
        of Spanwise Girders.
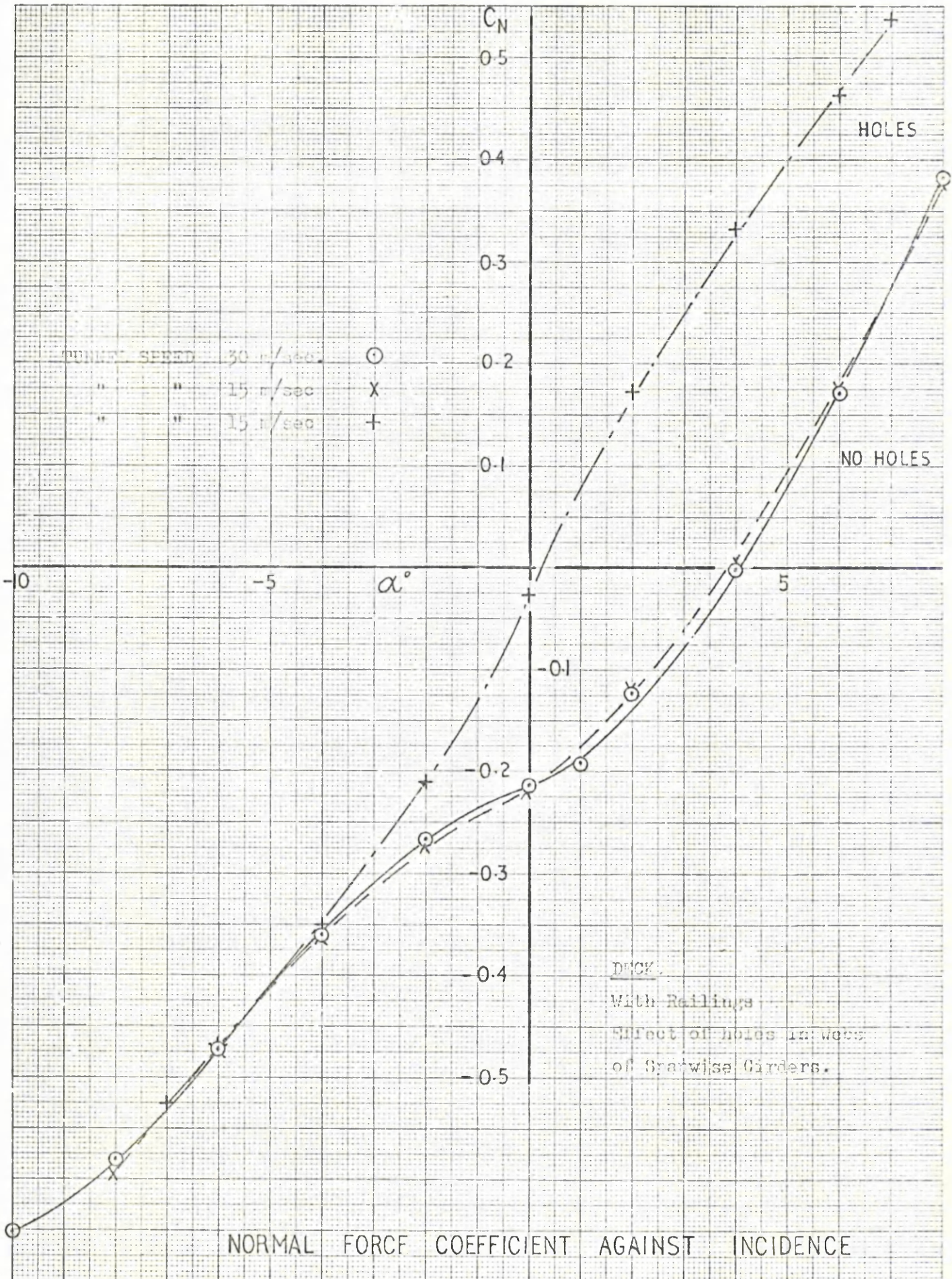
-10   -5   0 $\alpha°$ 5
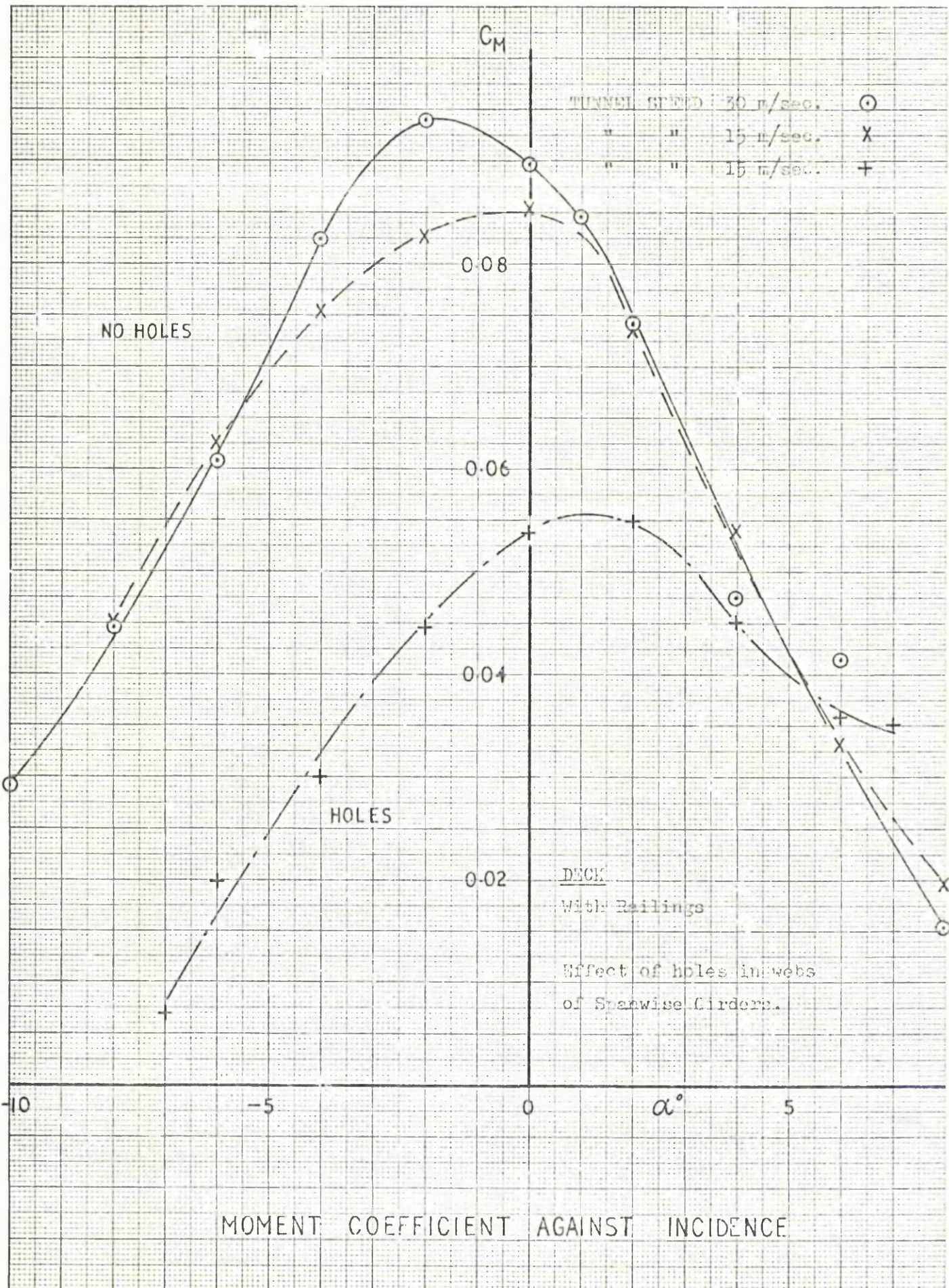
MOMENT COEFFICIENT AGAINST INCIDENCE

FIGURE 26

acting at a $\frac{1}{4}$ to $\frac{1}{3}$ of the deck chord above the surface, at some angle
to the horizontal Fig. 27. This is the rule for this type of structure,
as has been found in current and past investigations of bridge loads.

Figures 28, 29, 30 give C_H, C_N, and C_M for the final configuration,
with holes in the webs, parapet fairings, and representative mesh on
the railings. The Reynolds numbers are 4.78×10^6 and 7.66×10^6. The
mesh increases C_H, but has little effect on C_N or C_M as expected. The
gradient of C_N/α is still uniform, and has a value of 5.5/Radian
compared to 2 /radian for thin aerofoil theory. The major change due
to the parapet fairing is that the C_M curve is now linear, both with and
without the mesh. The flow is now reattached to the top surface of the
deck, and the airflow and wake stabilized throughout the incidence
range.

Figure 31, for the arch rib, shows C_H against incidence for the
original section, and the modified section with rectangular ducts
piercing the box beams. Between 4 and 5 degrees, for the original
section, the airflow begins to pass between the box sections, as though
through a slot, thus the width of the turbulent wake is reduced, and
with it, the drag. With the ducts, there is flow across the gap, which
now no longer acts as a slot at higher incidences due to the transverse
turbulent flow. This turbulence adds energy to the boundary layer, so
reducing the size of the wake, and the drag of the section. With
increasing incidence, the projected depth of the section increases,
giving an increase in drag due to the increase in thickness of the wake.

A comparison of the above C_H and C_N values with those obtained from
the British Standards Institution Code of Practice (Reference 37) is
interesting. For the arch rib, a single rib has a width of 0.047 m
and a depth of 0.1092 m and so the ratio $W/D = 0.43$.

TUNNEL SPEED 15 m/sec

47·87 N
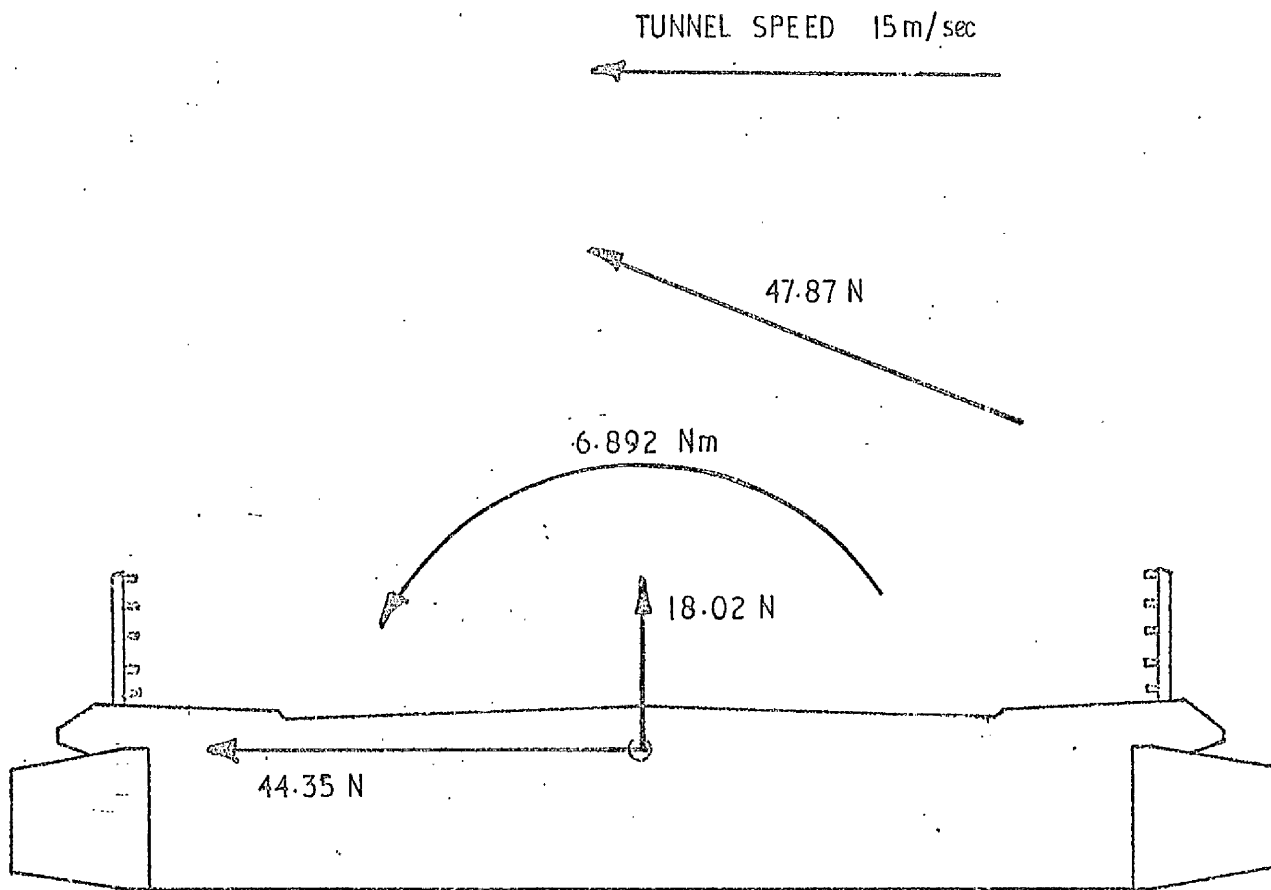
6·892 Nm

18·02 N

44·35 N

From TABLE 1 and FIGURES 28, 29, 30.

LIFT 18·02 N
DRAG 44·35 N
PITCHING MOMENT 6·892 Nm

RESULTANT FORCE 47·87 N
0·144 m from centre and 22·1° to horizontal
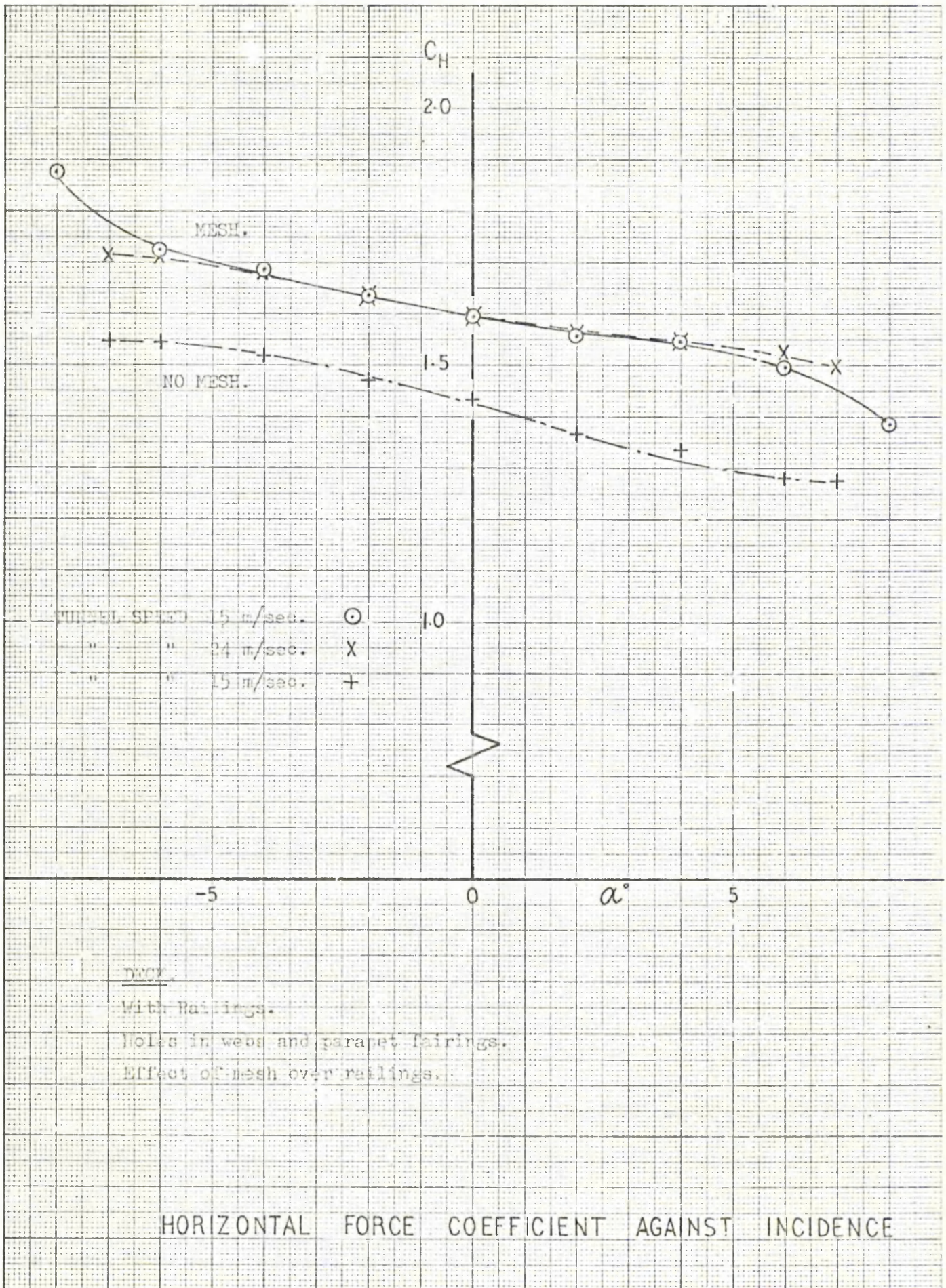
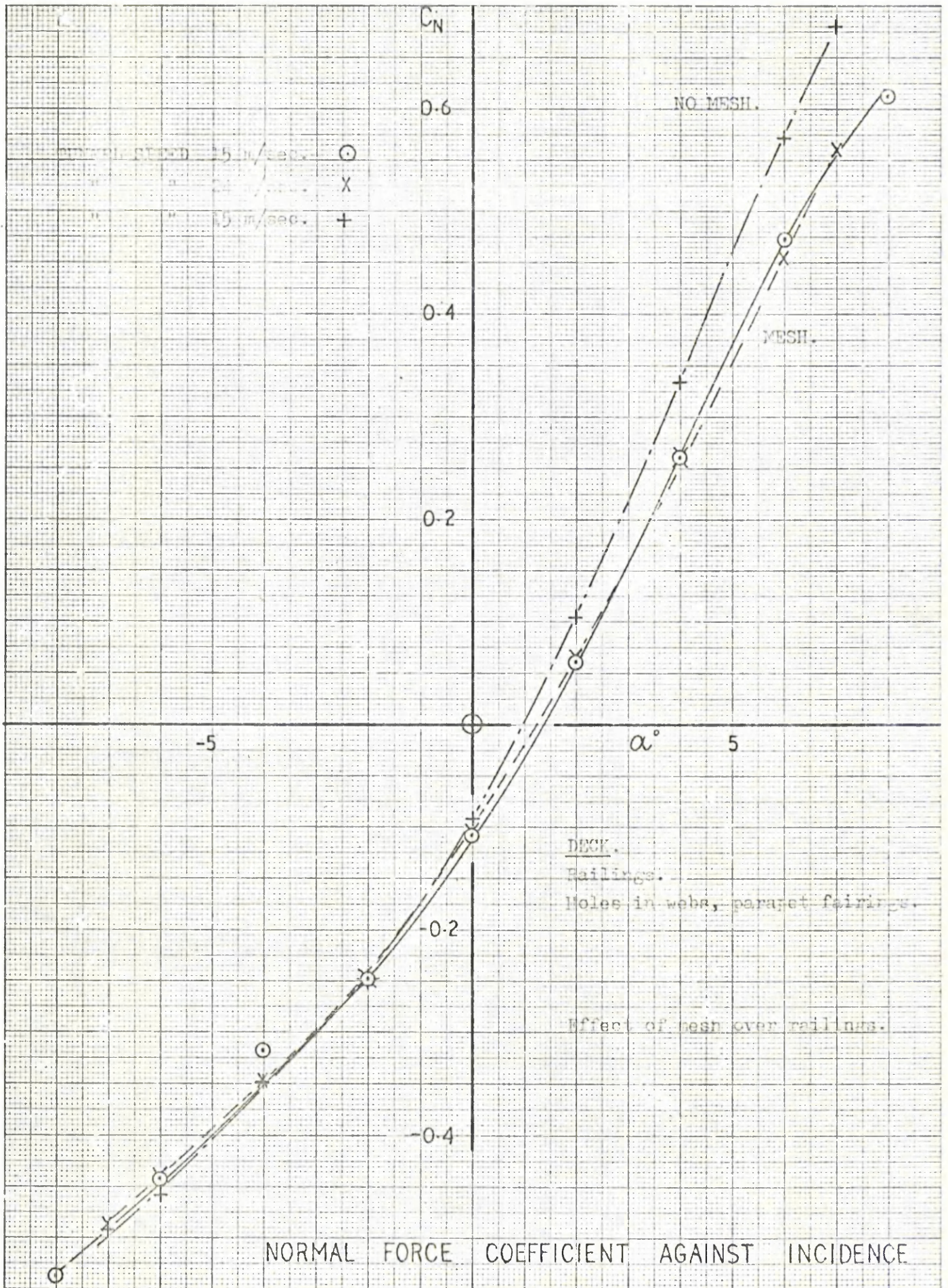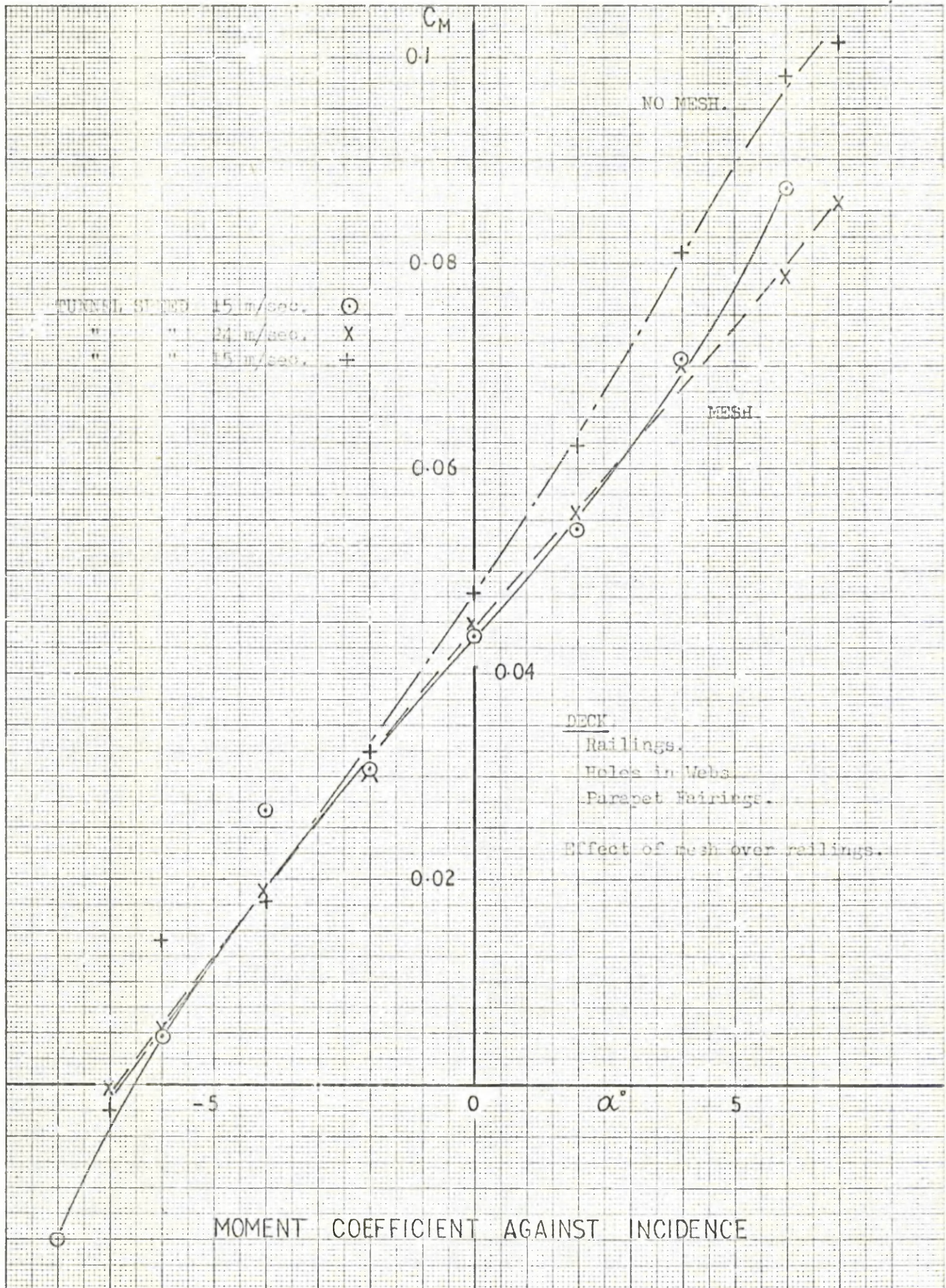STATIC FORCES EQUILIBRIUM FOR DECK

FIGURE 27

C_H

2·0

MESH.

NO MESH.

1·5

TUNNEL SPEED   15 m/sec.   ⊙   1·0

     "   "   24 m/sec.   X

     "   "   15 m/sec.   +

-5   0 $a°$ 5

DATA.

With Railings.

Holes in webs and parapet fairings.

Effect of mesh over railings.

HORIZONTAL   FORCE   COEFFICIENT   AGAINST   INCIDENCE

FIGURE   28

NORMAL FORCE COEFFICIENT AGAINST INCIDENCE

FIGURE 29

MOMENT COEFFICIENT AGAINST INCIDENCE

FIGURE 30

ARCH RIB

C_H

2·5

2·0

1·5

1·0

0·5

⊙ ——— ORIGINAL SECTION

X
+ —·—·— MODIFIED SECTION WITH
RECTANGULAR DUCTS PIERCING BOX BEAMS

TUNNEL SPEED   5.7   m/sec   ⊙
    "   "   13.4 m/sec   X
    "   "   15.0 m/sec   +

−10   −5   0   5   10

α°

HORIZONTAL   FORCE   COEFFICIENT   AGAINST   INCIDENCE

FIGURE 31

From the draft code of practice, $C_D = 2.22$ for box girders, which compares favourably with that of Figure 31 for the original section. The modified section is of such a configuration that tests are necessary to determine the drag coefficient, but the value for the box girder could be used as a first approximation.

For the deck without the fairing, the width is 0.351m, and with the fairing, 0.376m. The depth is 0.0598m, giving a width/depth ratio of 5.87 or 6.30 respectively. Using Figure 7 of reference 37, the corresponding C_Ds are 1.30 and 1.28.

From Figure 21, the value of C_D at zero incidence is 1.22, corresponding to the BSI value of 1.30, with no railings or wire mesh.

From Figure 24, at zero incidence, the measured C_D is 1.54, and the increment due to the railings must be added to the base calculated C_D. There are four railings 0.00159 x 0.00318m, one of 0.00159m square and thirteen posts .0381m by .00397m square. Thus

$$\text{Incremental } C_D = \frac{4 \times .00159 \times 1.1 + .00159 \times 1.5}{.0598} + \frac{13 \times .0381 \times .00397 \times 1.5}{.0598 \times 1.14}$$

$$= 0.200$$

This gives a calculated C_D of 1.50, comparing favourably with the measured value of 1.54.

To compare with the measured value from Figure 28 of $C_D = 1.60$ with railings and mesh, the incremental value of the mesh C_D is calculated. The mesh has 180 x 6 strands, and has a diameter of .00056m.

$$C_D = \frac{(180 \times .0381 + 6 \times 1.14) \ .00056 \times 1.2}{.0598 \times 1.14}$$

$$= .135$$

$$\text{BSI } C_D = 1.28 + .20 + .135$$

$$= 1.615$$

For railings alone, the measured C_D is 1.44 and the calculated C_D is 1.48.

Thus, the measured C_D for all the configurations of the deck agree favourably with those calculated using the BSI Code of Practice.

If the railings and mesh ice up, the depth is then 0.0979m and width/depth = 3.84, giving a C_D of 1.40.

For the deck normal force coefficient at zero incidence, the measured values are less than the allowable value of 0.4 from the Code of Practice.

The above comparisons have shown the accuracy of the Code of Practice when using the standard designs, and also the need for wind tunnel testing where there is an unusual design feature such as the holes in the arch rib.

Dynamic Tests.

It is also useful to use the Code of Practice to determine some of the criteria dependant on the dynamic characteristics of the structure, the most important being critical speed.

For the deck, the maximum width is 0.376m, the width between the main spanwise girders is 0.313m, and the depth is 0.0598m. The fundamental bending frequency is 2.86 hz., and the torsional frequency is 3.67 hz.

Using the smaller width,
$$\frac{b}{h} = \frac{.313}{.0598} = 5.23$$
$$\therefore \quad v = 6.5wh$$
$$= 6.5 \times 2.86 \times .0598$$
$$= 1.11 \text{ m/sec.}$$

For maximum width, $\frac{b}{h} = 6.30$
$$\therefore \quad v = 2.0wh\left(\frac{b}{h} - 2.5\right)$$
$$= 2.0 \times 2.86 \times .0598 \ (6.30 - 2.5)$$
$$= 1.30 \text{ m/sec.}$$

Using the torsional frequency of 3.67 hz, the corresponding speeds are
$$v = 6.5 \times 3.67 \times .0598$$
$$= 1.43 \text{ m/sec.}$$

and $v = 2.0 \times 3.67 \times .0598 (6.30 - 2.5)$

$\qquad = 1.67$ m/sec.

For the arch rib, the width is 0.445m, and the depth is .1092m, and the fundamental bending frequency is 3.33 hz.

$$\frac{b}{h} = \frac{.445}{.1092} = 4.08$$

$\therefore \qquad v = 6.5 \times 3.33 \times .1092$

$\qquad\qquad = 2.16$ m/sec.

From Figures 32 to 38, it can be seen that the calculated speeds closely match those of the low speed oscillations caused by the shedding of Karman vortex streets. This limited amplitude oscillation is non-catastrophic and, although it may cause fatigue damage eventually and public apprehension, it is not of primary importance for use in determining the safety of the structure. The high critical speeds illustrated in Figures 37 and 38 can not be calculated by this method, and can be discovered only by wind-tunnel testing.

For the deck, the measured low-critical speed is about 1.4-1.5 m/sec, and is due to the flexural frequency, and the motion is a vertical oscillation, so the calculated speeds are slightly low. Also, using the full width of the deck is more accurate than using the effective width as defined in the Code of Practice.

Using the Code of Practice to calculate maximum amplitude will give a result which is too low, as the given damping levels are assumed to be due only to the structure. At the critical speeds, a resonant condition occurs, and aerodynamic damping is negative, and the overall damping is greatly reduced, as can be seen from Figures 16 and 17, with Figure 17 being very close to a resonant condition.
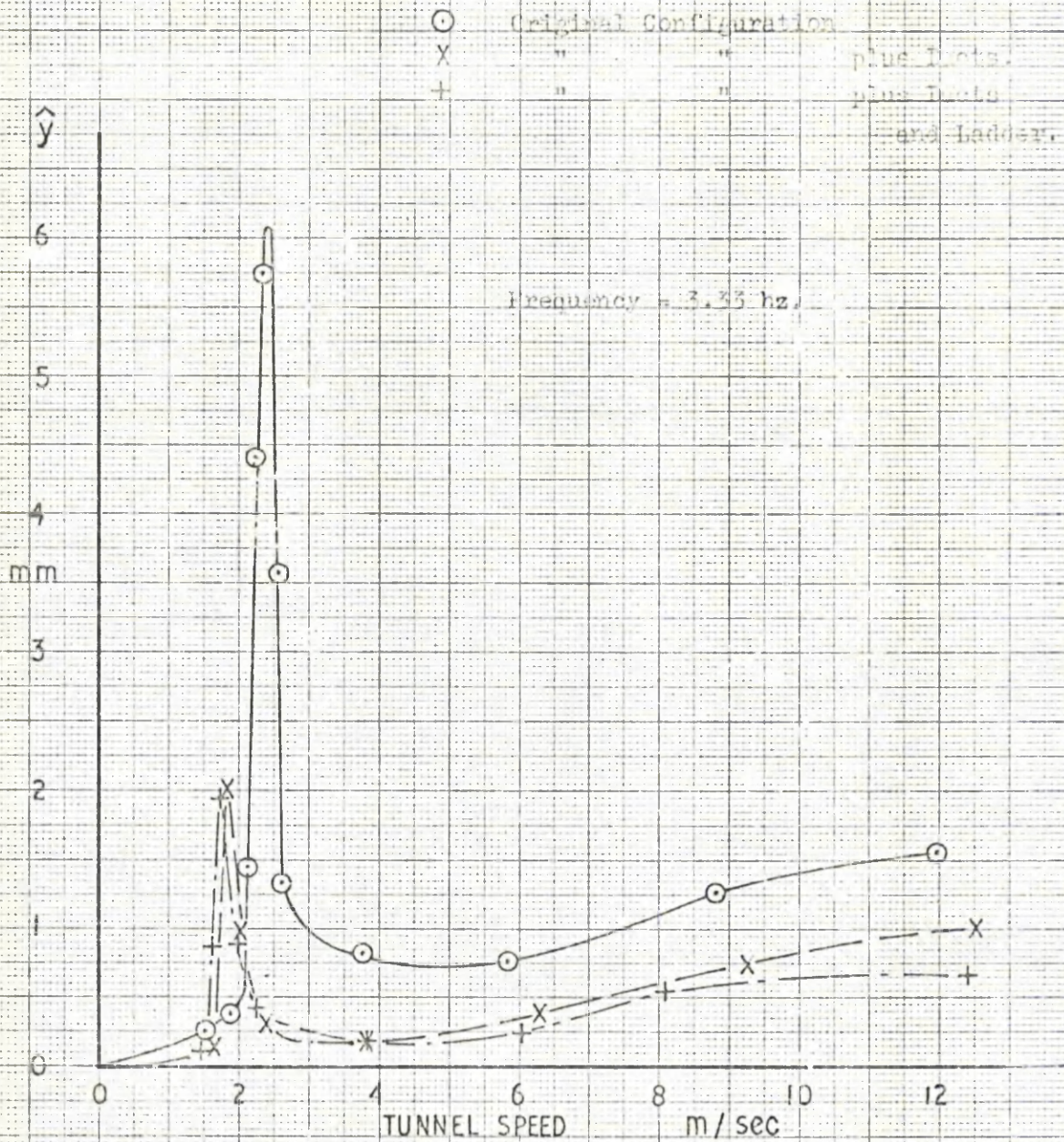
For a bridge, a more typical value of logarithmic decrement at a resonant condition should be 0.01, combining a positive structural value with a negative aerodynamic value.

The result of wind-tunnel testing of models is that the catastrophic critical speed for the bridge should be higher than the limiting wind speed as defined in the Code of Practice.

For the arch rib, Figure 32 shows the variation of steady state amplitude of oscillation with speed. The amplitude peaks at 1.3 m/sec. and 2.4 m/sec are the resonance peaks caused by the frequency of shedding Karman vortices matching the structural frequency of the model system. The Strouhal number for the arch rib with ducts is 0.193, and without the ducts, 0.146, at a frequency of 3.3 hz. The increasing amplitude of vibration above 4 m/sec. is caused by random buffet from the arch rib model, and the model does not exhibit any dynamic instability at high speeds. The effect of the ducts is to reduce the strength of the vortices by bleeding flow away from the edges of the box sections. The access ladder has the further effect of slightly disturbing the flow on the top surface, causing mixing in the boundary layer, and marginally reducing the strength of the vortex shed from the top surface. Figure 33 is a typical plot of logarithmic decrement against speed for the arch rib showing the amplitude resonance peak as a dip in the damping curve. The increase in damping at higher speeds shows good dynamic stability, although the effect of buffet increased the steady state amplitudes in this speed range. The model was free to translate vertically, and rotate in pitch.

Figures 34, 35, 36 show the variation of logarithmic decrement with speed for the deck in the final configuration, with parapet fairing and holes in the webs of the main beams.

The Strouhal number for the deck is 0.114 at a frequency of 2.86 hz in vertical translation. The tests were inadvertently carried out with the centre of gravity offset upwind, which affected the pitch inertia, and centre of rotation. Later tests showed that this offset was very important when determining the critical speed. The influence of incidence and pivot position on logarithmic decrement is also shown in

VARIATION OF MAINTAINED AMPLITUDE OF OSCILLATION WITH SPEED

FIGURE 32

VARIATION OF $\delta_{z\theta}$ WITH SPEED
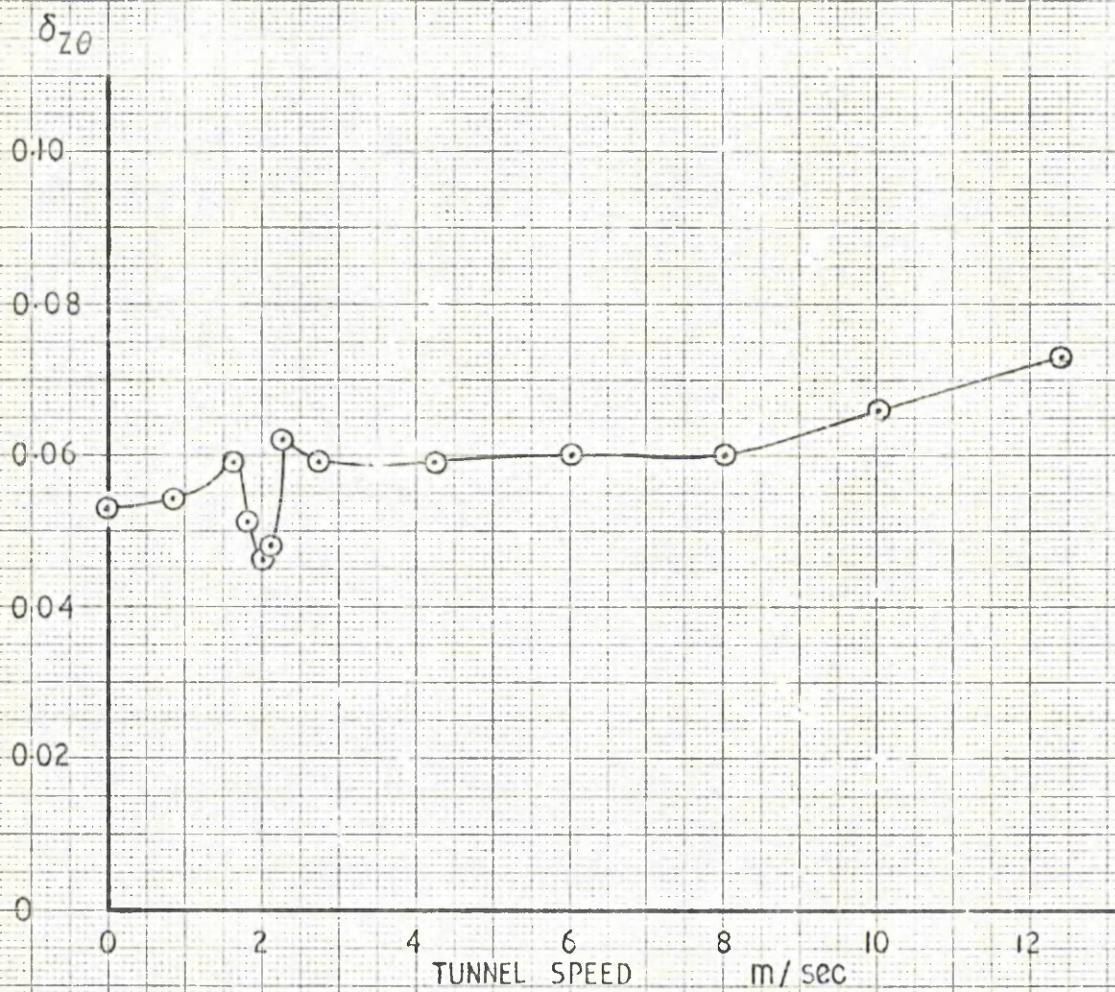
ARCH RIBS.

With ducts and access ladder.
Vertical translation and rotation.
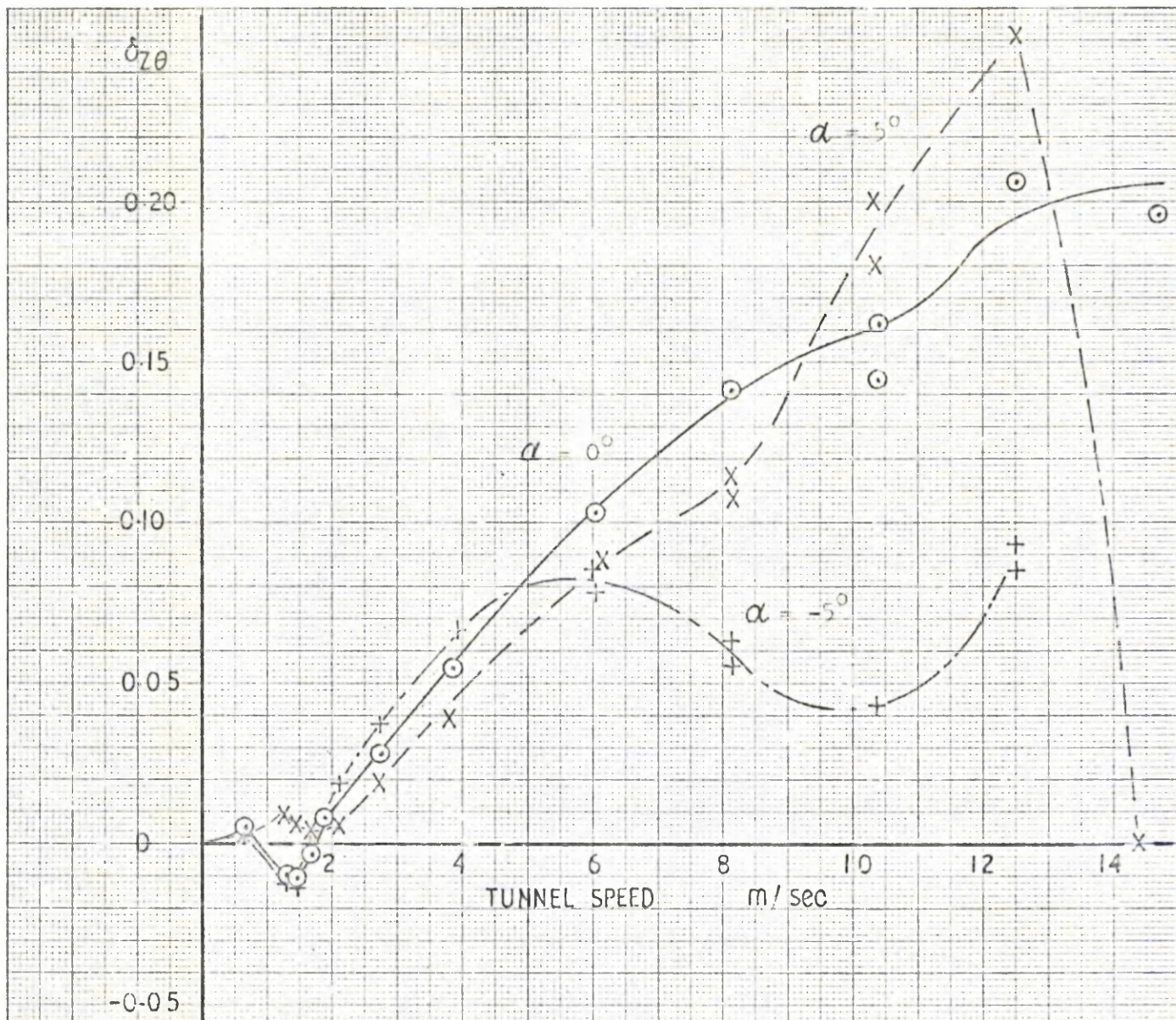
FIGURE 33

VARIATION OF $\delta_{z\theta}$ WITH SPEED
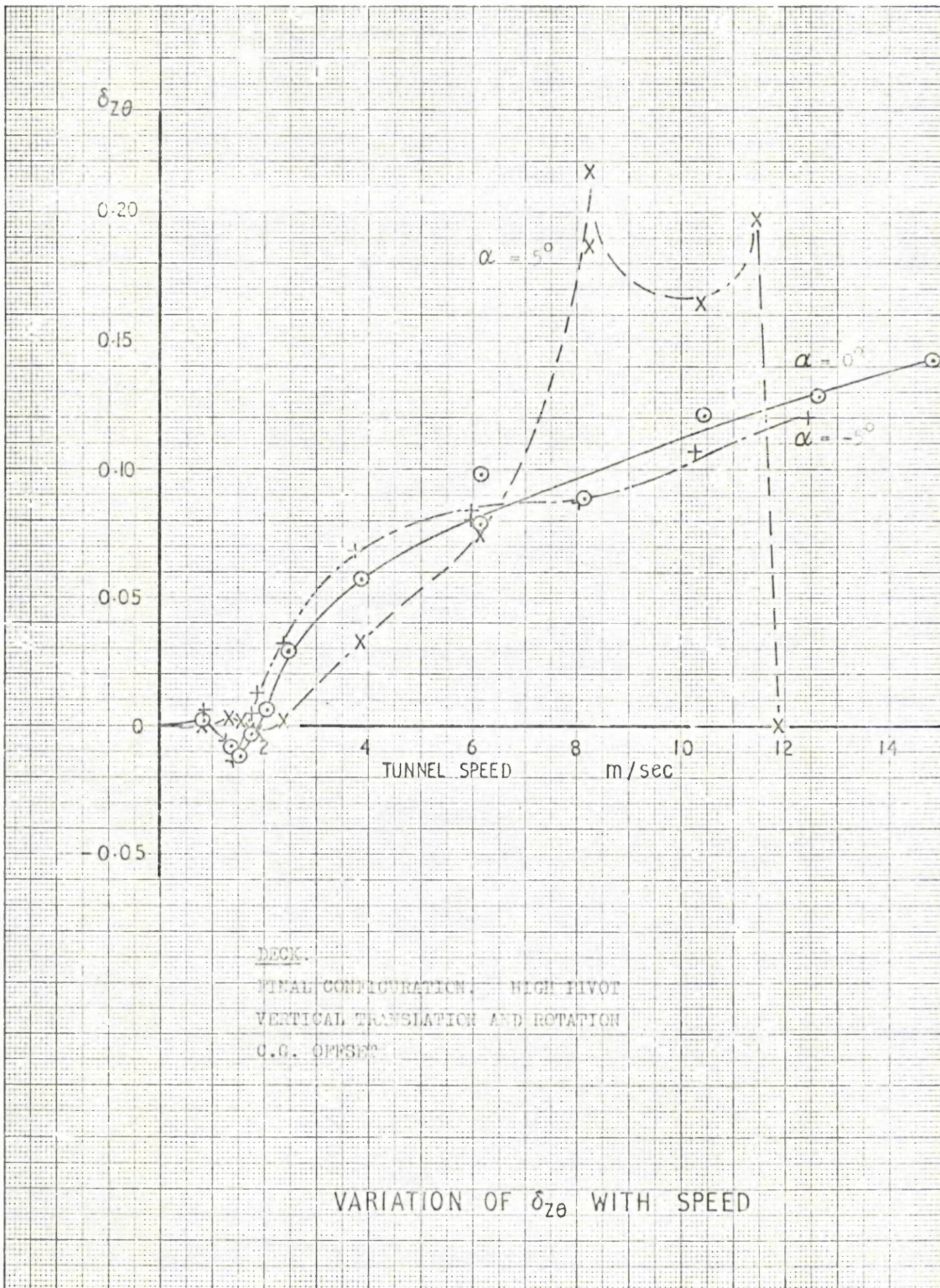
FIGURE 34
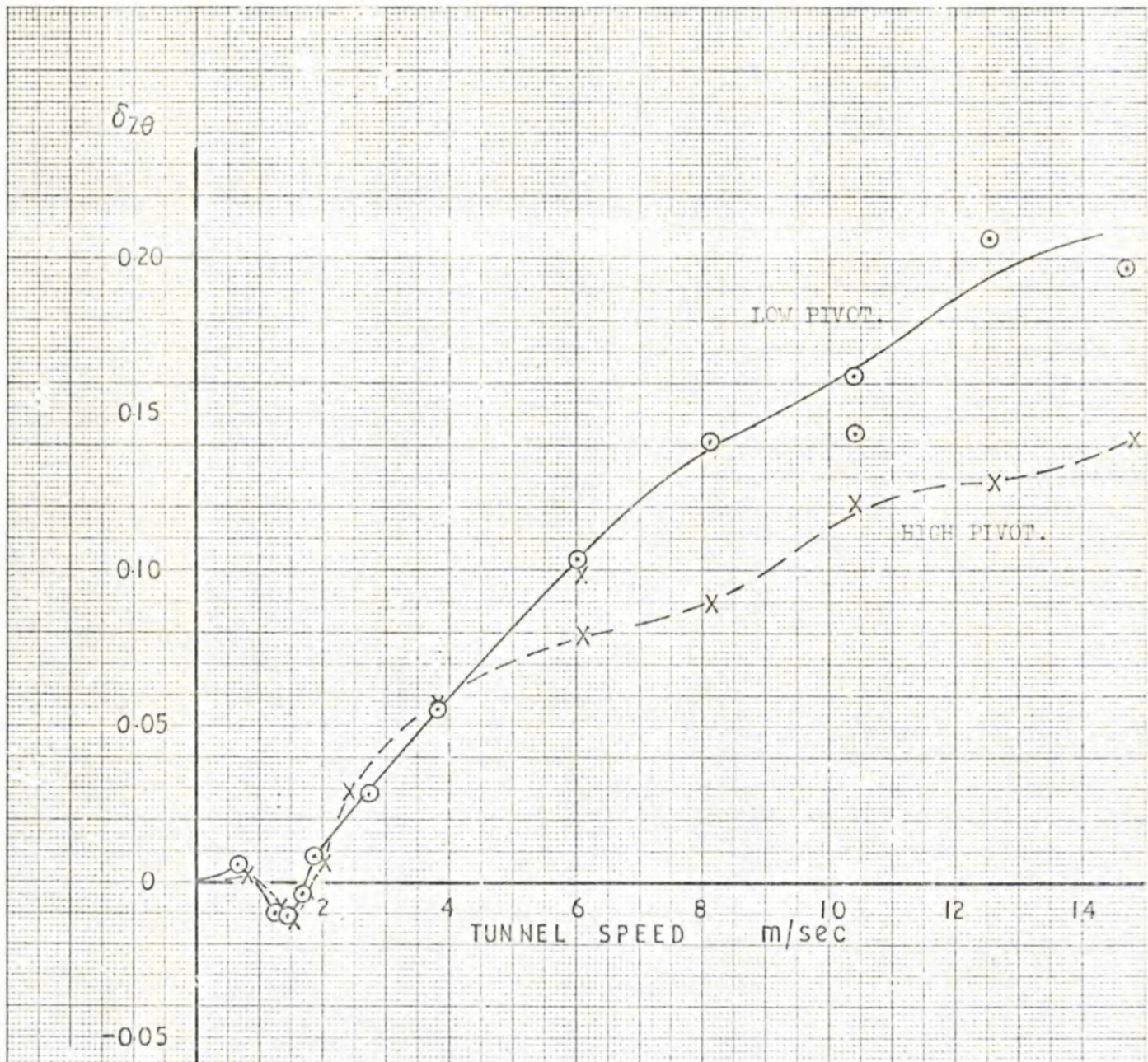
VARIATION OF $\delta_{z\theta}$ WITH SPEED

FIGURE 35

VARIATION OF $\delta_{z\theta}$ WITH SPEED

FIGURE 36

VARIATION OF $\delta_{z\theta}$ WITH SPEED
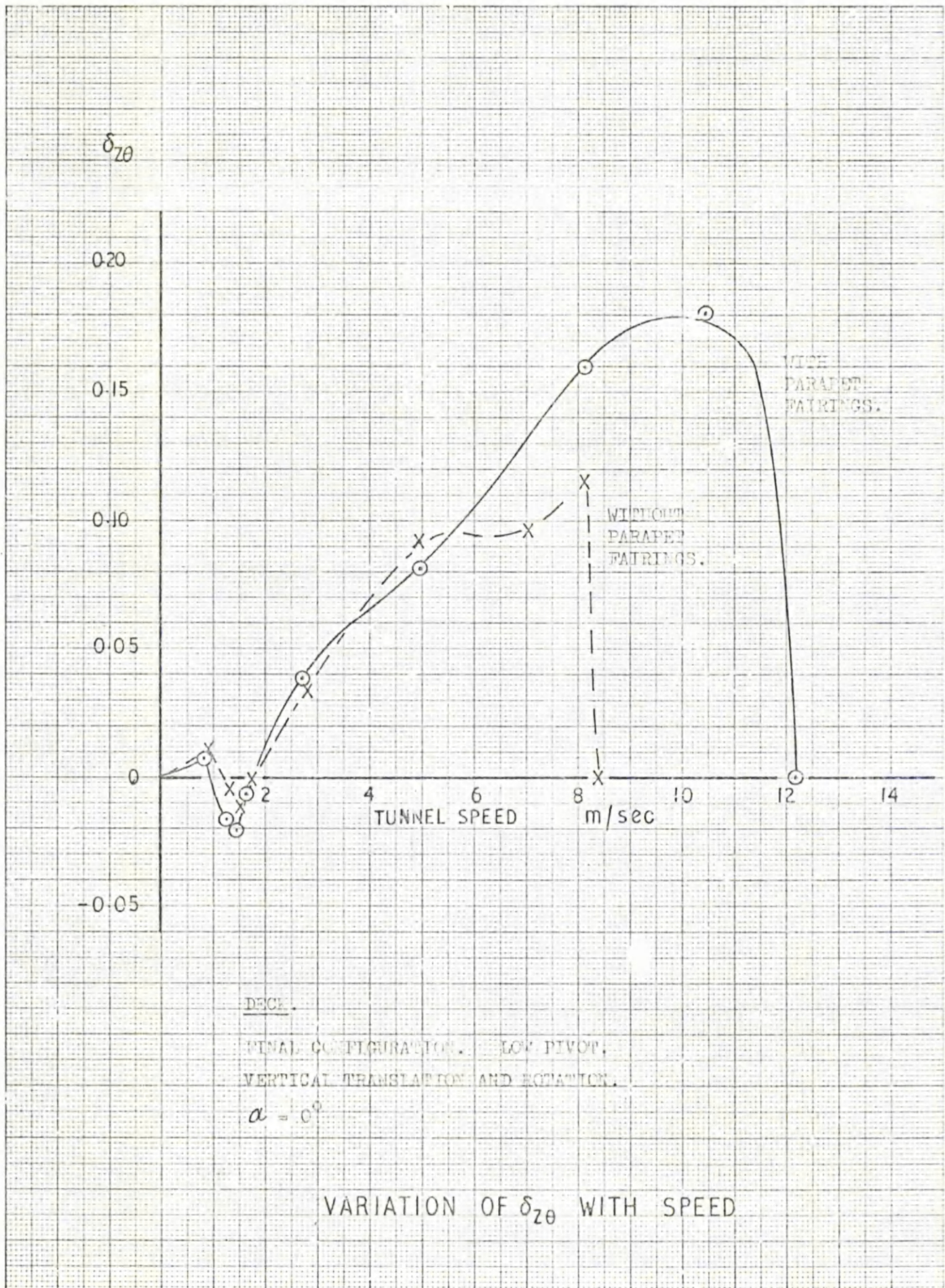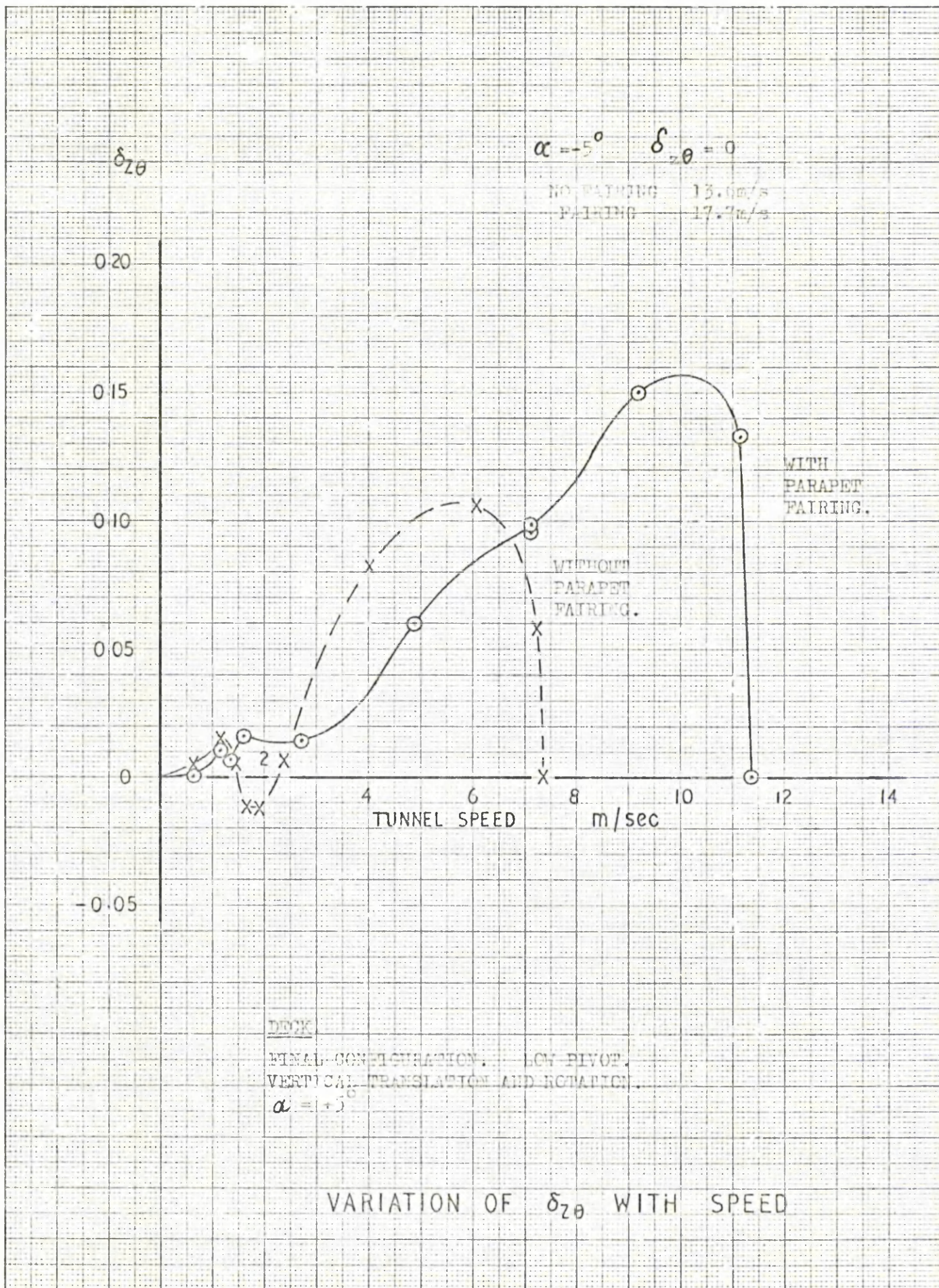
FIGURE 37

VARIATION OF $\delta_{Z\theta}$ WITH SPEED

FIGURE 38

Figures 34, 35 and 36. From these graphs, it would appear that the critical speed is determined by the flow over the top surface of the deck. At positive incidence, the flow is separated at the leading edge and over the whole upper surface, whereas for zero or negative incidence the flow either reattaches itself or remains attached. Flow visualisation using tufts confirmed the reattachment of the flow at 0 degrees. The very sharp drop in damping near the critical speed for $\alpha = 5^o$ indicated a resonance, and at the critical speed the motion was in the pitch mode only. The magnitudes of the logarithmic decrement above 0.1 were calculated by measuring the amplitude ratios over a number of cycles, and are not completely accurate, as the equation

$$\delta_{z\theta} = \frac{1}{n} \frac{\ln A_o}{A_N}$$

holds for small values of $\delta_{z\theta}$. The higher values were accurate enough for this study, as the main point of interest was the critical speed of each configuration. The damping was plotted from zero to give a measure of the aerodynamic damping at any speed.

Figures 37 and 38 give the variation of aerodynamic damping with speed for the deck in the final configuration, with the low pivot and correct centre of gravity. The sharp drop in damping is again noticeable, as is the marked increase in critical speed due to the parapet fairing. The effect of incidence is the same as before, the critical speed reducing as the incidence increases. For $\alpha = -5^o$, the critical speed without the fairing is 13.6 m/sec. and with the fairing 17.7 m/sec. At these negative incidences, the effect of the fairing is not marked, as the flow reattaches to the top of the deck anyway. The fairing causes the reattachment sooner. For each incidence, the fairing increases the critical speed by about 4 m/sec.

The reduction in damping between 1.5 and 2 m/sec. corresponds to the low speed shedding of Karman vortices, and the resulting forced oscillation in translation.

Figure 39, for the arch rib and deck shows the effect of initial logarithmic decrement on the maintained amplitude at the low speed resonance condition. The effect of the holes or ducts in the box beams of the arch rib and the holes in the webs of the main beams of the deck are also shown. Increasing the initial damping is equivalent to increasing the structural damping, and so any forced vibration would have a reduced amplitude with increased structural damping, as the aerodynamic damping will be constant at any given speed. The turbulent flow caused by the holes, and the reduction in the strength of the vortices is again illustrated.

In Figures 40 and 41, the variation of critical speed with centre of gravity offset is shown for the deck, with the centre and low pivots, and with and without the parapet fairing. The mode of vibration also changes, and becomes a coupled vertical and rotational motion with a frequency near that of the rotation mode. The coupling is mechanical rather than aerodynamic because of the offset of the centre of rotation from the pivot position. The forcing mechanism is still a vortex phenomenon, and not two degrees of freedom flutter. Typical frequencies are 3.78 hz for rotation, 2.96 hz for translation, and 3.79 hz for the coupled motion for zero c.g. shift, to 3.52 hz for rotation at 3% chord c.g. shift and 3.60 hz for the coupled. For the 3% shift, the 0.08 hz increase in the frequency of the coupled motion over the rotation motion is caused by the higher pitch inertia of the deck about the pivot when in the rotation mode only. In the coupled mode, the model rotates about the centre of gravity at the lower inertia and higher frequency, indicating that the exciting mechanism is constant.
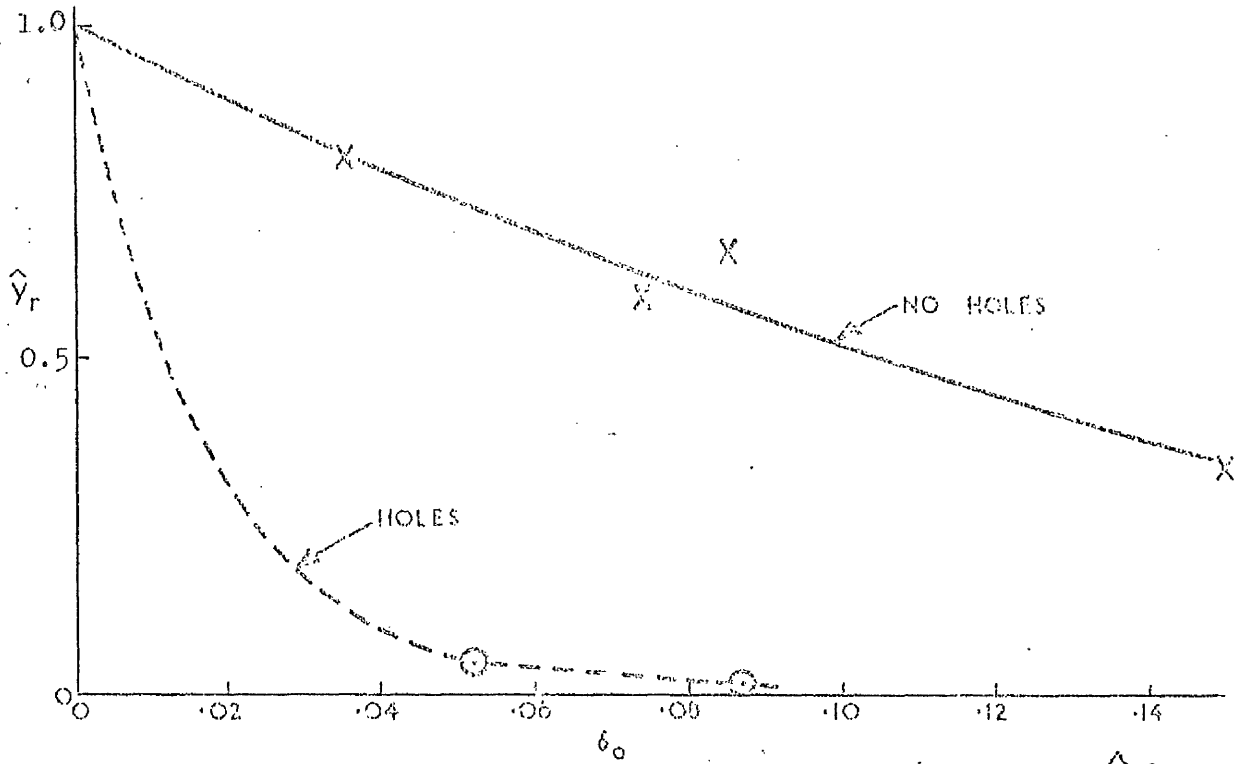
ARCH RIB. MAINTAINED AMPLITUDE AT RESONANCE $(\hat{y}_r)$
AGAINST ZERO WIND LOG. DECREMENT (δ_o)
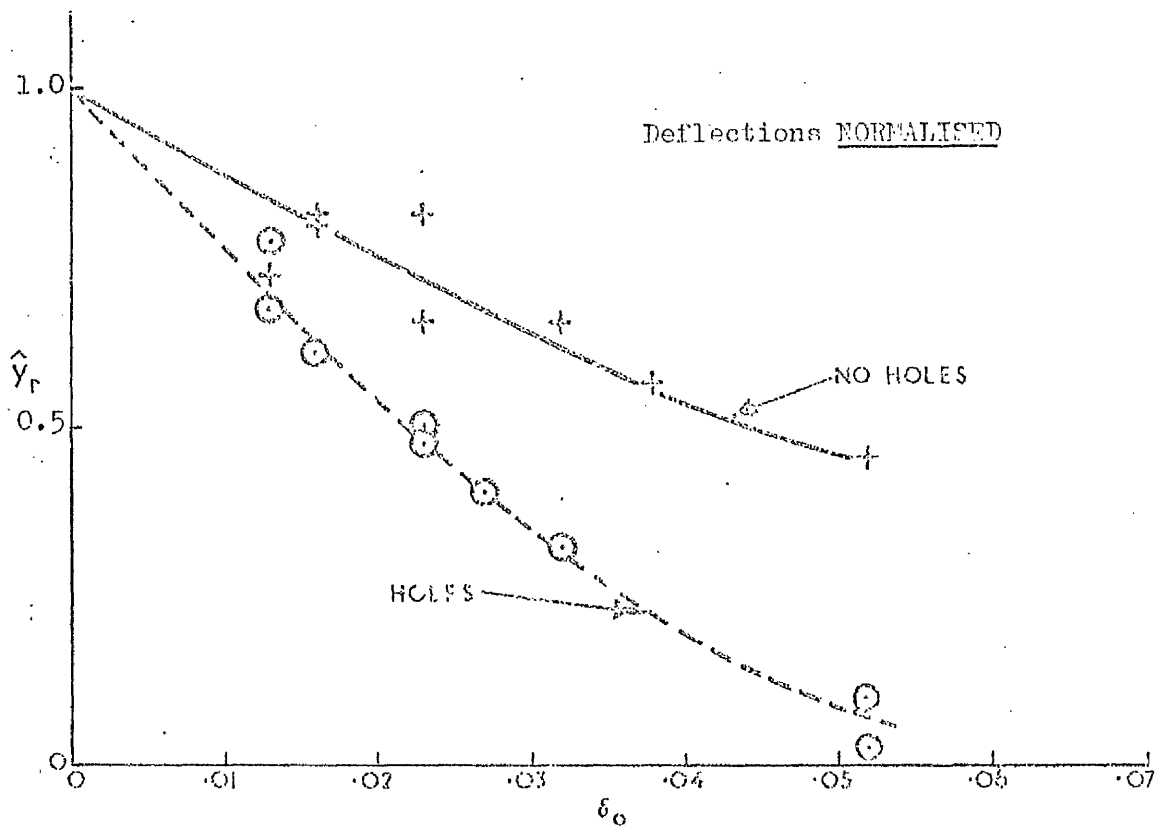
DECK. MAINTAINED AMPLITUDE AT RESONANCE $(\hat{y}_r)$
AGAINST ZERO WIND LOG. DECREMENT (δ_o)
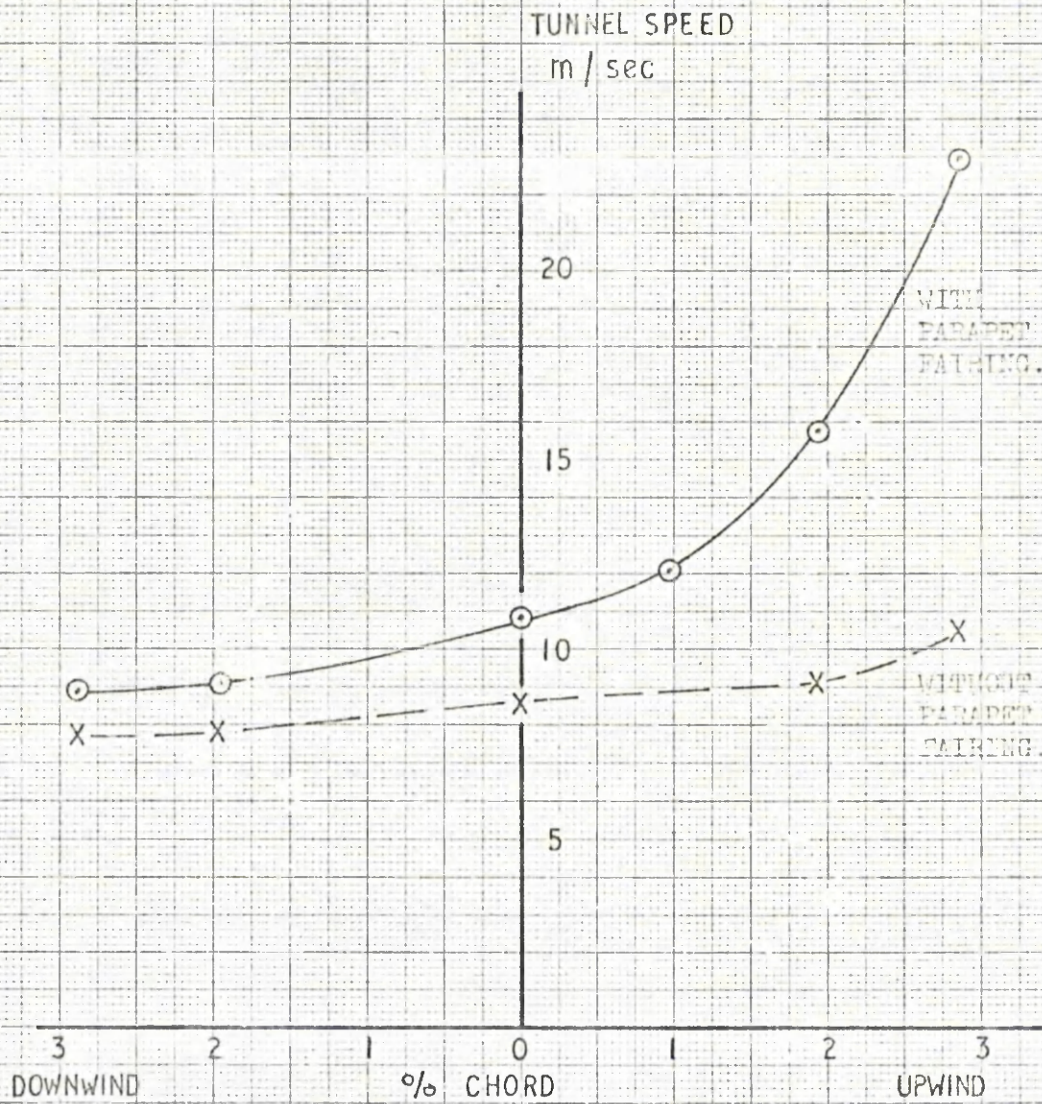
FIGURE 39

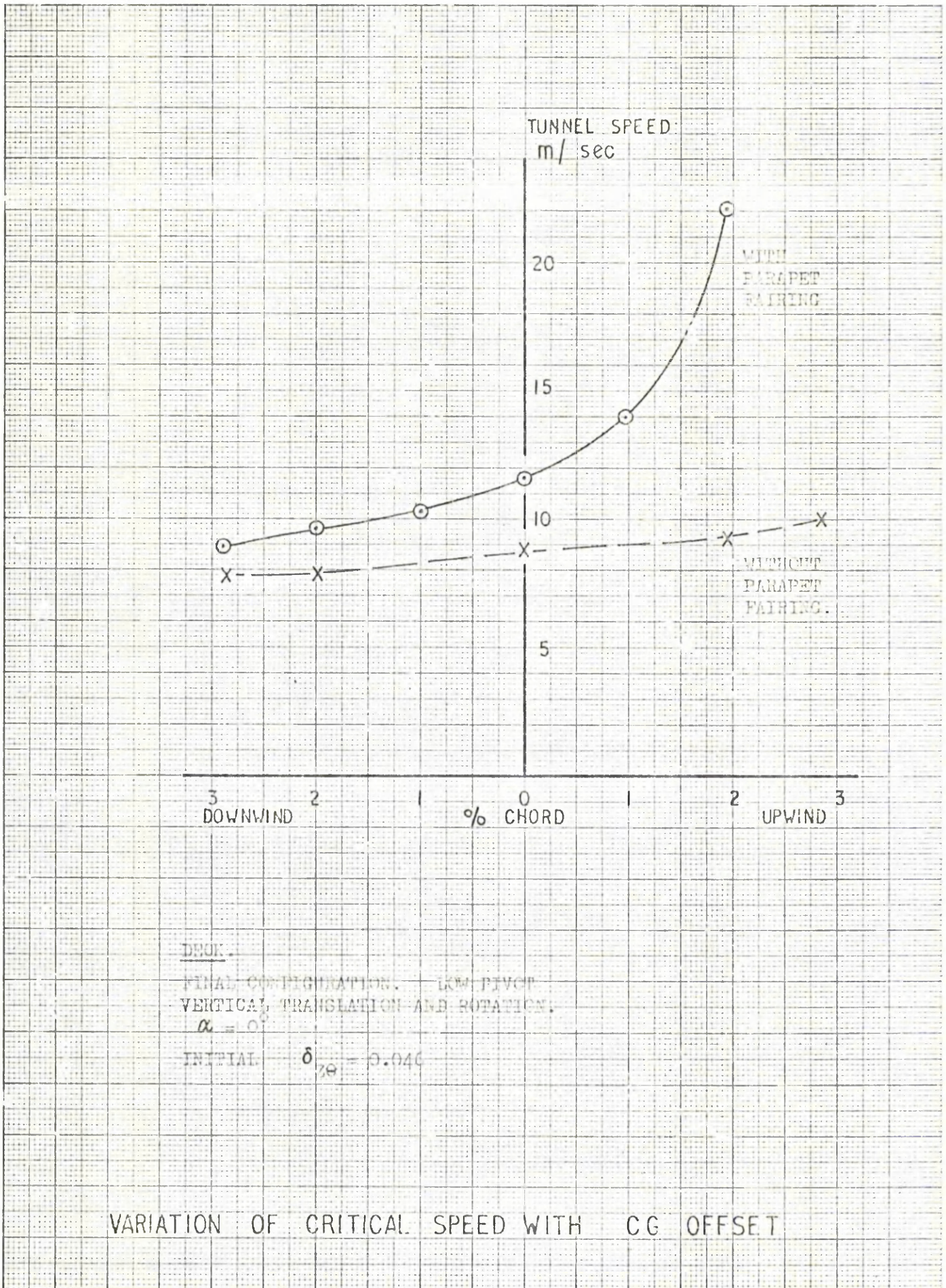VARIATION OF CRITICAL SPEED WITH CG OFFSET

FIGURE 40

VARIATION OF CRITICAL SPEED WITH CG OFFSET

FIGURE 41

For the deck, with centre pivot, fairing, etc. and the correct c.g.

Torsional frequency $w_{TOR} = 3.86$ hz

Spring stiffness in Torsion, $k_{TOR} = 110.765$ Nm/rad.

$$w = \frac{1}{2\pi}\sqrt{\frac{k}{I}}$$

$$I = \frac{k}{(2\pi w)^2}$$

$$= \frac{110.765}{4\pi^2 \; 3.86^2}$$

$$= 0.188 \text{ kg m}^2$$

For c.g. offset of 3% of chord, i.e. mass of 0.68 kg at 0.229 m radius

$$I_{PIVOT} = I + mr^2$$

$$= 0.188 + .68 \times (.229)^2$$

$$= 0.188 + 0.036$$

$$= 0.224 \text{ kg m}^2$$

$$w_{PIVOT} = w_{TOR} \times \sqrt{\frac{I}{I_{PIVOT}}}$$

$$= 3.86 \times \sqrt{\frac{.188}{.224}}$$

$$= 3.54 \text{ hz}$$

The experimental frequency with 3% offset c.g. $= 3.52$ hz.

Figure 42 compares the critical speed with c.g. offset for both the low and centre pivot, again indicating that the low pivot has better characteristics.

Figure 43 shows the effect of turbulence on the critical speed, with the turbulence intensity of 7% calculated using Whitbread's paper (Reference 38). The turbulence was not homogeneous as only a horizontal grid was used, but this was sufficient for vertical perturbations.

The effect of turbulence on the critical speed is curious. With a central c.g., the critical speed is raised slightly in turbulent flow, which could be caused by the flow delaying the formation of regular vortices from the leading edge. However, for the offset c.g. condition, another explanation is needed as the critical speed is reduced in turbulence. In turbulent flow, the critical speed is not so sharply defined
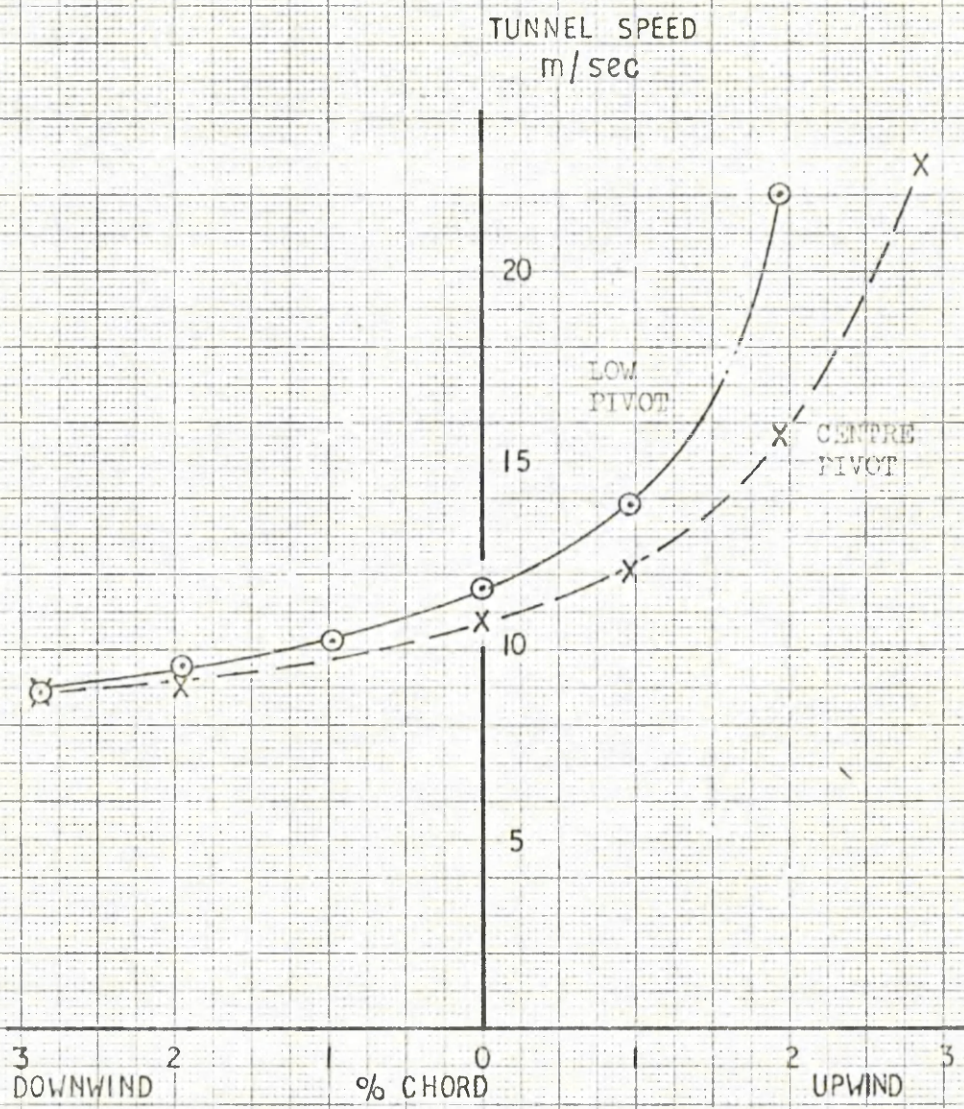
VARIATION OF CRITICAL SPEED WITH CG OFFSET

FIGURE 42

EFFECT OF TURBULENCE ON CRITICAL SPEED, WITH CG OFFSET

FIGURE 43
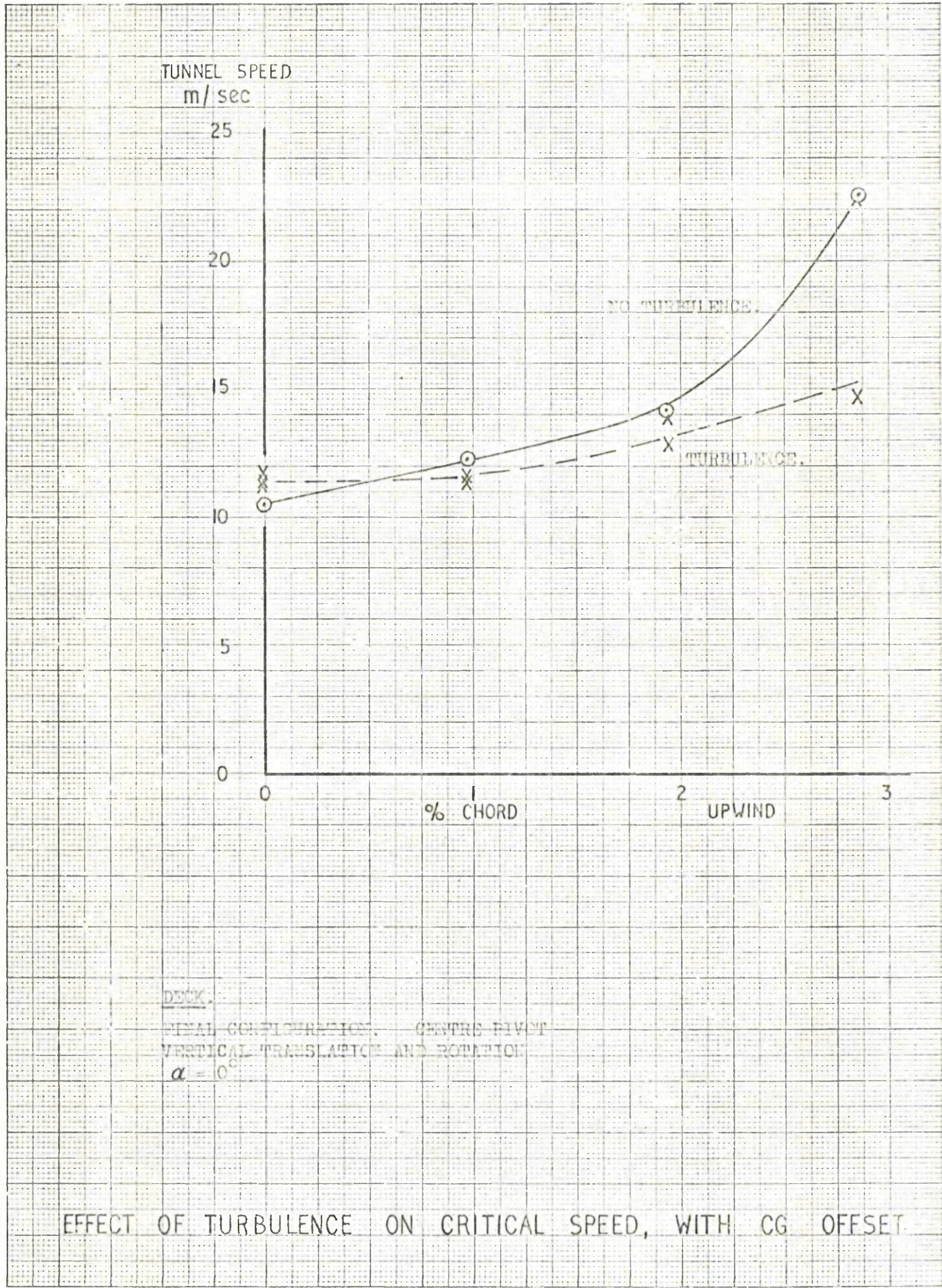
as in smooth flow, and this could lead to a slight error in the speed. Thus the overall effect of turbulence is to reduce the critical speed slightly or to have no effect at all.

The effect of turbulence on the limited amplitude oscillation at low speeds was not investigated as it was thought that the problem had been resolved sufficiently by the modifications.

Figure 44 gives the variation of critical speed with initial $\delta_{z\theta}$ and shows how important it is to determine the level of structural damping present. For the Severn Bridge tests, the experiments used a value of 0.01 for δ, but no structural damping was included in the calculations of critical speed (Reference 28). Welded structures tend to have lower damping than riveted or bolted ones. Large transport aircraft have logarithmic decrements of between 0.03 and 0.1 for the primary bending modes, as determined from ground vibration tests. With the spread in the values of damping for various slender structures, more experimental work is needed to allow good approximations to be made for new structures, incorporating the material used, type of construction, etc. For tall chimneys of a variety of construction types, approximate values for δ are (Reference 39)

Aluminium	0.007
Welded Steel	0.01 – 0.05
Welded Steel, Lined	0.03 – 0.07
Concrete, cast in situ	0.05 – 0.1
Precast concrete	0.07 – 0.15

Figure 45 is derived from Professor Scanlan's work on suspension bridges, in which flutter boundaries have been plotted for various box section models (Reference 32). The higher the reduced velocity v/wl, the more stable the section. Models E and B show increasing flutter boundaries when the natural frequency ratios are increased, a characteristic of classical flutter. The flutter boundaries of the other sections are more or less constant, indicating a torsional or a one
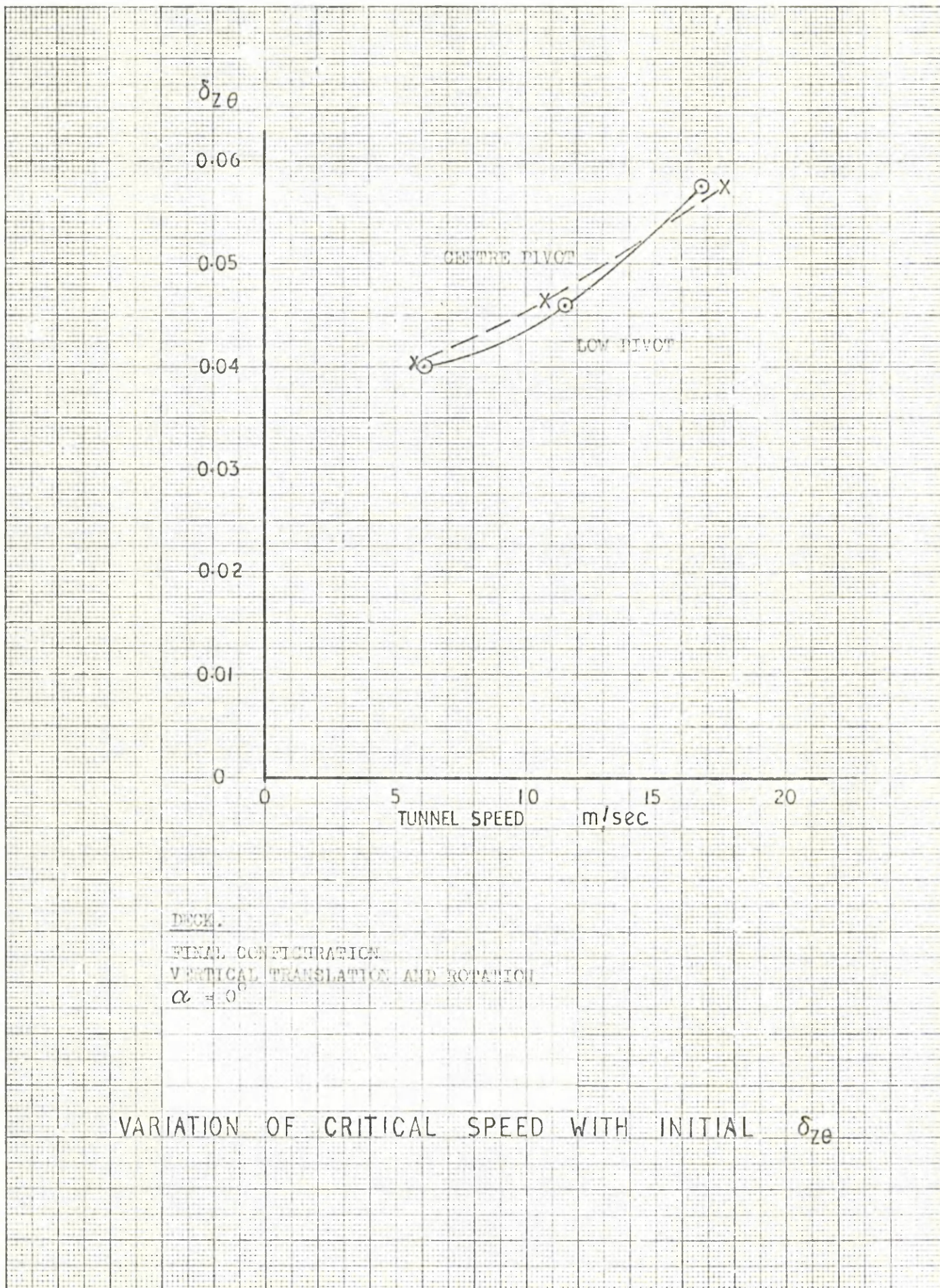
VARIATION OF CRITICAL SPEED WITH INITIAL δ_{ze}

FIGURE 44
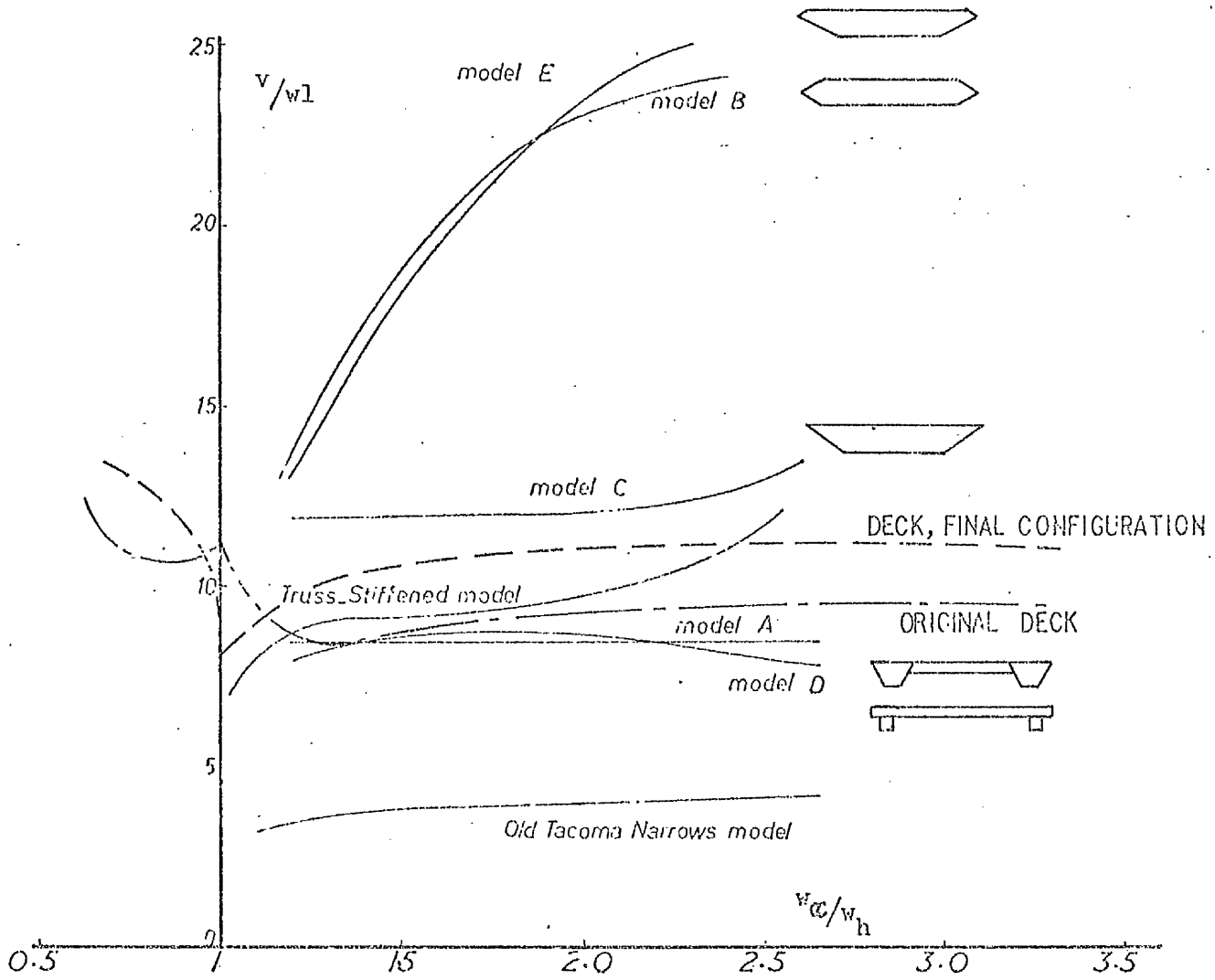
CRITICAL SPEED BOUNDARIES

FIGURE 45

degree of freedom instability. The bridge under consideration has an average flutter boundary, with the final configuration being more stable. An exact comparison between this and the other models depends on the value of the structural damping inherent in the system. The assumption was made that the lowest damping in any support system would tend to be the same. As models A, D and the original deck are similar in cross-section, and have similar boundaries, the assumption appears valid. About the frequency ratio of 1, the original deck and the final configuration have different characteristics in the critical speed boundary. Approaching a frequency ratio of unity the final deck has a similar boundary to that of the truss-stiffened model. The holes in the webs of the main beams of the deck give the webs a porosity of 19%, less than a truss structure, but still significant. The original deck is very similar to model D in cross-section, for which the frequency ratio does not go close enough to one to make a comparison possible.

CONCLUSIONS.

With any type of suspension bridge of non-aerodynamically faired cross-section, the wind causes two types of oscillatory motion to occur. The first and less serious motion is caused when the vortex shedding frequency matches that of the primary bending or torsional frequency of the structure. The torsional frequency is usually the higher and more difficult to force, and so the resonant frequency is in the bending mode. The resulting vibrations transverse to the airstream are of limited amplitude, and non-catastrophic. The amplitude can be reduced both by weakening the vortices and by increasing the structural damping in some way. As the level of damping is fairly constant, depending on the type of construction, the amplitude of the vibration is fixed by the strength of the vortices. These are formed alternately from the top and bottom leading edge of the body, and by disturbing this regularity of flow, their strength is reduced. The most powerful method found in this study was to perforate the webs of the spanwise girders, so bleeding a large volume of air from the stagnation point at the leading edge of the bridge. This took energy from the airstream which would otherwise have been used in the formation of the vortices. Using values of the static lift coefficient for low angles of incidence, and realistic values of damping, it is possible to calculate a reasonably accurate value for the amplitude at this low speed resonance. This will allow alternating stress levels to be calculated and thus an attempt can be made to predict the fatigue life of the structure. Public apprehension, reduced fatigue life, and damage to fittings are the main dangers of this stable oscillation.

Determining the critical speed at which the structure begins a divergent oscillation is the most important point of model testing or theoretical analysis. If the structure is such that it approximates

to a thin aerofoil, either a streamlined box section, or a truss design with a very thin deck, then the critical speed can be determined using thin aerofoil theory in a two degrees of freedom flutter analysis. If it is a bluff body, wind-tunnel testing of models is essential, and is also a necessary check on the other shapes.

This study found that the model in question had a torsional instability at high speed, and that the critical speed had to be increased. High speed Cine film showed that the instability was caused by a vortex phenomenon. The ensuing experimental work to reduce the vortex strength resulted in a trapezoidal fairing along the parapet edge. This had the effect of reducing the angle top corner of the leading edge of the deck, and thus the intensity of the vortex which was shed there. This allowed the critical speed to be raised by up to 30%. In comparison with the model, the fairing was not large, but being strategically placed, it emphasised greatly the importance of edge detail in wind-tunnel tests to determine critical speeds.

The value of structural damping that is assumed in any investigation is of great importance. This study indicated that the critical speed is very dependant on the initial damping values used, and the need for more full scale experimental work to determine damping values for existing bridges. This would allow better base-line assumptions to be made in future tests.

The arch rib has no indication of any torsional instability at high speeds, so the arch rib and deck acting together in high winds will also tend to increase the critical speed. An allowance was made for the effect of the mass and stiffness of one on the other, but the air-flow interaction was neglected. The cross-over points will cut down the length of the deck being forced by the vortices, and the inclination of the arch will also tend to cut down any vibration. The vibration analysis gives a beneficial coupling effect as the first mode of the

arch rib is asymmetric bending, and that of the deck is symmetric bending, thus opposing one another.

The resulting critical speed for the torsional instability will be higher for the bridge than is shown by the tests on the components.

The effect of turbulence on the bridge is hard to define. It certainly eased the very sharp onset of the torsional instability, making the exact definition of critical speed difficult due to a hysteresis effect. Once the model was vibrating, the wind speed could be reduced below critical to some extent, and the model could also remain stable above the defined critical speed.

For future work on bridge aerodynamic behaviour, Professor Scanlan's and Professor Duncan's approach is the best for determining an accurate critical speed. The model in the wind-tunnel should be used to develop the real unsteady aerodynamic derivatives, and these derivatives then used in a flutter solution. If the design is suitable, a comparison can be made using thin-aerofoil theory.

The pressure distribution over an oscillating model will help in understanding the exciting mechanism. Although the cine-film showed that the deck was being forced by a vortex phenomenon, a resonant condition between the deck torsional frequency and the vortex frequency could not be determined. A pressure distribution across both surfaces of a model starting a divergent oscillation from rest could be most useful in this problem.

REFERENCES.

1. Farquharson, F.B., et al. "Aerodynamic Stability of Suspension
    Bridges, with Special Reference to the Tacoma Narrows Bridge"
    University of Washington Engineering Experimental Station,
    Bulletin No. 116, Parts I - V.

2. Russell, J.S. "On the Vibration of Suspension Bridges and other
    Structures, and the means of Preventing Injury from this
    cause". Trans. Royal Scottish Society of Arts, 1841, Vol. 1.

3. Pasley, C.W. "On the State of the Suspension Bridge at Montrose
    after the Hurrican of 11th October, 1838".
    Inst. of Civil Engineers, Min. of Proc. Vol 1, 1839.

4. Rendel, J.M. "Memoir of the Montrose Suspension Bridge"
    Inst. of Civil Engineers, Min. of Proc., 1841

5. Provis, W.A. "Observations on the Effects produced by wind on the
    Suspension Bridge over the Menai Straits".
    Trans. of Inst. of Civil Engineers, 1842.

6. "Opening of the Great Railway Suspension Bridge at Niagara Falls"
    The Civil Engineering and Architect's Journal Vol. XVIII,
    1855.

7. Byrne, B.A. "Brooklyn Bridge - A Half Century of Service".
    American Society of Civil Engineers, Civil Engineering
    June, 1933.

8. "The East River Bridge"
    Engineering, May 25, 1883.

9. Vincent G. S. "Golden Gate Bridge Vibration Studies"
    Journal of Structural Division, Proc. A.S.C.E. Oct. 1958.

10. Frazer. R.A., and Scruton, C. "A Summarised Account of the Severn
    Bridge Aerodynamic Investigation".
    N.P.L./Aero/222

11. Scruton, C. "An Experimental Investigation of the Aerodynamic
    Stability of Suspension Bridges with Special Reference to the
    proposed Severn Bridge"
    Proc. of Inst. of Civil Engineers, Mar. 1952.

12. Walshe, D.E. "A resume of the Aerodynamic Investigations for the
    Forth Road and Severn Bridges."
    Proc. of Inst. of Civil Engineers, May, 1967.

13. Walshe, D.E. and Rayner, D.V. "A Further Aerodynamic Investiga-
    tion for the proposed River Severn Suspension Bridge".
    N.P.L./Aero/1010.

14. "Design cuts construction time on European-Asian Bridge"
    Engineering News-Record, Nov. 9, 1972.

15. "Verrazano Narrows Bridge"
    A.S.C.E., Civil Engineer, Dec. 1964.

16. "Tagus River Bridge opens ahead of schedule"
    A.S.C.E. Civil Engineering, Sept. 1966.

17. Lustgarten, P. "Suspension Bridge Spans Orinoco"
    A.S.C.E., Civil Engineering, Jan. 67

18. Bairstow, L. "Applied Aerodynamics" 2nd Edition p.273

19. Hirai, A., Okauchi, I., Ho, M., and Miyata, T. "Studies on the
    Critical Wind Velocity for Suspension Bridges".
    Symposium on Wind Effects on Buildings and Structures,
    Loughborough.

20. Scruton, C. "Aerodynamic Buffeting of Bridges"
    Engineer, Vol. 199 May 55.

21. "Tamar Bridge"
    Proc. of the Inst. of Civil Engineers, Vol. 31, Aug. 65.

22. Den Hartog, J.P. "Mechanical Vibrations"

23. Fung, Y.C. "The Theory of Aeroelasticity"

24. Victory, M.   "Flutter at High Incidence"

   R. & M. 2048, 1943

25. Bleich, F.   "Dynamic Instability of Truss-stiffened Suspension
   Bridges under Wind Action".

   Trans. American Society of Civil Engineers, Vol. 114, 1949.

26. Bleich, F., McCullough, C.B., Rosecrans, R., Vincent, G.S.   "The
   Mathematical Theory of Vibration in Suspension Bridges"

   U.S. Government Printing Office, 1950.

27. Smith, I.P.   "The Aeroelastic Stability of the Severn Suspension
   Bridge"

   N.P.L. Aero Report/1105, 1964.

28. Ostenfeld, C., Frandsen, A.G., Haas, G.   "Motorway Bridge across
   the Lillebaelt;   Aerodynamic Investigations for the
   Superstructure".

   Bygningsstatiske Meddelelser, Vol. 41, 1970.

29. Scanlan, R.H., Sabzevari, A.   "Suspension Bridge Flutter Revisited".
   A.S.C.E. Structural Engineering Conference, Seattle 1967.

30. Scanlan, R.H., Sabzevari, A.   "Aerodynamic Instability of
   Suspension Bridges".

   A.S.C.E. Journal of Eng. Mechanics Div.   April, 1968.

31. Sabzevari, A., Scanlan, R.H.   "Aerodynamic Investigation of Box
   Girder Bridges".

   A.S.C.E. Journal of Structural Div. July, 1969.

32. Scanlan, R.H.   "The Suspension Bridge;   Its Aeroelastic Problems".
   A.S.M.E. Vibrations Conference, Toronto 1971.

33. Frazer, R.A., Duncan, W.J.   "The Flutter of Aeroplane Wings"
   R. & M. 1155.

34. Duncan, W.J.   "The Fundamentals of Flutter"
   R. & M. 2417.

35. Dicker, D.   "Aerodynamic Stability of H Sections"

    Proceedings A.S.C.E. Jour. of Engineering Mechanics Div.1966.

36. Dicker, D.   "Critical Wind Speeds for Suspension Bridges"

    Phil. Trans. Royal Society of London, A269, 1971

    Discussion.

37. British Standards Institution.   Draft for Public Comment.

    Technical Committee B/116.

38. Whitbread, R.E.   "On the introduction of turbulence into wind

    tunnel investigations for the determination of wind-induced

    amplitudes of oscillation".

    Symposium on Wind Effects on Buildings and Structures,

    Loughborough.

39. Whitbread, R.E.   "Practical Solutions to Some Wind Induced

    Vibration Problems".

    Vibration Problems in Industry, 1973. U.K.A.E.A. and N.P.L.